# STUDYING LCHADD CHORIORETINOPATHY USING A NOVEL LCHADD MOUSE MODEL

By

Shannon J. Babcock

A Dissertation

Presented to the Molecular & Medical Genetics Department and the Oregon Health & Science University School of Medicine in partial fulfillment of the requirements for the degree of Doctor of Philosophy

May 2024

# Table of Contents

# Index of Figures

# Index of Tables

# List of Abbreviations

| | |
|---|---|
| $^{14}CO_2$ | Radiolabeled carbon dioxide |
| 3-KAT | 3-ketoacyl-CoA |
| ACAD9 | Acyl-CoA dehydrogenase |
| ACAD9-/- | ACAD9 deficient homozygous mouse model |
| ATP | Adenine triphosphate |
| BHB | β-hydroxybutyrate |
| CACT | Carnitine acylcarnitine translocase |
| CAG | Chicken beta-actin |
| CASTOR | CoA sequestration, toxicity, and redistribution |
| CNV | Choroidal neovascularization |
| CoA | Acyl-coenzyme A |
| CPT-1 | Carnitine palmitoyl transferase 1 |
| CPT-2 | Carnitine palmitoyl transferase 2 |
| CPT1 | Carnitine palmitoyltransferase 1 |
| CPT1a-/- | CPT1a (liver isoform) deficient homozygous mouse model |
| CPT1a+/- | CPT1a (liver isoform) deficient heterozygous mouse model |
| CPT1b-/- | CPT1b (adipose tissue, muscle, heart isoform) deficient homozygous mouse model |

| | |
|---|---|
| CPT1b+/- | CPT1b (adipose tissue, muscle, heart isoform) deficient heterozygous mouse model |
| CPT2 | Carnitine palmitoyltransferase 2 |
| CPT2A-/- | Adipocyte-specific CPT2 deficient homozygous mouse model |
| CPT2L-/- | Liver-specific CPT2 deficient homozygous mouse model |
| CPT2M-/- | Muscle- and heart-specific CPT2 deficient homozygous mouse model |
| DEGs | Differentially expressed genes |
| E510Q | Glutamate to glutamine mutation at amino acid 510 |
| ENU | N-ethyl-N-nitrosourea |
| ERG | Electroretinogram |
| FA | Fatty acids |
| FAO | Fatty acid β-oxidation |
| FAOD | Fatty acid oxidation disorder |
| FATP | Fatty acid transport proteins |
| FFA | Free fatty acids |
| H&E | Hematoxylin and eosin |
| HADH | 3-hydroxyacyl-CoA dehydrogenase |
| ISR | Integrated stress response |
| ITR | Inverted terminal repeat sequences |
| Jvs | juvenile visceral steatosis |

| | |
|---|---|
| Jvs/+ | Heterozygous mouse model for SCD |
| Jvs/jvs | Homozygous mouse model for SCD |
| KO | Knockout |
| LC-FAOD | Long-chain fatty acid oxidation disorder |
| LCAD | Long-chain acyl-CoA dehydrogenase |
| LCAD-/- | LCAD deficient homozygous mouse model |
| LCAD-/-//VLCAD+/- | LCAD deficient homozygous and VLCAD heterozygous mouse model |
| LCAD-/-/Slc22a5$^{jvs/+}$ | LCAD deficient homozygous and SCD heterozygous mouse model |
| LCHAD | long-chain 3-hydroxyacyl-CoA dehydrogenase |
| LCHAD-/- | LCHAD deficient homozygous mouse model |
| LCHADD | Long-chain 3-hydroxyacyl-CoA dehydrogenase deficiency |
| LV | Left ventricular |
| MADD | Multiple Acyl-CoA dehydrogenase deficiency |
| MCAD | Medium-chain acyl-CoA dehydrogenase |
| MCAD-/- | MCAD deficient homozygous mouse model |
| MCADD | Medium-chain acyl-CoA dehydrogenase deficiency |
| MCT | Medium chain triglycerides |
| MLCL AT-1 | Monolysocardiolipin acyltransferase |
| NBS | Newborn screening |
| OCT | Optical coherence tomography |

| | |
|---|---|
| OCTA | Optical coherence tomography angiography |
| OKT | Optokinetic tracking |
| PBS | Phosphate buffered saline |
| PCR | Polymerase chain reaction |
| rAAV | Recombinant adeno-associated virus |
| rAAV5 | Recombinant adeno-associated virus serotype 5 |
| rAAV8 | recombinant adeno-associated virus serotype 8 |
| rAAV9 | Recombinant adeno-associated virus serotype 9 |
| RER | Respiratory exchange ratio |
| RPE | Retinal pigment epithelium |
| RT-qPCR | Reverse transcription-quantitative PCR |
| SCAD | Short-chain acyl-CoA dehydrogenase |
| SCAD-/- | SCAD deficient homozygous mouse model |
| SCADD | Short-chain acyl-CoA dehydrogenase deficiency |
| SCD | Primary systemic carnitine deficiency |
| SD-OCT | Spectral domain-optical coherence tomography |
| TEM | Transmission electron microscopy |
| TFP | Mitochondrial trifunctional protein |
| TFP$\alpha$ | Alpha subunit of mitochondrial trifunctional protein |
| TFP$\alpha$-/- | TFP$\alpha$ deficient homozygous mouse model |
| TFP$\alpha$+/- | TFP$\alpha$ deficient heterozygous mouse model |
| TFP$\beta$ | Beta subunit of mitochondrial trifunctional protein |

| | |
|---|---|
| TFPβ-/- | TFPβ deficient homozygous mouse model |
| TFPD | Mitochondrial trifunctional protein deficiency |
| VLCAD | Very long-chain acyl-CoA dehydrogenase |
| VLCAD-/- | VLCAD deficient homozygous mouse model |
| VLCAD-/-//LCAD-/- | VLCAD and LCAD deficient homozygous mouse model |
| VLCADD | Very long-chain acyl-CoA dehydrogenase deficiency |
| WT | Wildtype |

# Outline

The goal of this dissertation is to improve understanding and treatment for the chorioretinopathy seen in long-chain 3-hydroxyacyl-CoA dehydrogenase deficiency (LCHADD) patients by examining the molecular mechanisms and testing potential treatments for LCHADD chorioretinopathy using a novel LCHADD mouse model. Specifically, this dissertation:

- Introduction to the history and current knowledge about LCHADD and LCHADD chorioretinopathy (Chapter 1)
- Reviews the currently available FAOD mouse models and the ways they have contributed to FAOD research (Chapter 2)
- Details the creation and characterization of a novel LCHADD mouse model (Chapter 3)
- Characterizes the progression of and molecular mechanisms involved in the chorioretinopathy of the LCHADD mouse (Chapter 4)
- Outlines the creation, packaging, and most effective dose for a subretinal injection of AAV2/5 encoding mHadha-3XFLAG transgene, and assesses the efficacy of gene addition therapy in treating the mouse LCHADD chorioretinopathy (Chapter 5)
- Conclusion and future directions (Chapter 6)

# Chapter 1 : Introduction

## Human Metabolism

A characteristic of **all** living organisms is that they have a **metabolism**, a system of chemical reactions that creates energy from nutrients in the environment. Every cell requires ATP, a currency for energy in humans, for proper functioning with some cells, such as neurons, requiring more ATP than other cells, such as skin cells. Therefore, dysregulation of metabolism can greatly impact human health.[2-5]

Human metabolism is an intricate network of **catabolic reactions** that degrade **carbohydrates, fatty acids (FA)**, or **amino acids**, for energy, and **anabolic reactions**, reactions that build macromolecules for energy storage. With the main goal of maintaining energy homeostasis, the body can switch between pathways depending on substrate availability and metabolic demand, known as **metabolic flexibility.**[6-8]

One example of this metabolic flexibility is shifting between a fed and fasted state (Figure 1-1). During a fed state, such as after eating, circulating glucose levels increase. This causes insulin release into the bloodstream and triggers cells to uptake glucose where glycolysis oxidizes it to make adenine triphosphate (ATP).[8] Insulin also increases triacylglycerol synthesis and glycogen storage to save energy for future situations.[7,8] When the body is low in circulating glucose, such as after an overnight fast or during exercise, there is a switch toward fatty acid oxidation. Because not all tissues, like the brain, are able to metabolize fat, glucagon stimulates glycogenolysis, gluconeogenesis, and ketogenesis in the liver.[8] These processes increase circulating glucose and ketone bodies, which can be metabolized by tissues that can't break down fat for energy. Glucagon also stimulates lipolysis, which increases circulating free fatty

acids (FFAs) and further stimulates fatty acid β-oxidation (FAO) in the liver, skeletal muscle, and heart.[7,8] Human metabolism relies on the ability to switch between processes depending on the substrate availability and energy demand, specifically from glycolysis to FAO during fasting. When metabolism is inflexible, it can result in disease, as evidenced by fatty acid oxidation disorders.[6-8]

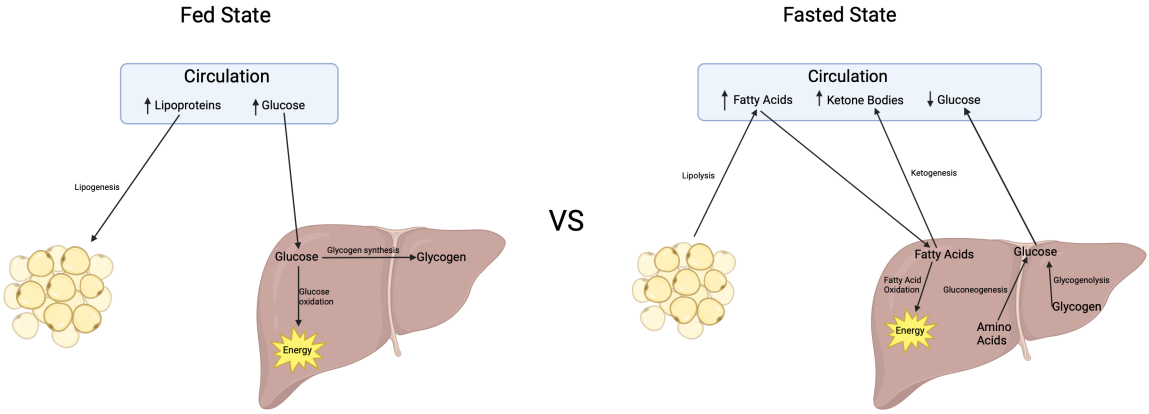


**Figure 1-1: A schematic of metabolism during a fed vs fasted state.** In the fed state, there are high concentrations of lipoproteins and glucose from the gut. Cells are triggered to take up glucose and it is used as the main source of energy. Anabolic reactions are also stimulated to create energy stores, such as triglycerides in adipose tissue and glycogen in the liver. In contrast, during the fasted state, there are low glucose and gut derived lipoprotein levels in circulation. Glucagon stimulates fatty acid oxidation in select tissues such as the liver in order to make ATP or ketone bodies, which can be used by tissue that are unable to metabolize fat. Lipolysis, the release of fatty acids from adipose, glycogenolysis, and gluconeogenesis are also stimulated in order to increase the levels of glucose and fatty acids in circulation. This figure was created using Biorender.com.

## Mitochondrial Long-Chain Fatty Acid β-oxidation

FAO occurs in the mitochondria and is the degradation of FFAs into acetyl-CoA and a new FA that is two carbons shorter. While this dissertation will be focusing on long-chain (C11-20) FAO (Figure 1-2), medium-chain (C6-10) and short-chain FAO (C4-6) follow similar enzymatic steps except use different proteins and medium/short-chain FAs are believed to freely diffuse across plasma and mitochondrial membranes.[9,10] The first step of long-chain FAO is the transportation of FAs across the plasma membrane using the fatty acid transport proteins (**FATPs**).[10] FATPs have acyl-coenzyme A (CoA) synthetase activity so FAs are rapidly converted to acyl-CoA after translocation.[11] The next step is for the acyl-CoAs to be transported into the mitochondria using the carnitine shuttle.[10,11] Carnitine palmitoyl transferase 1 (**CPT-1**), located on the outer mitochondrial membrane, converts the acyl-CoA into an acylcarnitine.[10,11] Acylcarnitines are then translocated across the inner mitochondrial membrane by the carnitine acylcarnitine translocase (**CACT**).[10,11] Once inside the mitochondria, **CPT-2**, which is located on the inner mitochondrial membrane, removes carnitine, and regenerates the acyl-CoAs.[10,11]

Once inside the mitochondrial matrix, long-chain acyl-CoAs undergo β-oxidation, a cyclic process of four enzymatic steps in which acyl-CoAs are shortened by two carbons and an acetyl-CoA is released. The acyl-CoA is first dehydrogenated to create a trans-2-enoyl-CoA by the very long-chain acyl-CoA dehydrogenase (**VLCAD**) protein. The mitochondrial trifunctional protein (**TFP**) conducts the last three enzymatic steps of long-chain FAO: enoyl-CoA hydratase, 3-hydroxyacyl-CoA dehydrogenase (LCHAD), and 3-ketothiolase.[11] The two-carbon chain-shortened acyl-CoA that results from this process goes back through the cycle. The acetyl-CoA fuels the tricarboxylic acid cycle and

electron transport chain where energy in the form of ATP is created. It can also be used by the liver to fuel ketogenesis during periods of fasting. This process produces the ketone bodies, acetoacetate and β-hydroxybutyrate (BHB), which are secreted from cells into circulation using monocarboxylate transporters and can be used for fuel by organs like the brain.[12,13]

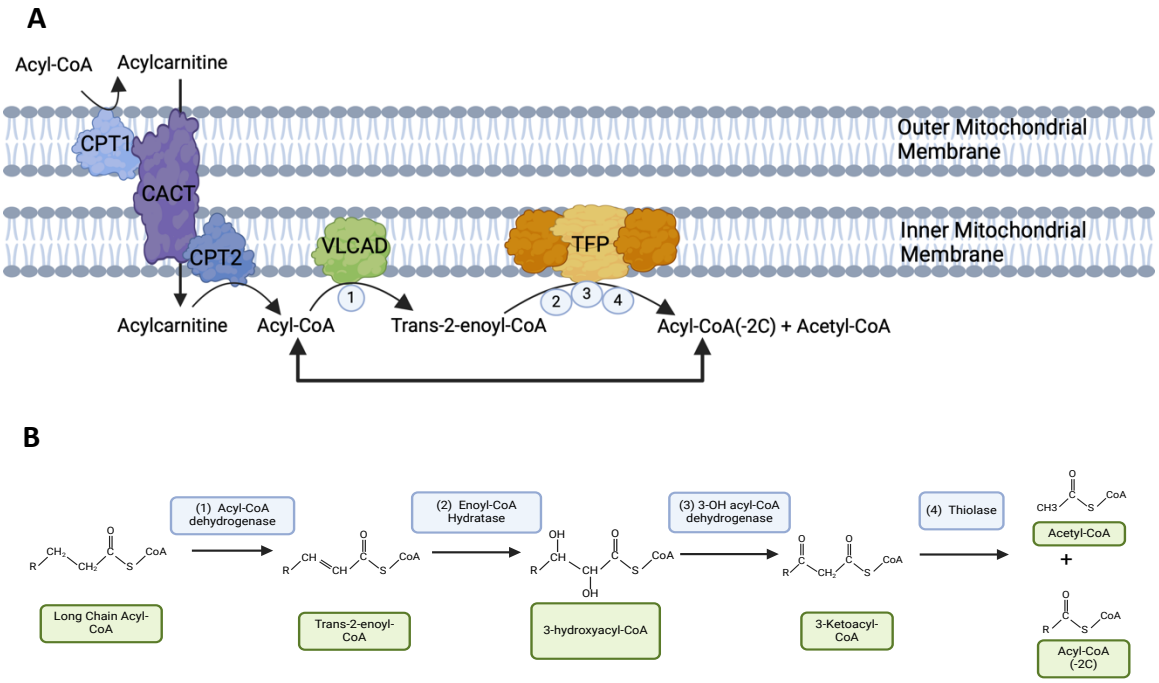


**Figure 1-2: Schematics of long-chain FAO.** Long-chain FAO is composed of many proteins that include transporting acyl-CoAs into the mitochondria and oxidizing it to a 2-carbon shortened acyl-CoA and acetyl-CoA. This figure shows (A) the proteins involved in and (B) the different enzymatic activities and intermediates formed in long-chain FAO. This figure was made using Biorender.com and is also seen in Chapter 4.

## Fatty Acid Oxidation Disorders

The importance of FAO can be highlighted by patients with FAO disorders (FAODs), a group of rare, genetic disorders that result from a reduced or loss of function in any protein involved in the mitochondrial β-oxidation pathway, including the transport of fatty acids into the mitochondria. These disorders are inherited in an autosomal recessive manner (Table 1-1).[14] All FAODs generally present with three common symptoms, but the severity of the presentation can range greatly depending on disorder and type of variants. First, patients will present with metabolic decompensation, which includes hypoketotic hypoglycemia and liver dysfunction, and is most life-threatening during infancy. These episodes are believed to be triggered during times when FAO is required, such as during fasting, exercise, or illness, although they can occur in severe patients without a trigger. Second, cardiac presentations, such as hypertrophic cardiomyopathy or arrhythmias, are another common finding and are observed mainly in young patients. Finally, adolescent FAOD patients can present with myopathies, such as elevated creatinine kinase levels, muscle weakness, and rhabdomyolysis. In addition to these common FAOD symptoms, some FAODs can present with disease-specific symptoms. [11,15-17]

**The main focus of this thesis will be the long-chain FAOD, long chain 3-hydroxyacyl-CoA dehydrogenase deficiency (LCHADD) (OMIM #609016)**.

**Table 1-1:** Table of FAODs

| Disorder | Incidence | Gene | Acylcarnitine elevations[18] | OMIM |
|---|---|---|---|---|
| Carnitine Transporter (CTD) | 1:100,000* | *SLC22A5* | Decreased C2, C16 | 212140 |
| CPT1 Deficiency | Rare* | *CPT1A* | C0/(C16+C18) | 255120 |
| CACT Deficiency | Very Rare* | *SLC25A20* | C16, C16:1, C18, C18:1, C18:2 | 212138 |
| CPT2 Deficiency | Rare* | *CPT2* | C16, C16:1, C18, C18:1, C18:2 | 255110 |
| SCAD Deficiency | 1:35,000 to 1:50,000[16] | *ACADS* | C4 | 201470 |
| MCAD Deficiency | 1:4,000 to 1:200,000[16] | *ACADM* | C8 | 201450 |
| VLCAD Deficiency | 1:42,500 to 1:120,000[16] | *ACADVL* | C14, C14:1, C14:2 | 201475 |
| LCHAD Deficiency | 1:250,000 to 1:750,000[16] | *HADHA* | C16-OH, C16:1-OH, C18-OH, C18:1-OH, C18:2-OH | 609016 |
| TFP Deficiency | Rare[16] | *HADHA, HADHB* | C16-OH, C16:1-OH | 620300 |
| HADH Deficiency | Rare[16] | *HADH* | C4-OH, C6-OH | 231530 |
| MADD | Rare[16] | *ETFDH, ETFA, ETFB* | C4, C5, C6, C8, C10, C12, C14, C16 | 231680 |

## Long Chain 3-hydroxyacyl-CoA Dehydrogenase Deficiency (LCHADD)

LCHADD is a rare, autosomal recessive long chain FAOD first reported in 1989 and is caused by a loss of the LCHAD enzymatic activity of the mitochondrial trifunctional protein (TFP).[19,20] TFP is a heterotetramer made up of two alpha and two beta subunits encoded by *HADHA* and *HADHB*, both located on chromosome 2p23.[21-23] The TFPβ subunits form a homodimer with one TFPα subunit on either side of the homodimer.[22] This mitochondrial membrane-bound complex contains three activities: TFPα contains the hydratase and LCHAD activity whereas TFPβ contains the thiolase activity.[24] The majority of LCHADD patients have at least one c.G1528C missense variant, which causes a glutamate to glutamine amino acid change at position 510 (E510Q) in TFPα.[25,26] This falls in the LCHAD active site in TFPα, which only reduces the LCHAD activity while the stability and other enzymatic functions of TFP are mostly retained.[22,25,26] This contrasts with TFP disorder, which is caused by any variant in *HADHA* or *HADHB* that affects the stability of TFP and reduces or eliminates all of the enzymatic functions of TFP.[24,27-29] **This unique loss of predominantly LCHAD activity leads to an accumulation of partially oxidized metabolites in tissues and in circulation, such as long-chain 3-hydroxyacylcarnitines which are a hallmark of LCHADD.**

LCHADD patients display all the common FAOD phenotypes. For example, LCHADD patients have a severe, acute clinical onset with episodes of hypoketotic hypoglycemia, cardiomyopathy, and hepatomegaly within the first years of life.[30,31] They also can have cardiac hypertrophy and arrhythmias during metabolic crises in infancy[9,17]; however, recent reports have shown cardiomyopathy with a risk of sudden cardiac arrest

and life-threatening arrhythmias in LCHADD patients who survived infancy.[32] Lastly, surviving LCHADD patients can experience skeletal myopathy and rhabdomyolysis.[9] In addition to the common FAOD symptoms, LCHADD patients who survived infancy develop chorioretinopathy and peripheral neuropathy: these two findings are unique to LCHADD patients and not observed in other FAOD patients. **We will specifically focus on the LCHADD-specific chorioretinopathy in this thesis where we will explore potential molecular mechanisms and treatments for the chorioretinopathy.**

*Newborn Screening and Dietary Management*

Newborn screening (NBS) has been crucial in decreasing the mortality of FAOD patients by identifying patients and applying preventative measures prior to fatal metabolic decompensations.[9,33,34] Prior to NBS, patients were identified due to family history or after the first metabolic decompensation, which caused severe morbidity within the first few years of life in the majority of patients.[30,31] Since FAODs cause sudden infant death and other life-threatening consequences, FAODs were added to NBS programs with the intention of implementing early treatment and preventing morbidity due to metabolic episodes. The main treatment for FAOD patients is dietary management. This includes avoiding extreme fasting and eating a high-carbohydrate, low long-chain fat diet. For long-chain FAODs, such as LCHADD, patients are also advised to supplement with medium chain triglycerides (MCT) or triheptanoin, an odd carbon, medium-chain FA, that can be metabolized for energy using the medium-chain FAO pathway.[35,36] There are currently five FAODs included on the Recommended Uniform Screening Panel Core Conditions, a list of disorders that the Secretary of the Department

of Health and Human Services recommends for states to screen on all newborn babies (https://www.hrsa.gov/advisory-committees/heritable-disorders/rusp). They are detected by a rapid acylcarnitine profile analysis by flow injection electrospray ionization tandem mass spectrometry on dried blood spots[33] (Table 1). For example, LCHADD is detected as an increase in long chain hydroxyacylcarnitines.

Studies have shown that NBS and early dietary treatment have improved outcomes compared to clinically diagnosed patients. FAOD patients detected through NBS have decreased cardiomyopathy, hypoglycemia, hypotonia, and mortality rate.[34,37] Specifically, for LCHADD patients, studies have shown that NBS and pre-symptomatic dietary management have improved the risk of mortality, improved quality of life for patients, and could improve some long-term complications.[34,38-43] Despite these promising results, NBS and early dietary management does not absolutely **prevent** lethal metabolic crises from occuring[34] nor the development of long-term complications.[44,45] **For example, early diagnosis and the current dietary treatment can slow the progression and/or delay the onset of the LCHADD chorioretinopathy but it does not fully prevent it.[39,41-43,45-47] This highlights the importance of studying the molecular mechanisms involved in these FAOD complications to improve prognoses and treatments.**

*Importance of Mouse Models in FAOD Research*

Mouse models have been especially crucial in understanding pathogenic mechanisms and developing treatments for rare disorders because the low prevalence of patients makes it more difficult to obtain more comprehensive natural history data.[48]

Mouse models are also more insightful than non-animal models for metabolic disorders because they can capture the interplay of different pathways and be manipulated by diet and environment. When it comes to studying FAODs, many mouse models have been created that recapitulate aspects of FAODs in patients. They have been used to study the molecular mechanisms involved in many prominent FAOD phenotypes, such as fasting-induced hypoglycemia and cardiomyopathy, and to investigate current and novel treatments.[49-52] Research into LCHADD has been limited because until recently, there has not been a mouse model that genetically and biochemically mirrors LCHADD or exhibits the LCHADD specific phenotypes, such as chorioretinopathy or peripheral neuropathy. **A LCHADD mouse model that specifically accumulates the hydroxyacylcarnitines and presents with FAOD- and LCHADD-specific symptoms will be crucial to understanding the phenotypes and developing potential treatments for LCHADD patients.**

## LCHADD Chorioretinopathy

Unlike any other FAOD, LCHADD patients develop chorioretinopathy, the progressive loss of the retina and choroid, which eventually leads to loss of vision. Located in the back of the eye, the retina is composed of several cell layers that absorb light and transduce electrical signals to the brain where it can be interpreted (Figure 1-3). First characterized in 1998, the progression of LCHADD chorioretinopathy can be categorized into four stages.[53-55]

- Stage 1: Visual performance is normal. The fundus (the back of the eye which is made up of retina, macula, optic nerve, and blood vessels) is also normal.
- Stage 2: Visual acuity and choroid are normal.

    - Stage 2A: Areas of fundus hypopigmentation appear in macular area and normal retinal cell function.
    - Stage 2B: Hypopigmentation spreads into the midperiphery and there is a mild to moderate decrease in retinal cell function.
- Stage 3: Partial atrophy of the retinal pigment epithelium (RPE) and photoreceptors in the posterior pole. Declined vision (progressive myopia), blind spots (scotomas), poor vision in the dark, and abnormal color vision develops.
    - Stage 3A: Mild to moderately decreased retinal cell function and mild choroidal thinning.
    - Stage 3B: Moderate to severely decreased retinal cell function and progressive atrophy of the choroid.
- Stage 4: Extensive atrophy of the choroid, RPE, and photoreceptors in the posterior pole and progressive atrophy in the periphery. There is a severe to complete loss of retinal cell function and loss of central vision.

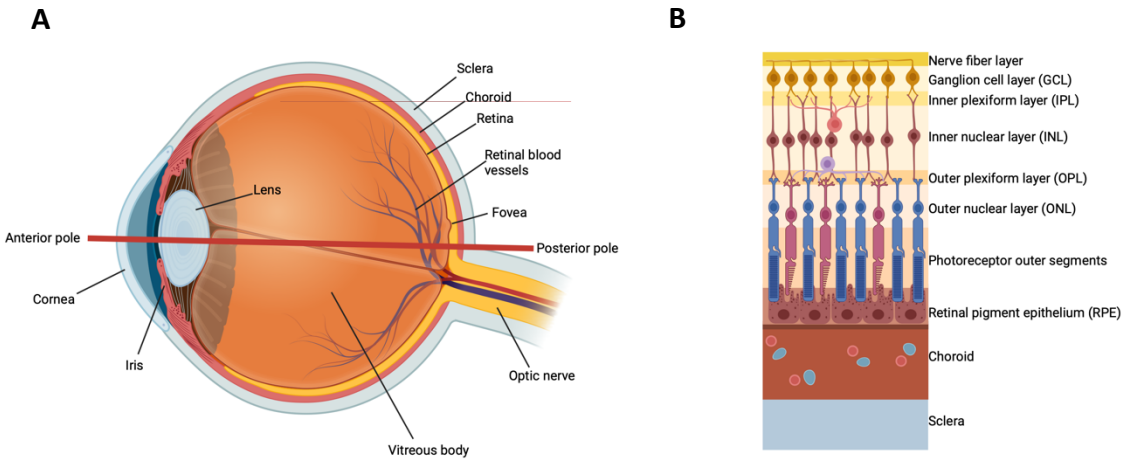


**Figure 1-3: A schematic of the human eye and retina.** (A) The human eye is composed of many types of tissues, including the retina. (B) The retina, located in the back of the eye, is made up of several cell layers and is crucial in absorbing light and transducing electrical signals to the brain where it can be interpreted. The choroid is a layer that separates the retina and sclera and vascularizes the outer layers of the retina. This figure was made using Biorender.com.

*Pathomechanisms of LCHADD Chorioretinopathy*

The LCHADD chorioretinopathy pathomechanisms are not currently fully understood and thus, further elucidating the molecular mechanisms will be crucial to developing a novel therapy. Because LCHADD chorioretinopathy presents as areas of hypopigmentation on fundus images, **it is believed that LCHADD chorioretinopathy is initiated by the loss of the retinal pigment epithelium (RPE) layer, which eventually leads to the death of photoreceptors and vision loss.**[53,54] The RPE is a retinal cell layer made up of post-mitotic, hexagonal epithelial cells that separates the choroid and photoreceptors. This layer has many functions that are crucial for the maintenance and function of the photoreceptors and choroid[56]:

- Transports nutrients, ions, and water between the choroid and photoreceptors.
- Crucial to visual cycle by converting 11-cis retinol to 11-cis retinal, which is necessary for the production of rhodopsin in the photoreceptors.
- Phagocytoses and degrades photoreceptor outer segments.
- Protects retina from light and free radicals.
- Produces growth factors.

**Recent research has suggested that the RPE relies on FAO for energy and that it is crucial in maintaining the "metabolic ecosystem" of the retina (Figure 1-4).**[57,58, 59] First, RPE must be able to efficiently metabolize substrates from photoreceptor outer segments, which are high in FAs. The RPE, therefore, relies on FAO to degrade FAs into energy to prevent lipid accumulation. FAO can stimulate ketogenesis, which uses acetyl-

CoA produced from FAO to produce BHB and acetoacetate. These ketone bodies are transferred to the photoreceptors as another form of energy.[59-63] Proline is also suspected to be an important nutrient for the RPE where it stimulates reductive carboxylation.[64-66] On the other hand, photoreceptors rely on glycolysis for function and outer segment biosynthesis.[67,68] This produces large amounts of lactate which is then transported to the RPE where it can be used as fuel.[57,69] All these pathways are interconnected and crucial for maintaining the health of the retina. For example, glucose from the choroid must pass through the RPE in order to reach the photoreceptors. Lactate, FAs, and proline downregulate glucose oxidation in the RPE so more glucose can pass through.[57,58,64] If any of the pathways are impaired, the RPE will rely more heavily on glucose oxidation and can result in retinal dysfunction and degeneration.[61,70-72] **It is therefore possible that the impaired FAO in the RPE is causing an energy deficiency and/or altering the metabolic pathways in the retina, thus causing LCHADD chorioretinopathy.**

This hypothesis is challenged by the fact that LCHADD is the **only** FAOD that causes chorioretinopathy; therefore, **another possible cause of LCHADD chorioretinopathy is the accumulation of toxic intermediates, specifically the 3-hydroxyacylcarnitines.** It has been shown that high plasma long-chain 3-hydroxyacylcarnitines are correlated with decreased retinal function[43] and that early diagnosis and treatment do improve chorioretinal functions.[38,39,41,45,46] **Determining whether LCHADD chorioretinopathy is due to an energy deficiency, an accumulation of 3-hydroxyacylcarnitines, or a mix of both will be crucial in developing a treatment for patients.**

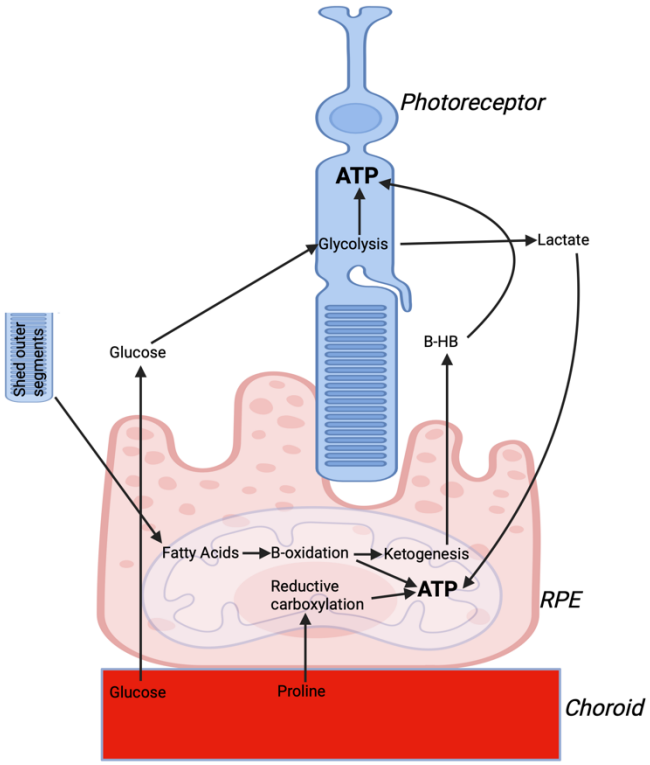


**Figure 1-4: A schematic of the hypothesized "metabolic ecosystem" of the retina.** Recent research has suggested that RPE rely on FAO to make ATP and degrade photoreceptor outer segments that are shed daily. This allows glucose to pass from the choroid to the photoreceptors where is can be used to make ATP. In addition, FAO stimulates ketogenesis in the RPE which can then pass the BHB to the photoreceptors as another source of energy. In exchange, lactate created in the photoreceptors can be used by the RPE to make ATP. This figure was made using Biorender.com.

*Gene Addition as a Potential Therapy for LCHADD Chorioretinopathy*

**Gene addition is one potential therapy for LCHADD chorioretinopathy.** Gene therapy uses genetic material to modify gene expression to treat disease. This can be done by adding a new copy of a gene (gene addition), fixing the endogenous copy (gene editing), or suppressing the mutated gene and adding a functional copy (gene insertion).[73] The most common way to introduce the new copy, also known as the transgene, is to package it in a viral vector, such as a recombinant adeno-associated virus (rAAV). AAV is a good option because of its low immunogenicity, and it rarely integrates into the genome (episomal or non-integrating) in non-dividing cells such as the photoreceptors or RPE. Extensive research on AAV has also led to a variety of capsids that allow for specific transduction of cells and tissues.[74,75] We will focus mainly on gene addition for the remainder of this thesis.

In 2017 the FDA approved Luxturna, a novel gene therapy, for patients with RPE65-mediated retinal dystrophy, an inherited form of vision loss. *RPE65*-mediated retinal dystrophy is an inherited form of vision loss that is caused when a patient is homozygous for a mutation in *RPE65* that results in a loss of RPE65 activity. Luxturna was the first gene addition therapy for these patients where a normal copy of *RPE65* was directly administered to RPE cells.[76] Since then, gene addition has become a promising therapy for many retinal dystrophies and currently there are many clinical trials.[73] This is because the retina is an ideal target organ.[73] First, it is relatively immune divergent meaning it will not have as high of an immune response towards the vector and transgene.[77] Next, the RPE can specifically be treated with the vector using a subretinal or intravitreal injection. This paired with the blood-retinal barrier prevents systemic

circulation and other tissues from being transduced. This targeted injection also allows for a lower efficacious dose which can also lower the chance of an immune response. Finally, retinal cells are post-mitotic. This allows for the use of non-integrating vectors, such as AAV, because the transgene will not be lost due to cell turnover.

LCHADD chorioretinopathy is an excellent candidate for gene addition therapy. First, LCHADD is an autosomal recessive, monogenic disorder that is caused by a loss of LCHAD function. Therefore, restoring some LCHAD activity by adding a functional *HADHA* gene may be sufficient to prevent the chorioretinopathy. Second, because the chorioretinopathy progresses slowly and patients receive a diagnosis before the chorioretinopathy begins, gene therapy can be administered prior to the onset of the chorioretinopathy and prevent vision loss from occurring.

# Chapter 2 : Review of FAOD Mouse Models

**A Review of Fatty Acid Oxidation Disorder Mouse Models**

Shannon J. Babcock[1*], Sander M. Houten[2], Melanie B. Gillingham[1]

[1]Department of Molecular and Medical Genetics, Oregon Health & Science University, Portland, Oregon, USA, [2]Deparment of Genetics and Genomic Sciences, Icahn School of Medicine at Mount Sinai, New York, New York, USA

Published in: *Molecular Genetics and Metabolism. Feb 2024; 142(1)*[78]

## Author Contributions

SJB was responsible to writing. SMH was involved in reviewing and editing, and MBG was involved in reviewing, editing, and funding.


## Abstract

Fatty acid oxidation disorders (FAODs) are a family of rare, genetic disorders that affect any part of the fatty acid oxidation pathway. Patients present with severe phenotypes, such as hypoketotic hypoglycemia, cardiomyopathy, and rhabdomyolysis, and currently manage these symptoms by the avoidance of fasting and maintaining a low-fat, high-carbohydrate diet. Because knowledge about FAODs is limited due to the small number of patients, rodent models have been crucial in learning more about these disorders, particularly in studying the molecular mechanisms involved in different phenotypes and in evaluating treatments for patients. The purpose of this review is to present the different FAOD mouse models and highlight the benefits and limitations of using these models. Specifically, we discuss the phenotypes of the available FAOD mouse models, the potential molecular causes of prominent FAOD phenotypes that have been studied using FAOD mouse models, and how FAOD mouse models have been used to evaluate treatments for patients.



**Keywords:** Fatty acid β-oxidation; inborn errors of metabolism; mouse models; hypoglycemia; cardiomyopathy; exercise; gene addition

Graphical Abstract:

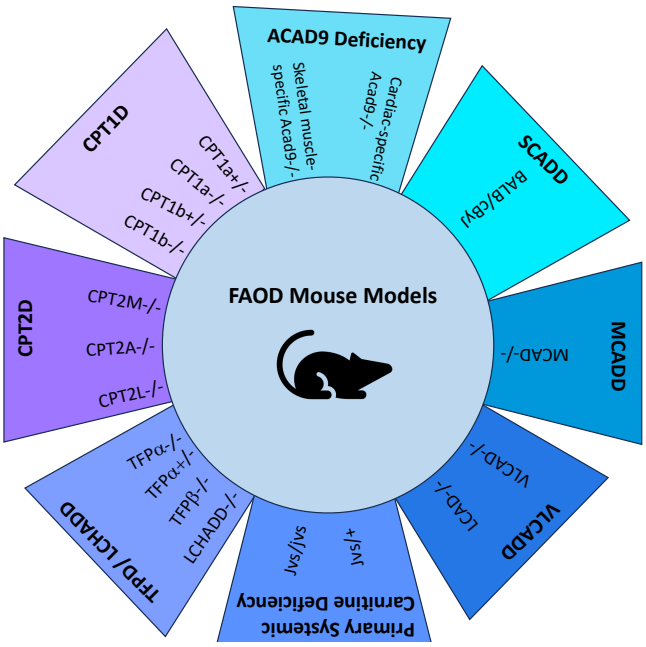


## Introduction

Mitochondrial fatty acid β-oxidation (FAO) is the degradation of fatty acids into acetyl-CoA and is crucial for energy homeostasis in humans. FAO can contribute to ATP synthesis by fueling the tricarboxylic acid cycle and oxidative phosphorylation or it can be used by the liver to generate ketone bodies. While high ATP consuming tissues, such as the heart, rely mainly on FAO, it becomes especially crucial during times of limited glucose, such as fasting, illness, or exercise. By relying on FAO instead of glycolysis, glucose can be preserved for use in the brain and central nervous system.[52,79]

The importance of FAO is highlighted by patients with fatty acid oxidation disorders (FAOD). FAODs are a family of rare, genetic disorders that are inherited in an autosomal recessive manner. FAODs can affect any part of the oxidation pathway (Figure 2-1). Fatty acids are first imported into the mitochondria. While medium-chain fatty

acids are believed to freely diffuse across the mitochondrial membrane, long-chain fatty acids must be imported using the carnitine cycle (*Cpt-1a/1b*, *Cact*, *Cpt2*). Free carnitine, which is essential for this cycle, is imported across the plasmalemmal membrane by OCTN2 (*Slc22a5*). Once inside the mitochondrial matrix fatty acids undergo a series of four enzymatic steps that result in an acyl-CoA that is two carbons shortened and an acetyl-CoA. While there are different enzymes responsible for long-chain FAO and medium/short-chain FAO, both undergo the same four steps: 1) the acyl-CoA is dehydrogenated to a trans-2-enoyl-CoA (*Vlcad*, *Mcad*, *Scad*), 2) a hydratase converts it to a 3-hydroxyacyl-CoA (*Hadha*, *Echs*1), 3) the hydroxyacyl-CoA is dehydrogenated to a keto-acyl-CoA (*Hadha*, *Hadh*), and 4) a thiolase cleaves the keto-acyl-CoA into the two carbon shortened acyl-CoA and an acetyl-CoA (*Hadhb*, *Acaa2*).[11] Patients with FAODs have a wide range of recognized phenotypes, but patients typically display the most severe phenotypes, such as hypoketotic hypoglycemia and rhabdomyolysis, during catabolic conditions. FAOD patients also commonly present with abnormal heart function, such as cardiomyopathy, arrhythmias, or conduction defects, and hepatomegaly.[52] FAODs are detected using newborn screening and are typically managed by diet and lifestyle such as avoidance of fasting and maintaining a low-fat, high-carbohydrate diet.

Animal models have been important in biomedical research and advancing human health. While non-animal models, such as cell or tissue culture, are useful models to study human disease, they are not able to fully recapitulate human physiology. On the other hand, animal, in particular mammalian models, have

physiologic similarities to humans and can mimic some of the complexity of human biology. Animal models are particularly useful when studying metabolic disorders because metabolism is a connection of many different pathways and influenced by diet and environment. Rodent models, which compromise about 95% of all laboratory animals, are commonly used due to their small size, short reproductive cycle and lifespan, and biological similarities to humans.[80] With the development of CRISPR/Cas9-mediated technologies, mice can also be more easily and precisely genetically manipulated to yield genetically manipulated strains on a variety of inbred backgrounds. This is crucial for studying rare diseases, such as FAODs, because knowledge about rare diseases is limited due to the small number of patients (Box 2-1).[48] In this review we discuss the FAOD mouse models that have been created, the phenotypes each mouse displays, and how they have been used to study the pathophysiology and potential novel treatments for FAODs.

## Phenotypes of the Available FAOD Mouse Models

Multiple mouse models have been created that recapitulate aspects of FAODs (Table 2-2).

*Carnitine palmitoyltransferase I (CPT1) deficiency:* CPT1 deficiency leads to an impairment of the carnitine cycle, which is crucial for the import of acyl-CoAs into the mitochondria. Two CPT1 deficient mouse models have been created. The first CPT1 deficient mouse model was created by knocking out exons 11-18 of the *Cpt1a* gene, resulting in a null allele (CPT1a-/-).[81] *CPT-1a* encodes for the liver isoform, and this

deletion is lethal prior to embryonic day 10.[81] Because the Cpt1a-/- is embryonic lethal, many studies have studied the CPT1a heterozygous mouse (CPT1a+/-) which has an over representation in het x het breedings.[81] This mouse displays phenotypes commonly associated with FAODs such as decreased glucose after a 24-hour fast[81], an increase in serum free fatty acids[81], and a fatty liver, which is suggestive of hepatic steatosis.[82] However, unlike some of the other FAOD mouse models, CPT1a+/- mice are able to maintain body temperature and glucose levels when exposed to cold temperatures.[81]

The other CPT1 deficient mouse model knocked out exons 1-3 of *Cpt-1b* which resulted in a null allele.[83] *CPT-1b* encodes the isoform predominantly found in adipose tissue, muscle, and heart[84], and this deletion is also embryonic lethal when knocked out.[83] The CPT1b heterozygous mouse (CPT1b+/-) has a different phenotype than the CPT1a+/-. For example, there was no difference in glucose levels after a 18-hour fast between WT and CPT1b+/- mice but they develop fatal hypothermia without hypoglycemia when exposed to cold.[83] The differences between the CPT1a+/- and CPT1b+/- mouse can be explained by the different tissues that have impaired FAO. Female CPT1b+/- mice have reduced fertility.[83]

*Carnitine palmitoyltransferase 2 (CPT2) deficiency:* CPT2 deficiency is another disorder that leads to an impaired carnitine cycle. Several tissue specific CPT2 deficient mouse models have been created. All these mice were created by crossing a tissue-specific Cre driver mouse strain and a mouse with loxP recombination sites surrounding exon 4 of *Cpt2* on both alleles. When crossed, the offspring has a tissue-specific loss of exon 4

which causes a frame-shift mutation in the remaining exons, and ultimately the loss of CPT2.

The first CPT2 mouse is an adipocyte-specific CPT2 deficient mouse (CPT2A-/-).[85] This mouse has a loss of CPT2 in both brown and white adipose tissue. FAO in brown adipose tissue is known to be crucial for generating heat; so, when exposed to cold temperatures, this mouse was unable to induce thermogenic gene expression in brown adipose tissue and was unable to maintain body temperature when exposed to cold temperature.[85]

Next, a muscle- and heart-specific CPT2-deficient mouse (CPT2M-/-) was created to specifically study how impaired FAO is linked to cardiac hypertrophy.[86] These mice are born at an expected Mendelian ratio, have increased heart acylcarnitines, and have lipid accumulation in the hearts. This mouse model also progressively develops severe cardiac hypertrophic remodeling, dilation, and eventually heart failure.[86] Dietary octanoate was not able to attenuate this cardiac phenotype[87], potentially because the heart and skeletal muscle may in fact need the carnitine cycle to import medium chain fatty acids.[88]

Finally, a liver-specific CPT2-deficient mouse (CPT2L-/-) was created.[89] When fasted for 24 hours at 9 weeks of age, these mice developed hypoketotic dyslipidemia, decreased gonadal white adipose tissue, and enlarged, fatty livers.[89] The mice, however, did not become hypoglycemic and there was no change in energy expenditure.[89] These mice showed similar symptoms when put on a low-carbohydrate ketogenic diet. After 6 days these mice exhibited a dramatic weight loss or death in addition to hepatomegaly,

liver damage, hypoglycemia and complete loss of white adipose tissue.[89] CPT2L-/- mice have also been used to study the response to a chronic high fat diet where they are shown to be resistant to high fat diet-induced obesity and maintain their glucose tolerance and insulin sensitivity.[90] On the HFD for 16 weeks, CPT2L-/- mice have suppressed ketone bodies, lowered glucose, and increased fatty acids in blood.[90] The livers, surprisingly, were not fatty nor did they show signs of damage even though there was increased oxidative stress.[90]

*Short-chain acyl-CoA dehydrogenase deficiency (SCADD) mouse model:* The SCADD mouse model is caused by a spontaneous variant in the *Acads* gene of the BALB/cByJ, a subline of the BALB/c inbred line. It was discovered as an organic aciduria with elevated concentrations of ethylmalonic acid, methylsuccinic acid, and N-butyrylglycine.[91] Studies have shown that the SCAD-/- mouse has decreased glucose levels after an 18-hour fast[91], has a fatty liver that is worsened after fasting[92], has enlarged brown adipose tissue and hearts[93], and are intolerant to cold exposure.[94] It is important to note that patients with SCADD display very few to no symptoms. Therefore, the difference in presentation between SCADD humans and mice highlights that differences between mice and humans can be a limitation to using mouse models to study human disorders.

*Medium-chain acyl-CoA dehydrogenase deficiency (MCADD) mouse model:* MCADD is an example of a medium-chain FAOD. The MCADD mouse model was created by introducing a duplication of exons 8, 9, and 10 into the *Mcad* gene.[95] When translated

the duplicated exon 8 region resulted in a truncated MCAD monomer due to a premature stop codon and ultimately knocked out the MCAD protein (MCAD-/-).[95] Like human MCADD patients, MCAD-/- mice had elevated acylcarnitine levels; however, they differ from the human MCADD acylcarnitine profiles (Table 2-1).[95] Specifically, the predominant species in MCAD-/- mice are C6 and C10:1 whereas the predominant species in patients is C8. MCAD-/- mice have decreased viability with an increase in neonatal mortality, are intolerant to cold exposure, and develop hepatic steatosis especially after a 24-hour fast.[95] Interestingly, when compared to WT mice, glucose levels do not decrease after a 24-hour fast.[95,96,97]

*Very long-chain acyl-CoA dehydrogenase deficiency (VLCADD) mouse models:* VLCADD is an example of a long-chain FAOD. There are two different mouse models that have been created to study VLCADD: one with a mutated *Acadvl* gene (VLCAD-/-) and the other with a mutated *Acadl* gene (LCAD-/-). Both the VLCAD-/- and the LCAD-/- mouse models have a milder phenotype when compared to VLCADD in humans; however, the LCAD-/- mice display a more severe phenotype than the VLCAD-/- model as evidenced by the decreased viability of LCAD-/- pups[98] and the more severe response to fasting. The milder phenotype of these mouse models compared to the human phenotype could be due to VLCAD and LCAD having overlapping functions in mice but not in humans.[99] Chegary et al showed that in human tissues that are known to have high FAO, such as heart, liver, and skeletal muscle, the LCAD protein and mRNA levels are either very low or undetectable. It is also important to note that LCAD deficiency hasn't been identified

in humans. On the other hand, FAO tissues in mice highly express LCAD. Chegary et al. also show that, in mouse fibroblasts, LCAD and VLCAD have substrate overlap where the absence of VLCAD can be fully compensated but LCAD deficiency is not fully compensated.[99] This suggests that in humans VLCAD is indispensable whereas in mice, there is more redundancy due to the functional overlap between VLCAD and LCAD. It also suggests that LCAD is a bit more important in the mouse which explains the difference in severity between the two models. The overlap of activity was investigated by creation of another mouse model that mutated both *Acadvl* and *Acadl*. Knocking out both VLCAD and LCAD proteins (VLCAD-/-//LCAD-/-) is neonatal lethal[98] and a LCAD-/-//VLCAD+/- mouse has a more severe phenotype when compared to either a VLCAD-/- and LCAD-/- mouse.[100] Even though there is a milder phenotype, both the VLCAD-/- and LCAD-/- models are good models of FAODs and have been used in multiple different studies.

There are two VLCAD-/- mouse models that have been created. Both VLCAD-/- models genetically mirror human VLCADD where mutations introduced in *Acadvl* result in an absence of the VLCAD protein.[98,101] Serum acylcarnitines from these mice do show an overall accumulation of long-chain acylcarnitines with the predominant species being C16, C18 and C18:1. The predominant species in the mouse do slightly differ from human VLCADD patients whose predominant acylcarnitine species are C14, C14:1, and C14:2 (Table 2-1).[98,102,103] These mice have cardiomyopathy[101,104-106], display a reduced ability to exercise[107-109], and develop hypoglycemia, hepatic steatosis, and hypothermia when exposed to cold temperatures.[110-112] Interestingly, in response to fasting for long

periods of time, these mice develop fatty livers but there is no reduction in serum glucose levels.[111-113] The VLCAD-/- mouse has been more extensively studied than other FAOD mouse models. For example, a hyperinsulinemic-euglycemic clamp showed that VLCAD-/- mice fed a high-fat diet are protected from insulin resistance.[114] These mice also had decreased glucose levels when infected with an influenza virus[115], did not develop renal failure when stressed potentially because the kidneys enhance glucose oxidation[116], and is the only model thus far to have a decreased respiratory function in response to a hypercapnic challenge.[117]

The other mouse model, LCAD-/-, was created by mutating the *Acadl* gene and knocking out the LCAD protein (LCAD-/-).[118] While this mouse is not genetically similar, the serum acylcarnitine profile in the LCAD-/- mouse mirror the human VLCADD profile with a prominent accumulation of C14:1-carnitine (Table 2-1).[98,118,119] Similarly to the VLCAD-/- mouse, the LCAD-/- mouse has cardiomyopathy[104,120,121] and exhibit hypothermia and reduced glucose when exposed to the cold[110]; however, the LCAD-/- mouse also has reduced glucose levels after fasting[122] and hepatic insulin resistance during a hyperinsulinemic-euglycemic clamp.[123] The LCAD-/- mouse has increased mortality from an influenza infection[124], similar to VLCAD-/-, and is the only mouse model reported to have altered lung mechanics.[125] Specifically, an accumulation of long-chain acylcarnitines in the epithelial lining fluid inhibits pulmonary surfactant's ability to reduce surface tension which prevents inflation of the alveoli and hinders breathing.[126]

*Mitochondrial trifunctional protein deficiency (TFPD)/Long-chain 3-hydroxyacyl-CoA dehydrogenase deficiency (LCHADD) mouse models:* TFPD and LCHADD are also long-chain FAODs and caused by mutations in the mitochondrial trifunctional protein (TFP); however, TFPD is caused when the stability or activity of all three of TFP's enzymatic activities are affected while LCHADD is caused by a common c.G1528C point mutation which impairs only the LCHAD enzymatic activity of TFP. While most of the phenotypes are similar, TFPD and LCHADD patients can have different presentations. For example, progressive chorioretinopathy is more pronounced in LCHADD patients. Fortunately, there have been mouse models for both TFPD and LCHADD.

Two TFPD mouse models have been created. The first model was created by deleting exon 1 and intron 1 of *Hadha.*[127] This resulted in a null allele and knocked out the TFP$\alpha$ protein in this mouse (TFP$\alpha$-/-).[127] Because TFP$\alpha$ and TFP$\beta$ rely on each other for TFP's stability and enzymatic activity[24,128], both the TFP$\alpha$ and TFP$\beta$ subunits were not detectable and all the activities of the TFP enzyme are eliminated in the TFP$\alpha$-/- mouse model.[127] The TFP$\alpha$-/- mouse was not viable due to sudden neonatal death, and fetuses suffered from significant intrauterine growth restriction.[127] Prior to death pups had increased long-chain acylcarnitines and 3-hydroxyacylcarnitines in serum, a significant decrease in glucose, severe hepatic lipidosis, and severe cardiomyocyte degeneration.[127] Because the homozygous TFP$\alpha$ mouse model is neonatal lethal, studies have used the heterozygous TFP$\alpha$ mouse (TFP$\alpha$+/-). They accumulate long-chain acylcarnitines and develop a fatty liver that is worsened after an overnight fast[129], but TPF$\alpha$+/- mice do not have a decreased glucose level after an overnight fast.[129] The TFP$\alpha$+/- mice have also

been used to study cardiolipin biosynthesis. It has been recently shown that TFPα exhibited monolysocardiolipin acyltransferase (MLCL AT-1) activity, which is involved cardiolipin remodeling. TFPα+/- mice have decreased MLCL AT-1 activity and reduced tetralinoleoyl cardiolipin in the heart and liver, suggesting an impaired cardiolipin remodeling process in these mice.[130]

The second TFPD mouse model is a TFPβ protein knockout mouse (TFPβ-/-). Created by treating C57BL/6J male mice with N-ethyl-N-nitrosourea (ENU), which is known to generate single-nucleotide mutations, this mouse had a T-to-A transversion mutation in exon 14 of *Hadhb* which causes a missense mutation of methionine 404 to lysine.[131] Western blots show that the protein levels and activity levels of both TFPβ and TFPα were significantly reduced.[131] In contrast to the TFPα mouse model, TFPβ-/- mice showed no gestational loss, had a normal inheritance pattern, and survived to adulthood.[131] These mice do have a decreased body weight compared to WT mice, decreased blood glucose after a 24-hour fast, and showed cardiac conduction defects as early as 6-months of age.[131] Finally, these mice showed an accumulation of lipids in both the livers and hearts.[131]

There have been two LCHADD mouse models that have been reported in the literature. The first LCHADD mouse model was created by deleting exon 15 of *Hadha* in C57BL6/SVEV129 chimeric mice.[132] Western blots showed that this deletion did not affect the concentration of TFPα or TFPβ even though liver palmitate oxidation was reduced, and it was embryonic lethal to homozygous mice.[132] When heterozygous mice

were studied, they were found to develop fatty livers by 5 months of age and ~20% had liver masses that were indicative of hepatocellular carcinoma by 18 months of age.[132]

Recently, we reported a new LCHADD mouse model that had been created using CRISPR/Cas9 to introduce the common LCHADD mutation, c.G1528C (p.E510Q), into the *Hadha* gene (LCHAD-/-).[133] This is unique because it is genetically and biochemically similar to the human LCHADD. Specifically, LCHAD-/- mice accumulate 3-hydroxyacylcarnitines which are a hallmark of human LCHADD (Table 2-1). This mouse expresses a stable TFP$\alpha$ protein, has decreased ketone bodies after fasting, a reduced ability to exercise, and cardiomyopathy. LCHADD patients also develop chorioretinopathy and peripheral neuropathy, phenotypes that are unique to LCHADD. This LCHAD-/- mouse model develops chorioretinopathy and potentially some neuropathy, highlighting that this mouse recapitulates common FAOD phenotypes as well as LCHADD-specific phenotypes.

*Primary systemic carnitine deficiency (SCD) mouse model:* The mouse model for SCD, also known as the juvenile visceral steatosis (jvs/jvs) mouse, is a C3H-H-2° mouse strain that had a spontaneous missense variant in the *Slc22a5* gene.[134,135] *Slc22a5* encodes for OCTN2, a carnitine transporter, and this specific mutation causes a L352R amino acid change and results in a loss of function.[135] Believed to be caused by an inability to reabsorb carnitine in the kidney[136], the jvs/jvs mouse has decreased serum carnitine and acylcarnitine levels, hepatic steatosis, lipid droplets in the kidneys, elevated serum ammonia levels, and cardiac hypertrophy.[134,136,137] After a 24-hour fast, jvs/jvs display a

decreased serum glucose level and decreased locomotor activity.[138-140] The heterozygous mice (jvs/+), while not as severe as jvs/jvs, also show decreased carnitine levels, increased lipid in the liver, and are potentially susceptible to cardiac hypertrophy and heart failure when subjected to pressure overload.[141-143]

*Acyl CoA dehydrogenase (ACAD9) deficiency mouse models:* ACAD9 deficiency is caused by mutations in the *ACAD9* gene which plays an essential role in the assembly of complex 1 of the respiratory chain. It may also still have a role in long-chain FAO. Whole body ACAD9 deficient mice have proven to be embryonic lethal; so, conditional heart and skeletal muscle-specific ACAD9 knockout strains (ACAD9-/-) were created by crossing a floxed *Acad9* mouse with Cre-expressing transgenic mice.[144] The cardiac specific ACAD9-/- mouse exhibited dramatic cardiomyopathy and reduced ejection fraction.[144] The skeletal muscle ACAD9-/- had an impaired exercise tolerance as seen as a reduced ability to hang in a hanging wire test along with higher lactate levels.[144]

*Pharmacologically inhibiting FAO in mice:* An alternative to genetically modified mouse models can be pharmacologic inhibition of the FAO pathway. There are many drugs that have been used to inhibit FAO by inhibiting specific proteins involved in FAO. For example, etomoxir and 2-tetradecylglycidate are common inhibitors of CPT1A/CPT1B and L-aminocarnitine can be used to inhibit CPT2.[145,146] Other enzymatic activities in the FAO pathway, such as 3-ketoacyl-CoA (3-KAT) and MCAD, can be inhibited using drugs such as trimetazidine and spiropentaneacetic acid.[147,148] Administration of these

inhibitors leads to an acute inhibition of FAO, which differs from the more chronic genetic models discussed in this review, and, therefore, is used to study more common diseases such as diabetes and obesity. In addition, the action of such inhibitors depends on their pharmacokinetic profile and therefore the degree of FAO deficiency may differ between tissues. Further analysis of FAO-inhibiting drugs and the mouse studies that have used them are beyond the scope of this review.

## Molecular Mechanisms of Phenotypes in FAOD Mouse Models

One benefit of using FAOD mouse models is the ability to study the molecular mechanisms involved in phenotypes. In this section we discuss potential molecular causes of prominent FAOD phenotypes including fasting-induced hypoglycemia, cardiomyopathy, and exercise intolerance, which have been studied using FAOD mouse models.

*Fasting-induced hypoglycemia:* During long periods of fasting, many FAOD mouse models have decreased serum glucose levels compared to WT, consistent with the development of hypoglycemia, and studies have suggested that increased systemic glucose catabolism with impaired gluconeogenesis and hepatic glucose output both contribute to hypoglycemia. Fasted CPT2L-/- mice have shown that the liver will attempt to mitigate the loss of FAO by upregulating whole-body catabolism to encourage compensation from other organs, such as the kidney. During a 24 hour fast, liver catabolic genes were upregulated in CPT2L-/- mice with increased circulating Fgf21, a hepatokine which increases systemic catabolism and depletes energy sources in

circulation.[89] Because FAOD models rely on glucose as the main source of energy, glucose in circulation would be rapidly oxidized by tissues and glycogen stores would be rapidly depleted.[111,112,122] Gluconeogenesis by the liver would then be crucial for maintaining euglycemia in circulation; however, there is evidence that suggests FAOD mouse models have an impaired gluconeogenesis. For example, Spiekerkoetter et al. reported impaired gluconeogenesis in VLCAD-/- mice in response to fasting and cold challenge.[112] Houten et al. further suggested using LCAD-/- mice that gluconeogenesis is impaired due to an impaired amino acid metabolism and decreased glucogenic precursors.[122] This was supported by proteomic data from Wang et al. taken from fasted VLCAD-/- mice.[149] Finally, in contrast to the previous LC-FAOD models, Martines et al. aimed to study how MCAD-/- mice were able to maintain blood glucose levels during fasting. Using transcriptomics data, they observed an increase in CoASH and NAD(P)(H) metabolism and increased levels of free CoA and NAD+. The increased levels stimulate more FAO flux of long-chain fatty acids, increases the glucogenic precursors, and lead to more gluconeogenesis and glucose output.[97] Increased LC-FAOD in MCAD mice might be protective during fasting but this is not the case in the CPT2L-/-, LCAD-/-, and VLCAD-/- models. While more evidence is needed to confirm these results, recent research provides preliminary evidence that an increased systemic glucose catabolism, rapid depletion of glycogen stores, and an impaired gluconeogenesis could be contributing to the fasting-induced decrease in glucose levels in FAOD mouse models. It is important to note that mice have been reported to have a higher average blood glucose level, deplete

glycogen stores faster, and have a greater reliance on gluconeogenesis than humans. This should therefore be considered when conducting fasting experiments.[1]

*Cardiomyopathy*: FAOD mouse models display cardiac phenotypes, such as cardiac hypertrophy[86,104,106,121,150], evidenced by increased left ventricular mass and decreased ejection fraction, and cardiac arrhythmias that can cause sudden death.[101,105,131] Therefore, these FAOD mouse models have been important for studying the molecular mechanisms involved in the cardiomyopathies. As seen from the CPT2M-/- mouse model, FAO is crucial for cardiac health and function and the loss of FAO is devastating for the heart.[87] One potential molecular cause of the cardiomyopathy in FAOD mice is that the heart has a chronic energy deficiency despite using significantly more glucose that WT mice.[106,151,120] A cardiac-specific VLCAD KO mouse model, which develops impaired cardiac function and cardiac abnormalities by 6-months of age, and VLCAD-/- mice have energy deficiencies in the heart.[106,151] Fasted LCAD-/- mice (fasting exacerbates the cardiac phenotype which is believed to be more severe than the cardiomyopathy in VLCAD-/- mice) were also shown to have a cardiac energy deficiency, observed as a decreased PCr/ATP ratio *in vivo*, despite having an increased uptake of glucose.[120] In fact, fasting worsens the cardiac function of both VLCAD-/- and LCAD-/- mice, suggesting that further limiting glucose decreases energy production and exacerbates the cardiomyopathy.[151,120] These studies suggest that FAOD cardiomyopathy can, at least in part, be due to the hearts inability to generate sufficient ATP even with an elevated reliance on glucose oxidation.

Another potential mechanism that could be contributing to the cardiomyopathy is lipotoxicity. Both VLCAD-/- and LCAD-/- mice have been shown to have increased lipid droplet levels and an accumulation of myocardial triglycerides in the heart that is exacerbated when fasted.[101,118,121,150] It is therefore possible that an accumulation of lipids and triglycerides could be contributing to the impaired cardiac function. This is correlative so more studies will need to address cardiac lipotoxicity.

Finally, secondary impairment of other metabolic pathways, such as amino acid metabolism, is another potential cause of the cardiomyopathy. Transcriptome analysis of fasted LCAD-/- hearts suggest that there is impaired protein translation due to a decrease in cardiac amino acid availability. This in turns activates and sustains the integrated stress response (ISR). These authors also observed a sustained ISR and impaired amino acid metabolism in the heart of CPT2M-/- mice. The authors hypothesize that the impaired amino acid metabolism alters cardiac metabolic signaling which could be playing a role in the cardiomyopathy seen in multiple FAODs[152]; however, more research will need to be done to establish causality.

Overall, FAOD mice have been and will continue to be crucial in studying the molecular mechanisms that contribute to cardiomyopathy seen in FAOD patients as well as finding treatments. Using a variety of FAOD mouse models will allow us to identify common and disorder-specific types of cardiomyopathy and any potential sex differences.[104]

*Exercise Intolerance:* While not as well studied as other phenotypes seen in FAOD patients, exercise intolerance with recurrent rhabdomyolysis is a prominent problem in patients; therefore, VLCAD and LCHADD mouse models have and will continue to be important mouse models for studying exercise intolerance. Both VLCAD-/- and LCHAD-/- mice are not able to run on a treadmill at a moderate pace as long as WT mice and reach $VO_2$ max or lactate threshold at a lower workload.[107,109] Research into the mechanisms behind the exercise intolerance is limited; however, studies suggest that the exercise intolerance in FAOD mice could be due to an energy deficiency in muscles even with an increased reliance on glucose. Alternatively, pathology in other tissues, such as the heart, could be limiting exercise. First, indirect calorimetry on exercised VLCAD-/- and LCHAD-/- mice have a significantly higher respiratory exchange quotient than WT mice[109] and VLCAD-/- muscle tissues have more glycolytic fiber types.[153,154] This suggests that there is a higher reliance on glucose especially during exercise. It is therefore possible that exercise intolerance could be due to the muscles not receiving enough energy because of the high reliance on glucose. On the other hand, it has also been shown that VLCAD-/- mice have an anaplerotic deficiency in the heart after a prolonged exercise.[109] This anaplerotic deficiency could limit energy production in the heart, and so it is possible the heart energy deficiency could also be contributing to exercise intolerance. Creating and exercising a striated muscle-specific[155,156] or a cardiac muscle-specific FAOD mouse model would contribute greatly to determining the heart's contribution to the exercise intolerance. Overall, research on the exercise intolerance in FAOD mouse models is very limited, so more research is needed to understand more of the

mechanisms behind this phenotype. Specifically, more research will need to address if exercise intolerance or exhaustion is related to rhabdomyolysis in human patients. Having multiple FAOD mouse models to study the exercise intolerance could provide crucial insight into why patients with FAODs develop rhabdomyolysis and how to prevent it.

*CoA sequestration, toxicity, and redistribution (CASTOR):* It has been proposed that the phenotypes seen in patients with FAODs, as well as some other inborn errors of metabolism, are due to an accumulation of acyl-CoA and/or a decreased availability of CoASH.[157,158] It is hypothesized that the reduction in CoASH can directly impact metabolism because it is a crucial substrate and an important regulator in many metabolic reactions. It is also possible that the accumulation of excess acyl-CoA is toxic. It has been shown that inducing CoA deficiency in mice does cause a fatty liver and death due to hypoglycemia, symptoms seen in FAODs; however, because of the difficulty in measuring acyl-CoAs and CoASH levels in tissues, evidence of CASTOR in FAODs is limited.[159] Computational modeling of MCAD, in human fibroblasts and mice, predicted decreased CoASH concentrations, but this has yet to be confirmed in FAOD mouse models.[160,161]

## Uses of FAOD Mouse Models

Mouse models are also a critical model for preclinical research and can help direct treatment for patients. In this section we will discuss how FAOD mouse models

have been used to study the effects of carnitine supplementation and other potential treatments, in the forms of both dietary recommendations and gene addition.

*Carnitine Supplementation:* Carnitine is crucial for energy homeostasis, as indicated by the jvs/jvs mouse, and carnitine supplementation has been shown to be beneficial in this particular mouse model.[140,162,163] Secondary carnitine deficiency is commonly observed in FAOD patients; however, the use of carnitine supplements in human patients is controversial. Mouse models may provide more insight on the role of carnitine in FAODs and potentially provide some insight to determine if carnitine supplements are needed.

The effects of a secondary carnitine deficiency have been recently studied in a LCAD-/- mouse model that had a defective *Slc22a5*, a carnitine transporter responsible for tissue carnitine uptake (LCAD-/-/Slc22a5$^{jvs/+}$). By creating a LCAD-/-/ Slc22a5$^{jvs/+}$, Ranea-Robles et al. genetically reduced carnitine availability. They found that the carnitine and acylcarnitine levels in plasma and tissue were decreased in LCAD-/-/Slc22a5$^{jvs/+}$ mice when compared to LCAD-/- mice, suggesting that decreased carnitine levels limit the acylcarnitine concentrations. Even though carnitine levels were lowered, phenotypes, such as fasting-induced hypoglycemia and cardiac hypertrophy, were not changed in the LCAD-/-/Slc22a5$^{jvs/+}$ compared to LCAD-/-. This suggests that a carnitine deficiency may not play a major role in the pathophysiology and does not aggravate the LCAD-/- mouse phenotype.[164]

Part of the controversy with carnitine supplementations is the risk of increasing acylcarnitine levels. VLCAD-/- mice supplemented with carnitine have increased acylcarnitine levels in muscle, which are potentially toxic to cells, yet it doesn't prevent a decrease in free carnitine levels in muscle after exercise.[165] This could indicate the carnitine supplementation is not beneficial for patients with a FAOD. On the other hand, Bakermans et al. conducted a longitudinal study in LCAD-/- and WT mice that were supplemented with carnitine. They found that while the acylcarnitines were raised in LCAD-/- mice supplemented with carnitine compared to no supplementation, the carnitine supplementation attenuated the myocardial lipotoxicity and did not worsen the cardiac hypertrophy and performance in LCAD-/- mice.[121] This suggests that carnitine supplementation can alleviate lipid overload in FAOD hearts. These studies highlight that the consequences of carnitine supplementation are complicated, and more research is needed with FAOD mouse models to enhance our understanding.

Overall, these mouse models have been important in analyzing carnitine levels, how they contribute to the phenotype of FAOD patients, and the consequences of altering them. Studying the effects of carnitine have also presented interesting questions about the toxicity of long chain acylcarnitine accumulation[121,164,165] and using other FAOD mouse models will be useful in determining how carnitine and acylcarnitine levels impact FAOD phenotypes.

*Dietary Treatments:* Patients with long-chain FAODs are typically prescribed a low-fat diet and supplementation of either medium-chain triglycerides (MCT) or triheptanoin,

an odd-chain medium fatty acid. FAOD mouse models have been crucial in studying the effects of the different dietary treatments and supplementations.

First, long-chain FAOD mouse models were used to show that a high-carbohydrate diet alone is not sufficient in providing energy especially during times of metabolic stress and that supplementation is important for providing energy. Schuler et al. showed that serum glucose levels were not predictive of survivability in a cold challenge for LCAD-/- mice and treating LCAD-/- mice with glucose prior to a cold challenge did not make the mice cold tolerant. This indicated that just raising the glucose levels was not sufficient to prevent metabolic decompensation.[166] Tucci et al. reported that VLCAD-/- mice fed a low-fat, carbohydrate-rich diet still show signs of pronounced energy deficiency at rest[167] and the diet treatment cannot prevent the exercise intolerance.[168] These studies suggest that just maintaining a long-term low-fat, high-carbohydrate diet does not mitigate fasting and exercise-induced phenotypes. Another source of energy is potentially needed.

Patients with long-chain FAODs supplement their diet with either MCT or triheptanoin, and FAOD mouse models have shown that both supplementations can improve responses during times of catabolism. For example, VLCAD-/- mice have been used to show that they are able to run longer on a treadmill when on a diet supplemented with MCT or triheptanoin[169,109], and LCAD-/- mice on an MCT diet were more tolerant when exposed to the cold.[166]

While these supplementations have been shown to be beneficial, research has also shown that MCT has potential negative effects in the long-chain FAOD mouse

models. First, it has been shown that chronic intake of medium-chain fatty acids stimulates genes involved in de novo fatty acid biosynthesis and elongation.[170] It is possible that the elongation of the medium-chain fatty acids to long-chain fatty acids can contribute to the accumulation of lipids, induce lipotoxicity, and exacerbate the hepatopathy and cardiomyopathy.[113,171,106] A chronic MCT diet has also been shown to prevent tissue-specific metabolic adaptations.[154] For example, white skeletal muscle in VLCAD-/- mice fed a chronic MCT diet did not have the shift toward glycolytic muscle fibers that a VLCAD-/- mouse on normal chow undergoes.[153] It is important to note that the negative effects seen in the FAOD mouse models could be a species-specific response to the MCT or triheptanoin supplementations. Regardless, the long-chain FAOD mouse models have and will continue to be useful in investigating effects of dietary treatments for FAOD patients. This includes when and how supplements should be taken[169] and if there are any sex-specific differences.[172-174]

*Gene Therapy:* Gene addition is an enticing treatment for patients with FAODs and FAOD mouse models have already been used to conduct pre-clinical trial research. Gene addition therapy has been shown to be effective in multiple FAOD mouse models and correcting many different symptoms. The most studied FAOD mouse model used for gene addition treatments has been the VLCAD-/- model. These studies have shown that systemic administration of recombinant adeno-associated virus 8 (rAAV8) or rAAV9 that express human *VLCAD* is able to transfect the heart, liver, and skeletal muscles and had positive effects up to 20 weeks post-injection.[175,176] Specifically, acylcarnitine levels and

lipid content were decreased in the serum, liver, heart, and skeletal muscles in treated animals, glucose levels were maintained when fasted, treated mice had increased survival when cold challenged, and respiratory insufficiency following fasting and exercise intolerance were ameliorated.[175,176] An intravenous injection of a lipid nanoparticle encasing a human VLCAD mRNA transfected the VLCAD-/- mouse liver without causing extra inflammation, decreased serum acylcarnitine levels, increased the tolerance to cold exposure, and decreased lipid accumulation in the liver.[177] Other mouse models, such as MCAD-/-, SCAD-/- and LCAD+/- mice, have been used to study gene addition treatments and have shown improvements, such as improved cold-tolerance, decreased acylcarnitines, and decreased lipid accumulation.[178-181] While more research needs to be done to see the effect of gene therapy in preventing metabolic decompensation when the mouse is stressed and include studies in more severe mouse models, the FAOD mouse models have been used to provide promising evidence that gene therapy may prove a beneficial treatment approach for FAOD patients.

## Conclusion

Mouse models have been crucial for studying different FAODs and potential treatments for patients with these disorders. These mouse models have shown to recapitulate many phenotypes seen in patients with different FAODs and have provided insights into the molecular mechanisms that cause these phenotypes. A major limitation of mouse models is that the responses or molecular mechanisms studied in the mouse may not be the same in humans due to the inherent genetic and physiological differences. This is exemplified by the functional overlap in VLCAD and LCAD in mice but

not humans, phenotypes presenting in mice but not humans with SCADD, and the neonatal lethality of some of the FAOD mouse models, such as TFP$\alpha$-/- and Cpt1 mouse models. Therefore, it is important to note both the genetic and biochemical differences between the FAO mouse models and human patients (Box 2-1). Negative effects of an MCT/triheptanoin and sex-specific differences have also been noted in FAOD mouse models but not human. This could be a mouse-specific response, or it could be that these side effects have not been identified in humans because of the small number of patients. To answer this question, more research into effects of MCT/triheptanoin and sex-specific differences in mice will need to be studied as well as more attention will need to be directed toward these questions in clinical research. While FAOD mouse models are not perfect, they have been and will continue to be crucial in understanding more about FAODs, trialing and advancing new treatments, and bringing attention to potential consequences that are unanticipated prior to testing potential treatment approaches in human patients with a FAOD.

## Funding

This study was funded by generous support from the Scully-Peterson foundation and the National Eye Institute (R01EY032889).

## Disclosure Statement

The authors have nothing to disclose.

Figures

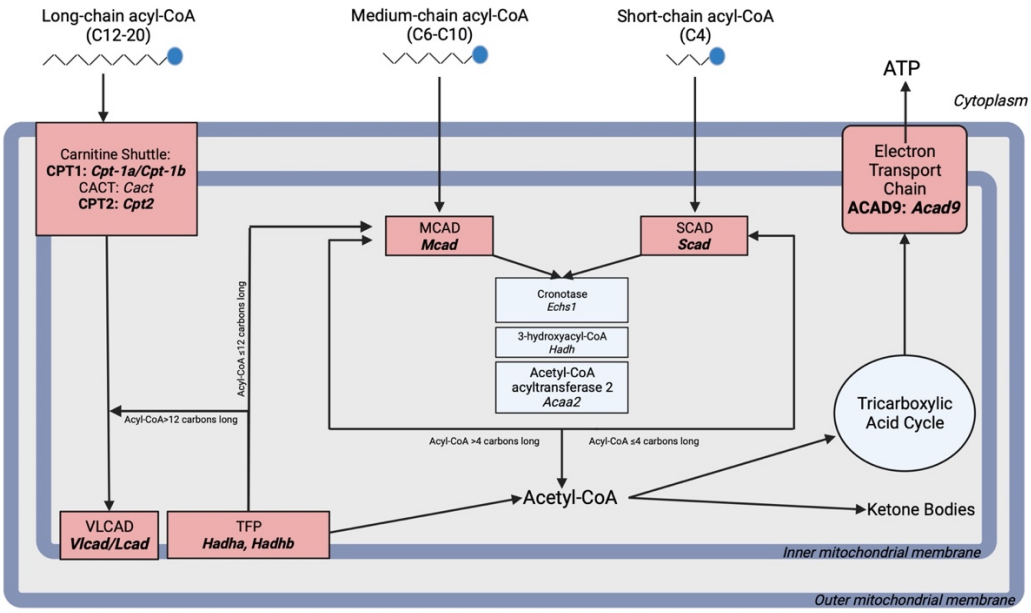


**Figure 2-1: Pathways of fatty acid oxidation**. Proteins highlighted in red indicate the fatty acid oxidation disorders that have a mouse model associated, and bolded genes indicate the genes that when mutated cause those fatty acid oxidation disorders. CPT= carnitine palmitoyltransferase; CACT= carnitine-acylcarnitine translocase; VLCAD= very long-chain acyl-CoA dehydrogenase; TFP= mitochondrial trifunctional protein; MCAD= medium-chain acyl-CoA A dehydrogenase; SCAD= short-chain acyl-CoA dehydrogenase. Figure was created in Biorender.com

## Table 2-1: Serum acylcarnitine changes in human FAOD vs mouse model

| Human Disorder | Changed Serum Acylcarnitines[18] | | Mouse Model | Changed Serum Acylcarnitines | |
|---|---|---|---|---|---|
| | Increased | Decreased | | Increased | Decreased |
| CPT1D | C0, **C0/(C16+C18) ratio** | C16, C18, C18:1, C18:2, **(C16+C18:1)/2** ratio | CPT1a-/- | - | - |
| - | - | - | CTP1b-/- | - | Decreased C16 and C18 in females[83] |
| CPT2D | **C16, C16:1, C18, C18:1, C18:2** | C2 | CPT2A-/- | - | C2, C4, and C5 in white adipose tissue[85] |
| | | | CPT2M-/- | Increased C16:0, C16:1, C18:0, and C18:1, C18:2, C20, C20:1 in heart tissue[86,87] | - |
| | | | CPT2L-/- | - | - |
| SCADD | **C4** | No decreases | SCAD-/- | - | - |
| MCADD | **C8**, C10, C10:1 | C2 | MCAD-/- | C6, C8, C10, C10:1[95] | - |
| VLCADD | C12, C12:1, **C14, C14:1, C14:2,** C16, C16:1, C18, C18:1, C18:2 | No decreases | VLCAD-/- | C14, **C16, C18, C18:1**[98,102] | - |
| | | | LCAD-/- | C10, C12, C12:1, **C14, C14:1, C14:2,** C16, C16:1, C18:1, C18[98,118,119] | C3, C4, C5[119] |
| TFPD | C14, C14:1, C14:2, **C16-OH,** C16:1, **C16:1-OH**, C18-OH, C18:1-OH, C18:2-OH | No decreases | TFP$\alpha$-/- | C14, C16, C16-OH, C16:1, C16:1-OH, C18:1, C18:2[127] | - |
| | | | TFP$\beta$-/- | C12-OH, C14-OH, **C16-OH**, C16:1, C16:1-OH, C18, **C18-OH**, C18:1, **C18:1-OH**[131] | - |
| LCHADD | C14, C14-OH, C14:1, C14:1-OH, C14:2, **C16-OH**, C16:1, **C16:1-OH**, C18, **C18-OH,** C18:1, **C18:1-OH,** C18:2, **C18:2-OH** | No decreases | LCHAD-/- | C16-OH, C18:1, C18-OH, C18:1-OH | - |
| PSCD | - | Decreased carnitine (C0) and total acylcarnitines[182] | Jvs/jvs | - | Decreased C0 and acylcarnitines[136] |

- More relevant abnormalities in bold

**Table 2-2: Mouse model phenotypes**

| Mouse Model | Viability/Fecundity | Glucose/Ketone Levels after Fasting | Exercise Intolerance | Cold Intolerance | Cardiomyopathy |
|---|---|---|---|---|---|
| CPT1a-/- | Embryonic Lethal[81] | Decreased Glucose after 24 hrs (Het)[81] | - | Normal (Het)[81] | - |
| CPT1b-/- | Embryonic Lethal[83] | Normal[83] | - | Yes[83] | - |
| CPT2A-/- | Normal[85] | - | - | Yes[85] | - |
| CPT2M-/- | Normal[86] | - | - | - | Fibrosis-free cardiac hypertrophy[86] |
| CPT2L-/- | Normal[89] | Normal Glucose; Decrease Ketones after 24 hrs[89] | | | |
| SCAD-/- | Normal[91] | Decreased Glucose after 18 hrs[91] | - | Yes[94] | Enlarged heart[93] |
| MCAD-/- | Decreased viability[95] | Normal[95-97] | - | Yes[95] | - |
| VLCAD-/- | Normal[98,101] | Normal[111-113] | Yes[107-109] | Yes[110-112] | Arrhythmia susceptibility[101]<br>Cardiac hypertrophy[104,106]<br>Longer QTc interval[105] |
| LCAD-/- | Decreased fecundity[98] | Decreased Glucose after 6 hrs[122] | - | Yes[110] | Cardiac hypertrophy[104,120,121,150] |
| TFPα-/- | Neonatal death[127] | Normal (Het)[129] | - | - | - |
| TFPβ-/- | Normal[131] | Decreased Glucose after 24 hrs[131] | - | - | Cardiac arrhythmias from prolonged PR interval which leads to complete atrio-ventricular dissociation and sudden death[131] |
| LCHAD-/- | Decreased fecundity[133] | Decreased Ketones after 6 hrs[133] | Yes[133] | - | Cardiac hypertrophy[133] |
| Jvs/jvs | - | Decreased[138-140] | - | - | Cardiac hypertrophy[137] |

- Hypertrophy is indicative of increased LV mass and decreased ejection fraction

**Box 2-1: Benefits and limitations of FAOD mouse models**

-

## Box 1: Benefits and Limitations of FAOD Mouse Models

Benefits of FAOD Mouse Models:

- Mice are physiologically similar to humans. Specifically, FAOD mouse models are biochemically similar and exhibit similar phenotypes to patients with the corresponding FAOD.
- Mice can be used to study the influence of diet and environment. FAOD mice can be used to evaluate potential treatments such as diet management and gene therapy.
- Mice can be precisely genetically manipulated so that specific variants, such as the LCHADD G1528C pathogenic variant, can be studied.
- Mice have a short reproductive cycle and lifespan.

Limitations of FAOD Mouse Models:

- Mouse models are genetically homogenous, so patient heterogeneity, such as in phenotype severity and disease-causing variants, is not well modelled.
- Differences in pathways may exist. For example, LCAD is important in long-chain FAO in mice but not humans.
- Sex-specific differences have been reported in FAOD mice but not patients.
- Mice have a higher average blood glucose level, deplete glycogen stores faster, and have a greater reliance on gluconeogenesis than humans.[1] This could affect the translatability of fasting and insulin-sensitivity experiments.

# Chapter 3 : A G1528C *Hadha* knock-in mouse model recapitulates aspects of human clinical phenotypes for long-chain 3-hydroxyacyl-CoA dehydrogenase deficiency

**A G1528C *Hadha* knock-in mouse model recapitulates aspects of human clinical phenotypes for long-chain 3-hydroxyacyl-CoA dehydrogenase deficiency**

Garen Gaston[1]; Shannon J. Babcock[1]; Renee Ryals[1,2]; Gabriela Elizondo[1]; Tiffany DeVine[1]; Dahlia Wafai[2]; William Packwood[3]; Sarah Holden[4]; Jacob Raber[3,4,5]; Jonathan R. Lindner[3#]; Mark E. Pennesi[2]; Cary O. Harding[1]; Melanie B. Gillingham[1*]

[1]Department of Molecular and Medical Genetics Oregon Health and Science University, Portland, Oregon, USA, [2]Casey Eye Institute Oregon Health and Science University, Portland, Oregon, USA, [3]Knight Cardiovascular Institute Oregon Health and Science University, Portland, Oregon, USA, [4]Department of Behavioral Neuroscience Oregon Health and Science University, Portland, Oregon, USA, [5]Departments of Neurology and Radiation Medicine Oregon Health and Science University, Portland, Oregon, USA, Division of Neuroscience, Oregon National Primate Research Center (ONPRC), Oregon Health and Science University, Portland, Oregon, USA

# Present address: Cardiovascular Division, University of Virginia Medical Center, Charlottesville, VA.

*Published in: Communications Biol. Aug 2023; 6(1):890*

## Author Contributions

GG helped with the design of mouse model, organized breeding of mice, conducted western blots, fasting and exercise experiments, worked on data analysis and assisted with writing the manuscript. **SB conducted RT-qPCR, metabolic flux studies, and assisted with manuscript writing.** GE assisted with mouse colony management, genotyping, data analysis and manuscript writing. TD assisted with genotyping, western blots, data analysis and manuscript writing. RR conducted visual acuity and retinal testing, and data analysis of the retinal phenotype. DW conducted visual testing and retinal testing. MEP helped designed and coordinate retinal experiments, and data analysis. WP conducted echocardiography. JRL analyzed echocardiography results and data analysis and assisted with manuscript writing. SH conducted the behavior testing. JR and SH analyzed the behavioral data and related data analyses. JR assisted with the manuscript writing. COH helped with the design of the mouse model, and overall study design and assisted with manuscript writing. MBG designed the overall project, conducted data analysis and drafted the manuscript. All authors read, edited, and approved the manuscript.

## Abstract

Long chain 3-hydroxyacyl-CoA dehydrogenase deficiency (LCHADD) is a fatty acid oxidation disorder (FAOD) caused by a pathogenic variant, c.1528G>C, in *HADHA* encoding the alpha subunit of trifunctional protein (TFP$\alpha$). Individuals with LCHADD develop chorioretinopathy and peripheral neuropathy not observed in other FAODs in addition to the more ubiquitous symptoms of hypoketotic hypoglycemia,

rhabdomyolysis, and cardiomyopathy. We report a CRISPR/Cas9 generated knock-in murine model of G1528C in *Hadha* that recapitulates aspects of the human LCHADD phenotype. Homozygous pups are less numerous than expected from Mendelian probability, but survivors exhibit similar viability with wildtype (WT) littermates. Tissues of LCHADD homozygotes express TFP$\alpha$ protein, but LCHADD mice oxidize less fat and accumulate plasma 3-hydroxyacylcarnitines compared to WT mice. LCHADD mice exhibit lower ketones with fasting, exhaust earlier during treadmill exercise and develop a dilated cardiomyopathy compared to WT mice. In addition, LCHADD mice exhibit decreased visual performance, decreased cone function, and disruption of retinal pigment epithelium. Neurological function is affected, with impaired motor function during wire hang test and reduced open field activity. The G1528C knock-in mouse exhibits a phenotype similar to that observed in human patients; this model will be useful to explore pathophysiology and treatments for LCHADD in the future.

## Introduction

Long-chain 3-hydroxyacyl CoA dehydrogenase deficiency (LCHADD, OMIM# 609016) is a rare, recessively inherited disorder of fatty acid oxidation (FAO) caused by the presence of a common pathogenic variant, c.1528G>C, in at least one allele of the *HADHA* gene.[183,184] *HADHA* encodes the alpha subunit of mitochondrial trifunctional protein (TFP$\alpha$) that together with the beta subunit (TFP$\beta$), encoded by *HADHB*, form a heterotetrameric multi-functional complex catalyzing the last three steps in mitochondrial long-chain fatty acid $\beta$-oxidation: long-chain enoyl CoA hydratase, long-chain 3-hydroxyacyl CoA dehydrogenase (LCHAD) and long-chain ketothiolase (Supplementary Figure 1a).[185] The common LCHADD pathogenic variant results in a glutamic acid to glutamine amino acid change (E510Q) in the LCHAD active site of TFP$\alpha$ reducing its activity but leaving the other two enzymatic activities relatively intact.[183] The biochemical consequence is reduced FAO capacity with activation of alternate energy metabolism pathways and the accumulation of partially oxidized plasma 3-hydroxy-acylcarnitines. In contrast, global trifunctional protein deficiency (TFPD, OMIM #609015) is caused by other less common variants in either the *HADHA* or *HADHB* genes that lead to decreased protein stability and loss of all three enzymatic functions.[29] Similar to other long-chain FAO disorders, humans with LCHADD or TFPD frequently present in infancy with hypoketotic hypoglycemia, liver dysfunction, and dilated cardiomyopathy, but then develop recurrent rhabdomyolysis later in life.[186] However, several disease complications are unique to disorders impacting mitochondrial TFP activity including peripheral axonal sensorimotor neuropathy and a progressive retinopathy with vision loss. Patients with LCHADD and TFPD have similar peripheral

neuropathy characterized by relatively ubiquitous infantile or childhood loss of peripheral deep tendon reflexes with variable progression to foot drop, numbness, muscle weakness and loss of mobility that waxes and wanes over time.[187,188] In contrast, retinopathy, characterized by a steady decline in visual acuity, increased myopia, and progressive atrophy of the outer retina with choriocapillaris loss, appears to progress more rapidly in patients with LCHADD.[54]

Multiple knockout mouse models have been created for studying FAO disorders; however, a viable mouse model that recapitulates LCHADD did not exist. Two prior TFPα knockout models resulted in neonatal lethality in homozygous pups.[132,189] Because there has not been a mouse model that successfully recapitulates the human disorder, we sought to use CRISPR/Cas9 gene editing technology to introduce the common LCHADD pathogenic variant into mouse embryos and create a model that could be used to study LCHADD *in vivo*. Here we report a LCHADD mouse that exhibits features of the human disorder including impaired fatty acid oxidation, accumulation of 3-hydroxy-acylcarnitines, low fasting ketone concentrations, impaired motor function, exercise intolerance, and dilated cardiomyopathy. They also develop a retinal phenotype with decreased visual performance.

## Results

### *Generation of G1528C LCHADD mice*

Similar to humans, the murine c.1528G nucleotide is located in *Hadha* on exon 15 and in the same codon position of amino acid 510, which is in a stretch highly conserved at the amino acid level. Using the CRISPR/Cas9 system, the c.1528G to C (GAA to CAA)

mutation was introduced into exon 15 by homology-directed repair in fertilized C57Bl/6J embryos, and a silent mutation (ACC to ACG) was introduced to the PAM sequence to prevent the binding and re-cutting of the edited allele by the Cas9 system post-repair (Figure 3-1:a). The G1528C sequence results in a glutamic acid to glutamine amino acid change (E510Q) in the LCHAD active site of the protein identical to that observed in human patients with LCHADD (Supplementary Figure 1b). Embryos treated with editing reagents were implanted into pseudo-pregnant females and allowed to develop to term. Progeny were then screened for the presence of the c.1528G>C variant by allele-specific polymerase chain reaction (PCR) on tail biopsy DNA to detect heterozygotes. Homozygous mice were then generated by mating heterozygous breeding pairs. The line was further propagated by mating LCHADD homozygous males with heterozygous females. Week old homozygous mouse pups were identified at ~50% lower frequency than expected regardless of breeding approach, suggesting reduced LCHADD mouse pup viability similar to observations in the long-chain acyl-CoA dehydrogenase (LCAD) knockout mouse (Table 3-1).[190,191] However, after weaning, surviving homozygous LCHADD mice grew normally with similar body and liver weights to wild-type (WT) littermates (Supplementary Figure 2a & b). Hereafter, the terminology LCHADD mice will refer to mice homozygous for the *Hadha* c.1528G>C allele.

Normal levels of TFP$\alpha$ have been detected in fibroblasts of human patients homozygous for c.1528G>C so we anticipated normal protein expression in LCHADD mouse tissues.[29,183] We analyzed heart and liver tissue for protein levels of TFP$\alpha$, TFP$\beta$ and very long-chain acyl-CoA dehydrogenase (VLCAD), the FAO pathway enzyme

immediately proximal to mitochondrial trifunctional protein. Protein bands were normalized to GAPDH and compared between genotypes by sex. Similar levels of TFP$\alpha$, TFP$\beta$ and VLCAD protein were detected in heart of male and female WT and LCHADD mice (Figure 3-1:b & c, Supplementary Figure 6). VLCAD protein in liver was similar between genotypes. However, TFP$\alpha$ and TFP$\beta$ was reduced in male and female LCHADD liver compared to sex-matched WT liver (Figure 3-1:b & c, Supplementary Figure 6). To determine if decreased protein levels were related to decreased mRNA levels, we analyzed gene expression of *Hadha* and *Hadhb* by reverse transcription-quantitative PCR (RT-qPCR). We found similar *Hadha* and *Hadhb* mRNA expression in both heart and liver of male and female LCHADD and WT mice (Figure 3-1:d, Supplementary Figure 3-2:c). Decreased TFP$\alpha$ and TFP$\beta$ protein levels but similar gene expression in liver of LCHADD mice suggests decreased protein stability and/or increased turnover of TFP$\alpha$/TFP$\beta$ in the liver.

To determine the impact of the G1528C mutation on FAO in tissues, palmitate oxidation studies were performed on liver and cardiac tissue. Fresh tissue homogenates were incubated with $^{14}$C-palmitate for 30 minutes then measurements were taken for the radiolabeled carbon dioxide ($^{14}CO_2$) production and residual radioactivity in acid soluble products. Both liver and cardiac tissue exhibited lower metabolized $^{14}$C compared to those seen in liver and cardiac tissue of WT mice (Figure 3-1:e). Palmitate oxidation was approximately 60% of WT suggesting reduced but not absent FAO capacity. A 60% residual palmitate oxidation seems relatively high for LCHADD. However, our assay measures total metabolized $^{14}$C including $\beta$-oxidation in the

peroxisome and $w$-oxidation in microsomes. Peroxisomal oxidation may compensate for lower mitochondrial oxidation in tissues with impaired mitochondrial $\beta$-oxidation and may explain higher than anticipated tissue palmitate oxidation.[110] Regardless, total metabolized $^{14}C$ was significantly lower in the LCHADD tissues compared to WT mice.

*Male LCHADD mice oxidize less fat and more glucose than WT mice*

Indirect calorimetry was used to determine whole body substrate oxidation. The volumes of consumed oxygen and released carbon dioxide were analyzed in individual mice in a Columbus Oxymax chamber and the data was analyzed in CalR software.[192] Male LCHADD mice had a higher respiratory exchange ratio (RER; $VCO_2/VO_2$) than WT mice during the dark period when mice are most active, suggesting increased glucose metabolism and decreased fat oxidation (Figure 3-2:a & b). This was due to higher $VCO_2$ during dark hours while the $VO_2$ was not different (Supplementary Figure 3). RER was not different between female LCHADD and WT mice (Figure 3-2:c & d; Supplementary Figure 3).

Patients with LCHADD accumulate partially oxidized long-chain 3-hydroxy-acylcarnitines in blood that is a biochemical marker for LCHADD. We measured plasma 3-hydroxy-acylcarnitines in blood from fasted LCHADD and WT mice by LC-MS/MS and found significantly higher long-chain 3-hydroxy-acylcarnitine species in blood from LCHADD male (Figure 3-2:e) and female mice (Figure 3-2:f); similar to levels observed in human patients **(**C16:1OH mean=0.13 and C18:1OH mean =0.86 $\mu mol/L$).[193] Higher RER and elevated long-chain 3-hydroxy-acylcarnitines suggest decreased whole body FAO with the accumulation of partially oxidized fatty acids similar to humans with LCHADD.

*LCHADD mutant mice exhibit lower ketone concentrations with fasting and impaired exercise tolerance*

Other mouse models of FAO disorders develop fasting-induced low blood glucose, and low ketones with or without the additional stress of a cold challenge.[51] We measured blood glucose and ketone concentrations in LCHADD and WT mice during an 18-hour fast at room temperature. Serum glucose decreased with fasting in both groups over time (Figure 3-3:a). The 2-way ANOVA indicated an overall genotype effect suggesting LCHADD male and female mice had slightly lower serum glucose compared to WT male and female mice but post-hoc comparisons only observed a significant difference between LCHADD and WT females after 6 hours of fasting (Figure 3-3:a). Total blood ketone concentrations increased with fasting in both groups over time, but ketones were significantly lower in LCHADD male and female mice compared to WT mice (Figure 3-3:b). Overall, LCHADD mice exhibited hypoketosis with fasting compared to WT mice.

Previous FAO disorder mouse models also exhibited reduced exercise capacity during a moderate intensity exercise test and lower $VO_2$ max during maximal exercise.[109] Time to exhaustion with moderate intensity exercise was assessed and LCHADD mice exhausted much earlier than WT mice (Figure 3-3:c). During $VO_2$ max testing, LCHADD mice reached or neared lactate threshold, as indicated by a respiratory exchange ratio (RER) of >1.0, at 11 meters/min while WT mice never attained an RER above 0.9 (Figure 3-3:d). During the same $VO_2$ max exercise test, LCHADD mice achieved maximal $VO_2$

consumption at 5 to 7 meters/min that then decreased at higher treadmill speeds (Figure 3-3:e); maximal $VO_2$ was significantly lower in LCHADD mice in comparison to WT mice at 9 and 11 meters/min. This data indicates LCHADD mice experience decreased $VO_2$ max and impaired exercise tolerance as compared to WT littermates.

*Evidence of cardiomyopathy in LCHADD mutant mice*

Because dilated cardiomyopathy with systolic dysfunction is a common phenotype in human LCHADD patients, heart function was assessed. Two-dimensional and Doppler echocardiography was performed on 12- to 15-month-old mice to assess left ventricular (LV) dimensions and function. Male and female LCHADD mice had lower ejection fraction associated with lower cardiac output and stroke volume (Figure 3-4:a, b, & c), and increased left ventricular wall mass (Figure 3-4:d) compared to male and female WT mice. To support this finding, we observed an increase in heart tissue weight (Figure 3-4:e) and heart-to-body weight ratio (Figure 3-4:f) among LCHADD males and females compared to WT males and females. This suggests eccentric hypertrophy with a dilated cardiomyopathy phenotype. The cardiac dilation in our LCHADD mouse model may be related to our observed impaired exercise tolerance. Similar cardiac phenotypes have been observed in other related mouse models of FAO disorders.[194,195]

*Neurological assessment of LCHADD mutant mice*

Because peripheral neuropathy is a phenotype in human LCHADD patients, a panel of neurological function tests was performed on 13-month-old mice. LCHADD male and female mice showed decreased wire hang fall and reach scores (Figure 3-5:a &

b), indicating impaired motor function. LCHADD male and female mice also showed a non-significant trend for lower activity levels (Figure 3-5:c) and decreased time spent (Figure 3-5:d) in the center in an open field study, suggesting increased anxiety levels. In contrast to the wire hang test, there was no genotype difference in rotarod performance or grip strength (Supplementary Figure 4). Decreased motor function may also contribute to impaired exercise tolerance in LCHADD mice. Conversely, early exhaustion may contribute to changes observed in wire hang tests.

*Retinal phenotype of LCHADD mutant mice*

Because LCHADD patients develop a unique chorioretinopathy, we assessed retinal function in our LCHADD mouse. Visual parameters were tested in LCHADD and WT littermates of mixed sex at 1 year of age. Upon evaluating visual performance with optokinetic tracking (OKT) and retinal function with electroretinograms (ERG), LCHADD mice had significantly lower spatial frequency thresholds (Figure 3-6:a) and photopic b-wave amplitudes (52% reduction; Figure 3-6:b). As these two tests were evaluated in light-adapted conditions, these reduced responses indicate that cone mediated function is disrupted. Scotopic b-wave amplitudes, used to assess rod-mediated function, were not different (Supplementary Figure 3-5:a). However, scotopic c-waves, specifically measuring retinal pigment epithelium (RPE) function, were significantly reduced by 32% in LCHADD mice compared to WT mice (Figure 3-6:c) indicating RPE dysfunction. RPE degeneration was observed on fundus images as white or hypopigmented spots. When grading fundus images for presence or absence of these areas, 53% of LCHADD eyes evaluated had hypopigmented areas present. There were no hypopigmented areas

observed in WT eyes (Figure 3-6:d, arrowheads). H&E staining of retinal cross sections revealed numerous large areas of RPE disruption in LCHADD mice (Figure 3-6:e, red arrows). H&E cross sections were scored based on the percentage of RPE containing these areas of RPE loss or disruption (range from 0-100%). Some areas were observed in WT mice but LCHADD had a significantly higher percentage of RPE containing visibly disrupted areas (80% in LCHADD compared to 40% in WT) suggesting greater RPE disruption (Figure 3-6:e). The nature of the RPE disruption is currently unknown but does not appear to be lipid deposits based on oil-red-O staining of retinal cross-sections. The RPE loss may be indicative of immune infiltration, or dead cells as previously reported in human eyes.[196] There was no difference in the RPE or retinal thickness on spectral domain-optical coherence tomography (SD-OCT) images suggesting normal retinal structure (Supplementary Figure 3-5:b). Overall, LCHADD mice display visual performance decline and retinal dysfunction with specific evidence of RPE damage.

Figures

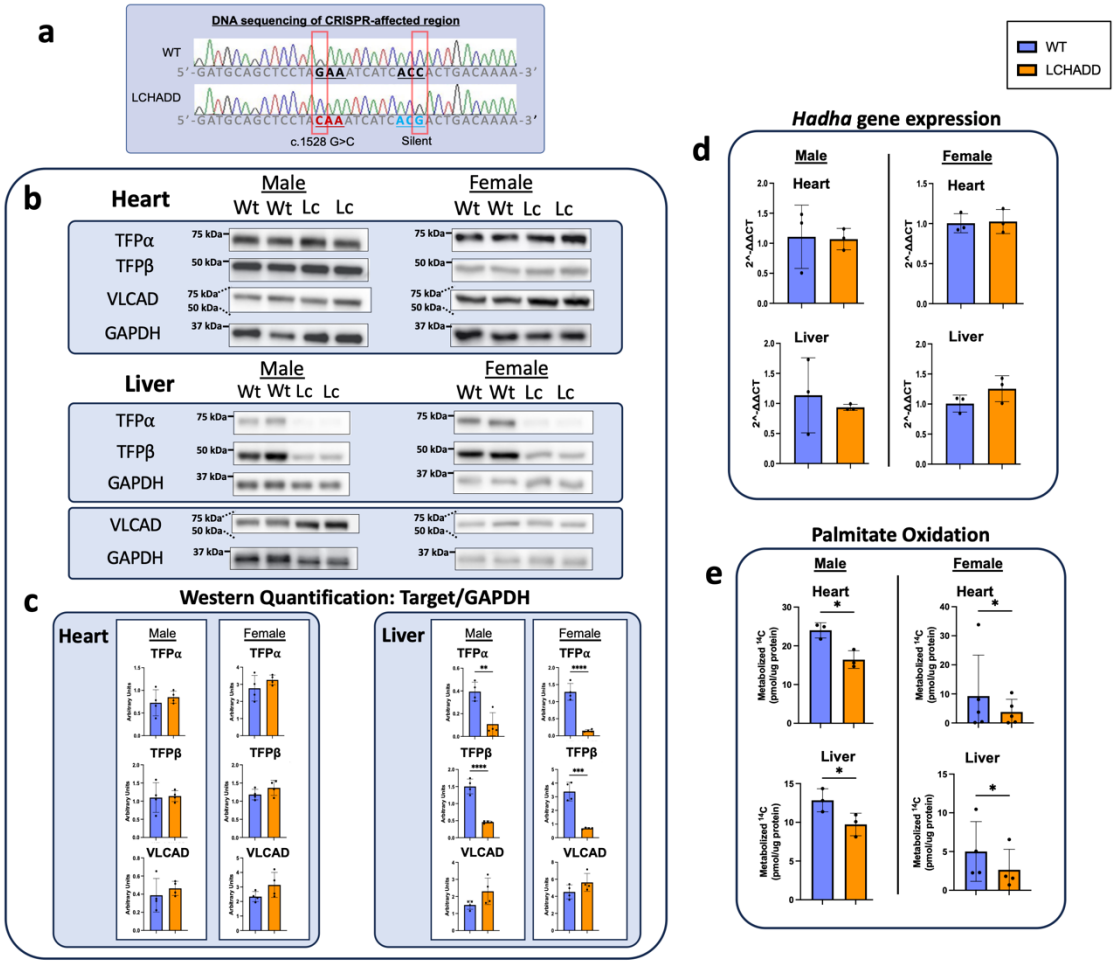


**Figure 3-1: Biochemical analysis of LCHADD mutant mouse.** The G1528C mutation and a silent mutation were introduced to C57Bl/J6 mice by CRISPR-Cas9 to model human LCHADD. (a) Sanger sequencing of a small region of exon 15 of *Hadha* in WT or G1528C mice. Red boxes represent CRISPR/Cas9 edited nucleotides. (b) Cropped images and (c) quantification of Western blots for TFP$\alpha$, TFP$\beta$, and VLCAD protein from 15-month-old mice (Wt=wildtype; Lc=LCHAD). TFP$\alpha$ and TFP$\beta$ show decreased protein expression in the LCHADD liver but not heart in both sexes (n=4 per group). Original blots can be found in Supplementary Figure 6. (d) RT- qPCR of *Hadha* mRNA from 12-18-month-old mice show no change in gene expression (n=3 per group). (e) Palmitate oxidation was measured by incubating radiolabeled palmitate with dounced tissue using age/sex matched pairs of each genotype. Heart and liver tissue metabolized-$^{14}$C are decreased in LCHADD mice (Male: age: 3-15 months; heart, liver n=3 per group; Female: age: 3-6 months; heart n=5, liver n=4). Data are presented as mean + SD. Genotypes were compared by unpaired t-test by sex; *p<0.05; **p<0.01; ***p<0.001; ****p<0.0001.

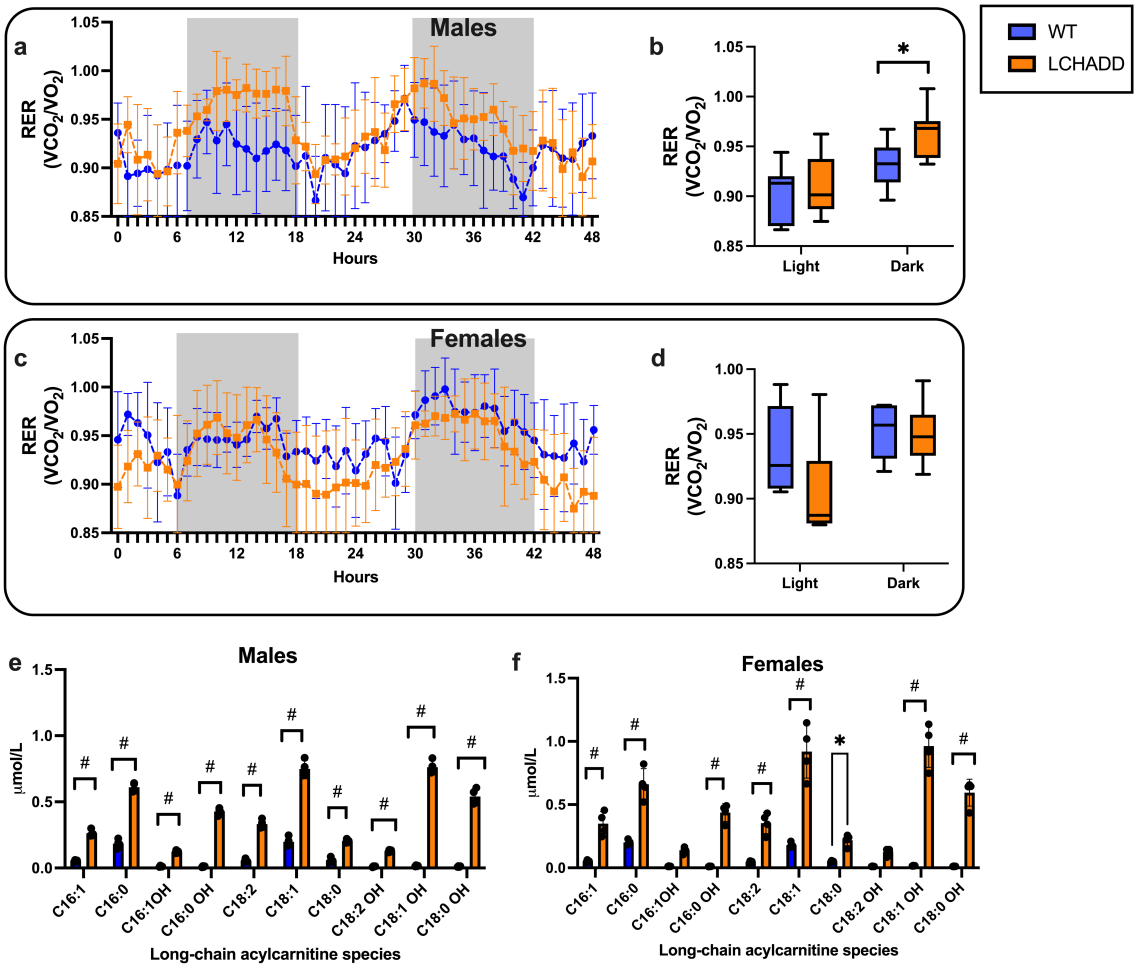


**Figure 3-2: Resting substrate oxidation and serum acylcarnitines.** Ten-month-old LCHADD and WT mice were placed in Oxymax chambers for 4 days; data for last 48 hours is displayed. Dark periods are indicated by gray shading regions. (a) Hourly Respiratory Exchange Ratio (RER; $VCO_2/VO_2$) and (b) light and dark period RER averages illustrate RER was higher in LCHADD males (n=7) compared to WT males (n=7) during the active/dark period. (c) Hourly RER and (d) light and dark period RER averages of LCHADD females (n=6) were not different than WT females (n=6). (e) LCHADD male mice (n=4) and (f) LCHADD female mice (n=4) had higher serum long-chain 3-hydroxyacylcarnitines compared to WT male (n=4) and female (n=4) mice. Data presented as mean ± SD. (a & c) Genotypes compared by repeated measures. (b & d) Box plots illustrates interquartile range; center line is median; whiskers are min and max. Genotypes compared by t-test. (e & f) Acylcarnitines compared by 2-way ANOVA; (main effects =genotype, species) with Sidak's multiple comparisons by sex; *p<0.05; #p<0.0001.

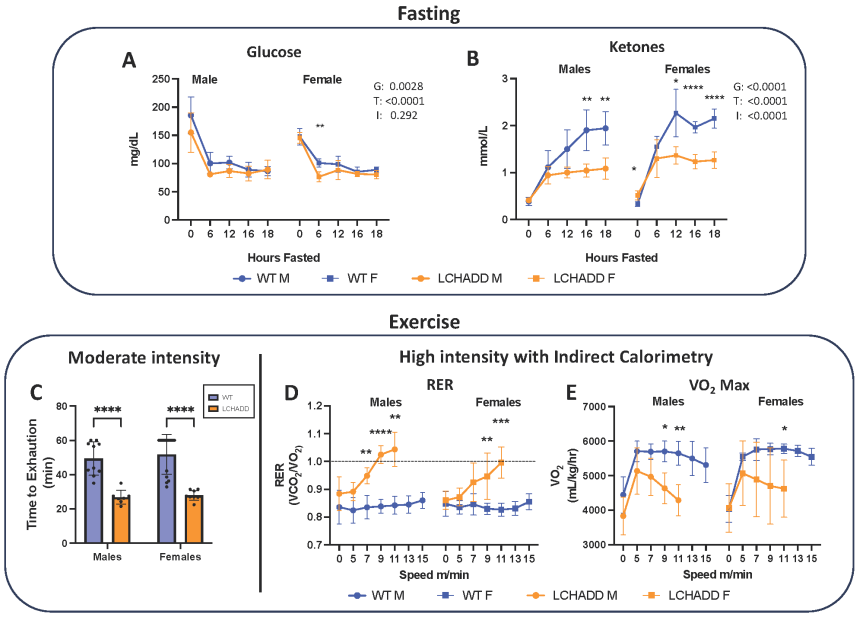


**Figure 3-3: Fasting and exercise response.** LCHADD (males, n=7; females, n=6) and WT (males, n=7; females, n=6) mice were fasted overnight for 18-hours. (a) LCHADD females had lower glucose at 6 hours and (b) both sexes had lower ketones over time. (Main effects: G=group; T=time; I=interaction). (c) In a moderate intensity exercise test, mice were run until exhaustion or up to 60 minutes. LCHADD male (n=7) and female (n=9) mice exhausted earlier than WT male (n=10) and female (n=14) mice. A maximal exercise protocol was implemented until animals completed the protocol, exhausted, or reached a Respiratory Exchange Ratio (RER or $VCO_2/VO_2$) > 1.0. (d) LCHADD mice (males, n=5; females, n=4) exhibited consistently higher RER than WT mice (males, n=5; females, n=4). LCHADD males exceeded RER > 1.0, while some females exhausted before achieving RER of 1.0 (e) LCHAD mice also exhibit lower $VO_2$ max compared to WT. Data are presented as mean + SD. Genotypes were compared by repeated measures ANOVA (a, b, d, e) or 2-way ANOVA (c) with Sidak's multiple comparisons; *p<0.05; **p<0.01; ***p<0.001; ****p<0.0001

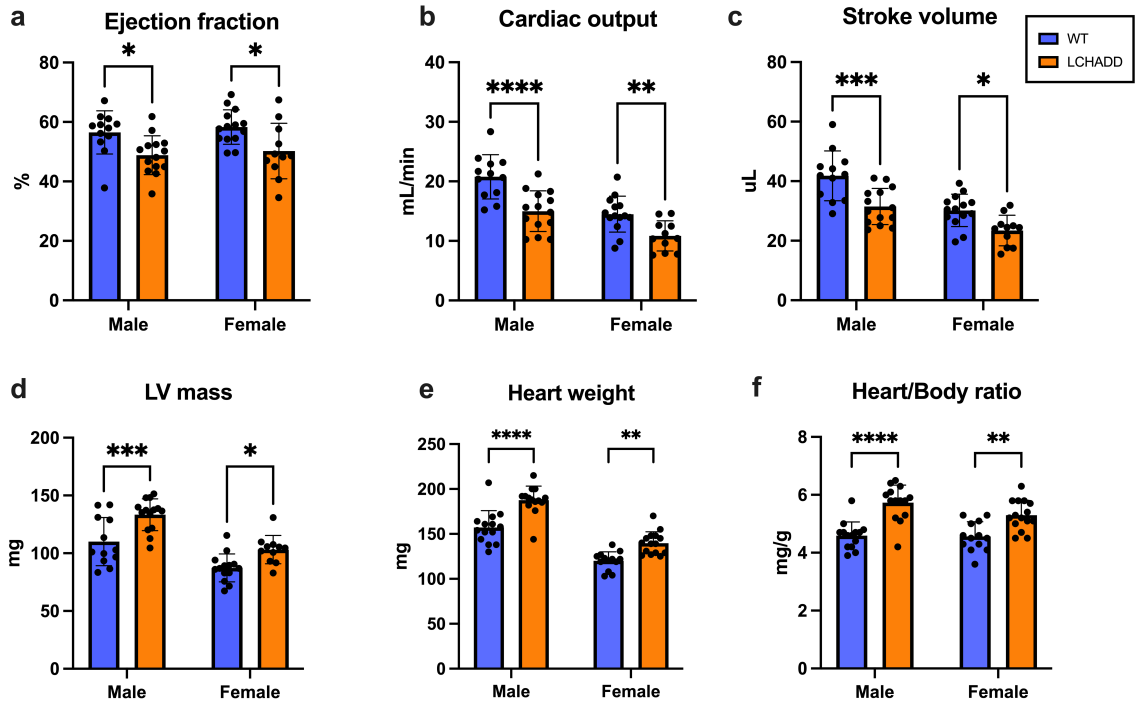


**Figure 3-4: Cardiomyopathy observed in LCHADD mice.** Echocardiograms and tissue dissections (n=11-15 per group) were completed on 12-15-month-old mice. (a) Ejection fraction, (b) Cardiac output and (c) Stroke volumes were lower in LCHADD males (n=14) and females (n=11) compared to WT (males n=12; females n=14). (d) Left Ventricular (LV) mass, (e) heart weight and (f) heart/body weight ratio were higher in LCHADD males and females compared to WT. Data are mean ± SD. 2-way ANOVA (main effects: sex, genotype) with post-hoc Sidak's multiple comparisons. ****p<0.0001; ***p<0.001; **p<0.01;*p<0.05.

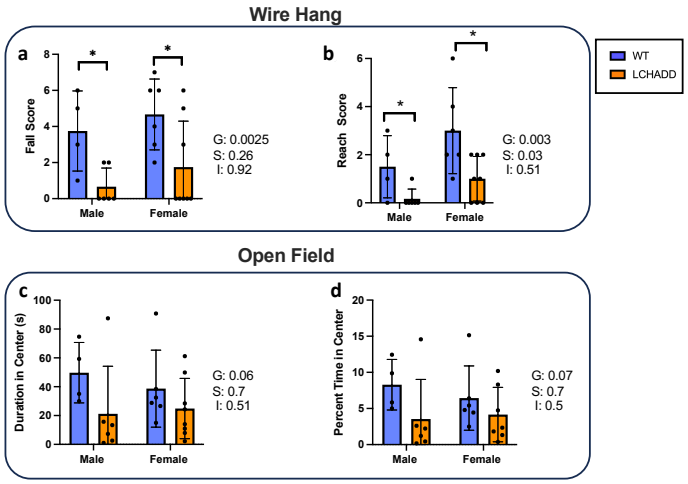


**Figure 3-5: Neurological and behavioral testing.** Tests were performed in 1 year old mice. (WT males n=4, females n=6; LCHADD males n=6, female n=8) (a-b) Wire hang tests showed a lower (a) fall score and (b) reach time in male and female LCHADD mice compared to WT male and female mice. (c-d) Open field tests showed non-significant trends for decreased (c) duration in the center and (d) percent time in center in LCHADD mice compared to WT (2-way ANOVA, Main effects: G=genotype; S=sex; I=interaction). Data are mean + SD. *p<0.05.

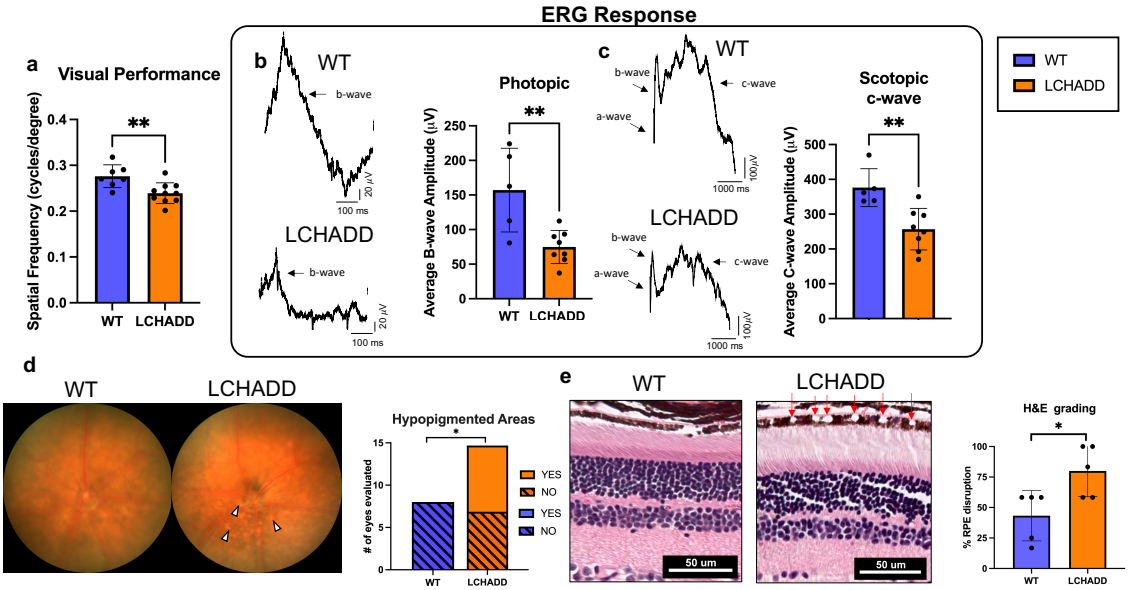


**Figure 3-6: Visual parameters in 1 year old WT and LCHADD mice.** (a) Spatial frequency of LCHADD mice (n=10) was lower than WT mice (n=7). (b-c) (WT: n=5, LCHADD, n=8) (b) Wave forms and bar graph illustrate lower photopic b-wave amplitudes and (c) lower scotopic c-wave amplitudes at the highest light intensity evaluated. (d) Representative fundus images demonstrate hypopigmentation in LCHADD retina (arrowheads) indicative of retinal atrophy. Quantification of hypopigmented areas observed in LCHADD only. Yes = observed hypopigmented areas; No = no observed hypopigmentation. (e) H&E staining of retinal sections highlights large areas of RPE disruption (red arrows) that are visible in the RPE of LCHADD mice. % of RPE with areas of disruption was greater in LCHADD mice. Data are presented as count or as the mean ± SD. Compared by unpaired t-test or fishers exact test *p<0.05; **p<0.01.

## Tables

**Table 3-1:** Pup viability by genotype and breeding strategy

| | **Het x Het** | | **Het x LCHADD** | |
|---|---|---|---|---|
| **Pup Genotype** | expected no. (ratio) | observed no. (ratio) | expected no. (ratio) | observed no. (ratio) |
| **+/+ (WT)** | 162 (25%) | 179 (30.8%) | - | - |
| **+/- (Het)** | 324 (50%) | 324 (55.8%) | 69 (50%) | 69 (73.40%) |
| **-/- (LCHADD)** | 162 (25%) | 78*** (13.6%) | 69 (50%) | 25*** (26.6%) |

Genotype numbers for het-het and het-LCHADD breeding strategies. Expected number based on Mendelian autosomal inheritance. Observed number given as total number and ratio of total pups. Stats by chi squared goodness of fit test ($\chi 2$). ***p<.001. no. = number het=heterozygous; WT= wildtype; LCHADD=Long-chain 3-hydroxyacyl CoA dehydrogenase deficiency.

**Table 3-2:** Antibody concentrations used for western blots

| Category | Target | Company | Cat # | Concentration |
|---|---|---|---|---|
| Polyclonal | HADHA | Thermo Scientific | PA527348 | 1:1000 |
| Polyclonal | HADHB | Thermo Scientific | PA5117024 | 1:1000 |
| Polyclonal | ACADVL | Invitrogen | PA529959 | 1:1000 |
| Monoclonal | HADHA (3E9B1) | Proteintech | 50-173-6347 | 1:1000 |
| Monoclonal | GAPDH | Santa Cruz Biotechnology | sc-365062 | 1:3000 |
| Monoclonal | GAPDH-HRP | Santa Cruz Biotechnology | sc-365062 HRP | 1:2000 |
| Secondary | Mouse TrueBlot® | Rockland Immunilogical | 18-8817-30 | 1:2000 |
| Secondary | Goat anti-rabbit | Thermo Scientific | 31462 | 1:8000 |

**Table 3-3:** Primer List for qPCR

| Gene | Sequence (5'-3') |
|---|---|
| *Hadha* FWD (mouse) | ATGGCGTCAAAGGGGATGTGGC (Exon 3) |
| *Hadha* RVS (mouse) | TGGTCGTTGGCCCAGATTTCGT (Exon 4) |
| *Hadhb* FWD (mouse) | CCCTGGGAGCTGGCTTCTCTGA (Exon 7) |
| *Hadhb* RVS (mouse) | CTCAACACCACCAGCCACGACG (Exon 8) |
| *β-actin* FWD (mouse) | CCCGGGCTGTATTCCCCTCCAT (Exon 2) |
| *β-actin* RVS (mouse) | TGGGCCTCGTCACCCACATAGG (Exon 3) |

## Supplemental Figures

For other supplemental information, please see published paper

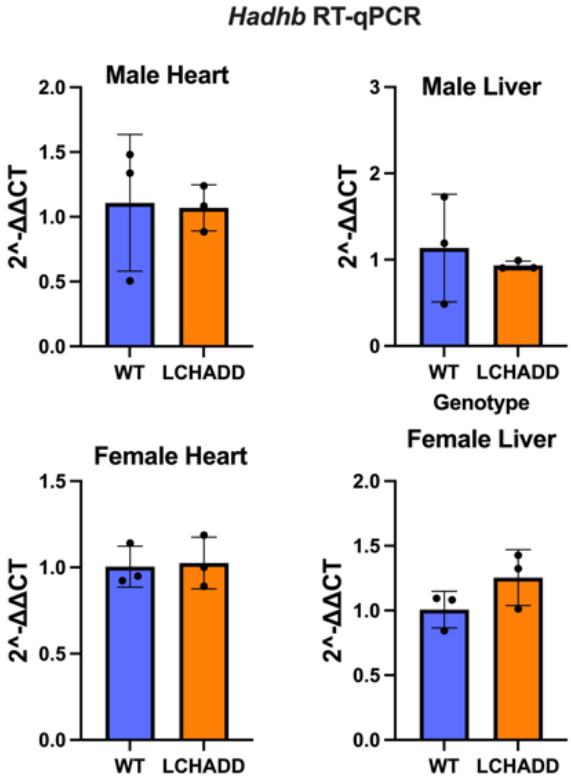


**Supplemental Figure 3-2:C:** *Hadhb* RT-qPCR in male and female heart and liver was not different between genotypes. Data are presented as mean +/- SD.

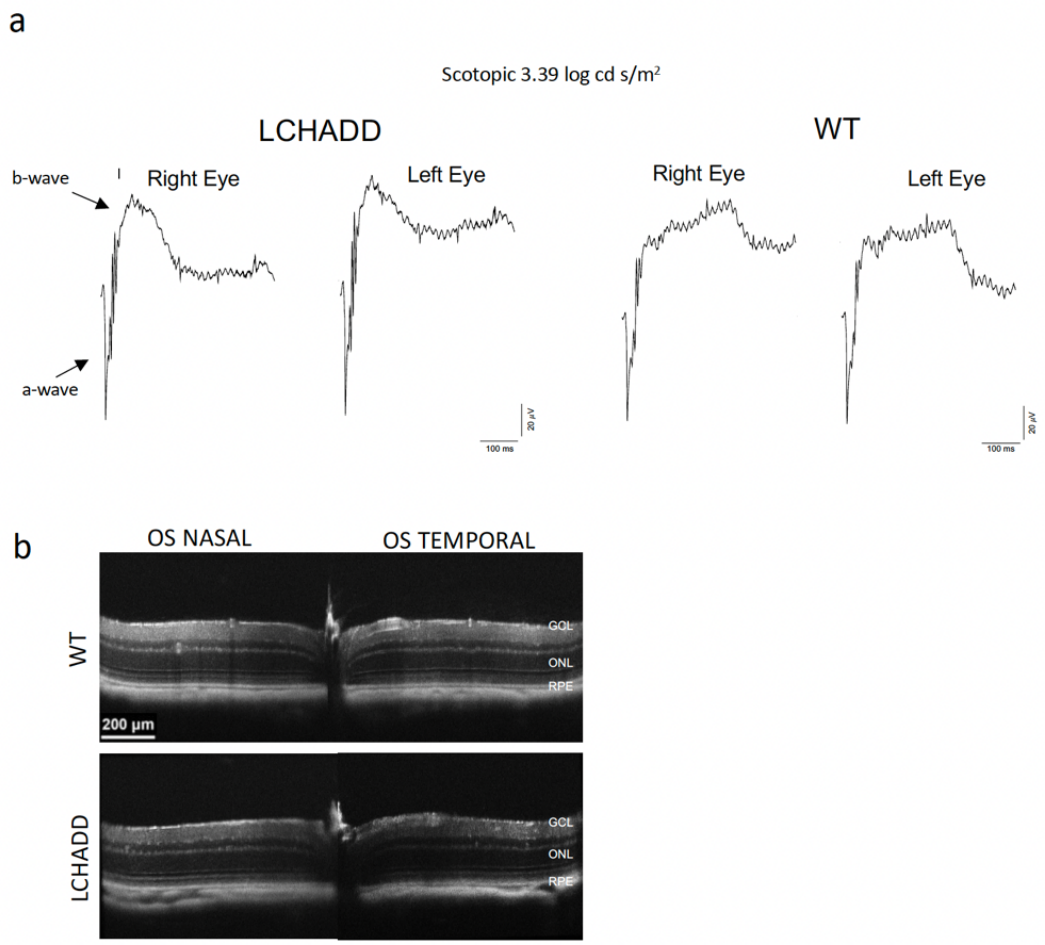


**Supplemental Figure 3-5: Scotopic a, b ERG amplitudes and SD-OCT images.** (a) Representative scotopic a and b waveforms in LCHADD and WT mice. No difference in a and b scotopic amplitudes were seen between genotypes. (b) SD-OCT images were captured in 1 year old mice (WT: n=5, LCHADD: n=8). There was no difference in SD-OCT images between genotypes. GCL-ganglion cell layer, ONL-outer nuclear layer, RPE-retinal pigment epithelium.

## Discussion

LCHADD is a severe long-chain FAO disorder characterized by hypoketotic hypoglycemia, dilated cardiomyopathy, exercise intolerance and recurrent rhabdomyolysis similar to other long-chain FAO disorders.[186,197] Patients with LCHADD also present with a unique retinopathy and peripheral neuropathy not apparent in the other FAO disorders.[187,198] Due to a lack of a LCHADD mouse model, we created a mouse model harboring the pathogenic variant c.1528G>C using CRISPR/Cas9 technology. Our murine model recapitulates many of these features of the human disorder including LCHADD-specific phenotypes. The LCHADD mouse exhibited reduced whole body and tissue FAO; accumulates partially oxidized 3-hydroxy-acylcarnitines in blood similar to human patients; develops lower ketone concentrations with fasting; and exhibits exercise intolerance. Importantly, the LCHADD mouse has a retinal phenotype that has not been reported in other mouse models and thus represents a unique animal model of LCHADD retinopathy. LCHADD mice also demonstrate evidence of a dilated cardiomyopathy. Cardiac complications are the most common cause of death among patients with LCHADD or TFPD. This mouse model could provide insight into cardiac pathophysiology when FAO is impaired and can be used as a model to test therapeutic interventions. LCHADD-associated peripheral neuropathy has a large impact on quality of life; a model to study this debilitating complication has been elusive. It is unclear at this point in time if the impaired motor function as assessed in the wire hang test and reduced activity levels in open field recapitulates features of the human disease. However, if these behavioral phenotypes prove to model the human disease

complication, it opens opportunities to study and therapeutically target under-investigated aspects of this rare disease.

Mouse models have been crucial for studying long-chain FAO disorders; however, development of a mouse model that has a substantial decrease in FAO but is not neonatal lethal has been difficult.[81,132,189,199] The most popular mouse models for long-chain FAO disorders are the very long-chain acyl-CoA dehydrogenase (VLCAD) and the long-chain acyl-CoA dehydrogenase (LCAD) knockout (KO) mice.[101,190,191] VLCAD and LCAD recapitulate some aspects of the human VLCAD deficiency; however, these models do not present with a phenotype as severe as the human deficiency potentially because VLCAD and LCAD appear to have overlapping function in mice while this overlap is not observed in humans.[200] This allows knockout mice to compensate, at least partially, for any loss of VLCAD or LCAD activity. Consequently, FAO is less impaired.[51] The LCHADD mouse model has a comparable, but in several ways more severe phenotype than VLCAD or LCAD KO mouse models potentially because there is no known protein that can compensate for the partial loss of LCHAD activity. LCHADD mice exhibit decreased FAO capacity as demonstrated by a higher RER in the LCHADD male mice, a phenomenon that has not been conclusively observed in either VLCAD or LCAD KO mice.[123,201,202] Similarly, fasting-induced hypoketotic hypoglycemia is a common phenotype tested in murine FAO models. LCAD KO mice become hypoketotic and hypoglycemic after an overnight fast but VLCAD KO mice require both fasting and cold stress to induce hypoglycemia.[111,112,122,201] This LCHADD mouse, like the LCAD KO mouse, has lower blood ketones than WT mice with only an overnight fast and without any cold challenge,

suggesting that there is a similar reliance on glucose with decreased ketosis during fasting when compared to the other models. The LCHADD mouse also experiences exercise intolerance like the VLCAD KO mouse.[169,203] Both LCHADD and VLCAD KO mice have a reduced ability to exercise for prolonged periods, and reach $VO_2$ max much earlier during exercise than WT. [107,202] All together this mouse model exhibits multiple relevant disease specific manifestations of LCHADD.

We anticipated normal protein expression of TFP$\alpha$ in tissues that rely on FAO for energy similar to what has been reported in cultured human LCHADD fibroblasts.[183,204] It was thus surprising when we measured decreased TFP$\alpha$/ TFP$\beta$ levels in the liver of LCHADD mice. It is unknown if TFP$\alpha$ expression in human tissues differ in LCHADD patients but it is possible that human patients with LCHADD may have lower liver expression of TFP$\alpha$ and TFP$\beta$ compared to normal liver. Alternatively, it may also be unique to the mouse or related to the timing of tissue collection such as the impact of feeding/fasting on protein expression. Pulse chase experiments indicate the TFP complex has a relatively long half-life in fibroblasts, around 48 hours,[29,205,206] so the fed or fasted state may have no impact on protein levels but this has not been tested. Alternatively, the lower protein level with similar mRNA by qPCR could suggest decreased protein stability in the liver. Liver protein instability, but not heart, is a surprising finding that will be further investigated.

Chorioretinopathy is a unique complication of LCHADD not observed in other FAO disorders.[196] Our LCHADD mouse model exhibits a retinal phenotype with evidence of decreased visual performance, reduced retinal function (RPE and cones) and disruption

of the RPE layer on H&E staining.[54] We have yet to elucidate the pathological etiologies of the LCHADD retinopathy in this mouse model. Two main hypotheses include 1) decreased FAO in the RPE disrupts the normal retinal metabolic ecosystem between RPE and photoreceptors and 2) selective retinal toxicity by LCHADD-specific circulating metabolites such as plasma long-chain 3-hydroxy fatty acids and/or 3-hydroxy-acylcarnitines.[207] Higher cumulative exposure to plasma 3-hydroxy-acylcarnitines is associated with decreased retinal function in humans.[43,54] However, these metabolites may simply be a biochemical marker for interrupted FAO in the body, and by extension, the retina. We are currently conducting a large natural history study of LCHADD retinopathy in humans and testing a retina-directed gene therapy treatment approach in our mouse model to further our understanding of LCHADD-associated retinopathy. In particular, we plan to use OCTA in future experiments to explore the choroidal phenotype in the LCHADD mice.

Cardiomyocytes preferentially oxidize long-chain fatty acids to generate the energy required for normal cardiac function[208], and patients with long-chain FAO disorders can present with heart failure, dilated cardiomyopathy, and arrhythmias during infancy, adolescence or later in life.[39,209,210] Symptomatic or asymptomatic ventricular dysfunction, from dilated or hypertrophic cardiomyopathy, is often the first manifestation among infants and children with LCHADD or TFPD.[211,212] Cardiac complications are the main cause of early demise in patients. The underlying etiology of cardiac complications in long-chain FAO disorders is hypothesized to be from decreased energy production in the heart or the accumulation of potentially toxic lipid

intermediates.[213] Our LCHADD mouse develops dilated cardiomyopathy with eccentric hypertrophy and provides an *in vivo* model to investigate the cardiac complications associated with LCHADD.

Peripheral neuropathy impacts patient mobility and quality of life, but little is known about the pathophysiology of this disease manifestation.[187,188] It appears in almost all infants around 18 months of age with a loss of peripheral deep tendon reflexes. Some patients never progress past this and the absent reflexes have little functional impact, but many patients exhibit a rapid progression during puberty with foot drop, numbness, and weakness that ultimately lead to reduced mobility.[187,188] Our mice do not develop immobility up to 1 year of age and the changes in neurological testing appear to be confined to performance in the wire hang and open field tests. The phenotypes appear to be more detectable in male mice and milder than observed in human patients. Additional studies, such as pathologic examination of nerve tissue, to determine if the LCHADD mouse neurological phenotype has some similarities to the human presentation are needed.

In conclusion, we generated an LCHADD mouse harboring the common G1528C mutation in exon 15 of *Hadha* using CRISPR/Cas9 technology. Mice homozygous for the LCHAD pathogenic variant recapitulate aspects of the human phenotype including decreased FAO, accumulation of plasma 3-hydroxy acylcarnitines, lower ketones with fasting, exercise intolerance, and cardiomyopathy. We present evidence of a neurological phenotype that needs further characterization. Additionally, these mice have a retinopathy that may be similar to that observed in human patients with LCHADD.

We are currently using this mouse model to investigate tissue specific effects of decreased FAO compared to the effects of potentially toxic circulating metabolites such as 3-hydroxy acylcarnitines. Future studies using this unique model of LCHADD will further elucidate the underlying pathophysiology of LCHADD and can be used to evaluate various therapeutic strategies.

## Methods

All animal procedures were reviewed and approved by the OHSU IACUC (eIACUC #B11243). All experiments were performed in accordance with AAALAC and ARRIVE guidelines. Age, sex, and N of the mice for each experiment can be found in Supplementary Data 1.

**Mouse creation:** Mice were created through Cyagen Biosciences (Santa Clara, CA). The target c.1528G-C mutation and a silent mutation, which prevents recutting by sgRNA, was introduced into exon15 by homology-directed repair. Cas9 mRNA, sgRNA and donor oligo were co-injected into C57Bl/6J zygotes for knock-in mouse production. Injected zygotes were implanted in pseudo-pregnant females. Positive founders were bred to produce F1. All pups were genotyped by PCR/Sanger sequencing using primers 5'-CCAAACCACCCAAGCCTGACTCT-3', 5'-CACCACTACTGTCCGTTTTGGAGAC-3. Five potential off-target sites were analyzed and no additional mutations detected.

**Western blots:** ~20 mgs of snap-frozen tissue were homogenized in ice-cold RIPA lysis buffer (Thermo Scientific Cat #89900) using a stick homogenizer followed by 3 rounds of

sonication (7 sec on; ~1 min rest) at ~11W. ~20-30 ng of protein per sample were electrophoresed using TGX Stain- Free gels (Bio-Rad) which allow visualization of total protein in the gel and on blot. After transfer to PVDF membrane, transferred total protein was visualized with a fluorescent dye (Bio-Rad) before blots were blocked in Tris buffered saline with 0.1% Tween (TBST) plus 5% milk and then incubated with appropriate primary (Polyclonal: HADHA, Thermo Scientific, PA527348; HADHB, Thermo Scientific, PA5117024; ACADVL, Invitrogen, PA529959. Monoclonal: HADHA (3E9B1), Proteintech, 50-173-6347; GAPDH, Santa Cruz Biotechnology, sc-365062 and sc-365062 HRP) and appropriate secondary antibodies. Concentrations of the antibodies used in Western Blots are provided in Table 2. Membranes used for successive blots were stripped using a 5%NaCl 5% Acetic acid solution. Target proteins were visualized using PicoPlus HRP Chemiluminescence kit (ThermoFisher). Size was estimated using Precision Plus Dual Color Standard (Bio-Rad).

Equipment and settings: All images are shown without additional contrast. Total protein was scanned on a GelDoc EZ Imager (Bio-Rad). Blots were scanned with an Azure Sapphire imager on chemiluminescent settings using wide range autoexposure for bands and visible light settings for ladders. Image densitometry for bands and total protein was analyzed on Bio-Rad Image Lab 6.1. Ratio of HADHA, HADHB, and VLCAD densitometry normalized to GAPDH and to total protein were compared between genotypes by sex with similar results (Supplementary Data 1).

**RT-qPCR:** Total RNA from was extracted from ~20 mg of snap-frozen tissue using RNeasy Fibrous Tissue Mini Kit (Qiagen) with an on-column DNase treatment. RNA

was converted to cDNA using the High-Capacity RNA-to-cDNA Kit (Thermofisher). The cDNA was used to perform quantitative PCR on the QuantStudio 5 Real-Time PCR System (Thermofisher) with ~10 ng of cDNA, 250 nm of forward/reverse primers (Table 3), and Power Syber Green PCR Master Mix (Thermofisher). Amplification was performed at 95°C for 10 mins, followed by 40 cycles of 95°C for 15 sec, 53°C for 15 sec, 60°C for 45 sec. Primers were designed to span across 2 exons of the gene (Table 3).

**Metabolic Flux:** Long-chain fatty acid oxidation was measured as described before.[214] Mice were anesthetized with isoflurane and euthanized, and liver (200 mg) or heart (whole heart) were quickly extracted and homogenized using a Dounce homogenizer (5 strokes) in STE buffer (0.25 M sucrose, 10 mM Tris-HCL, 1 mM EDTA, pH 7.4). Homogenates were centrifuged at 450 x g for 10 min at 4 °C. Samples (30 μL) from the homogenate supernatant were incubated with 370 μL of oxidation reaction mixture (100 mM sucrose, 10 mM Tris-HCl, 5 mM $KH_2PO_4$, 0.2 mM EDTA, 80 mM KCl, 1 mM $MgCl_2$, 2 mM L-Carnitine, 0.1 mM Malate, 0.05 mM Coenzyme A, 2 mM ATP, 1 mM DTT, 0.7% BSA/500 μM cold palmitate/0.4 μCi [1-$^{14}$C]palmitate, pH of 8) for 37 °C for 30 min. The reaction was stopped by adding samples to Eppendorf tube with 200 μL of 1 M perchloric acid and a Whatman filter-paper circle soaked with 20 μL of 1 M NaOH in the cap. After gentle shaking for one hour at room temperature, the Whatman filter-paper (containing released $CO_2$) was removed and the radioactivity was measured on a liquid scintillation counter. Eppendorf tubes were also centrifuged at 14,000 x g for 10 mins at 4 °C. 400 μL of supernatant (containing acid-soluble metabolites) was collected and the radioactivity was counted on a liquid scintillation counter. Total protein concentration

measured from homogenate supernatant using the Bradford Assay (Bio-Rad) was used for normalization.

**Fasting:** 11-month-old mice were fasted overnight from 6pm-12pm. Blood draws were taken every 6 hours by pricking the tail vein or removing the clot using a ~19ga needle. Ketones and glucose were measured using a KetoMojo (https://keto-mojo.com Napa, California) device and appropriate micosampling strips. Similar to a handheld glucometer, KetoMojo uses microsamples of blood applied to a testing strip to measure concentrations of ketone or glucose enzymatically (beta-hydroxybutyrate dehydrogenase (HBDH) or Glucose Oxidase, respectively).

**Energy Expenditure:** *Resting IC:* Mice were placed in enclosed cages with food and water starting early afternoon. Oxygen consumption and $CO_2$ production was measured for 4 days (12-hour light/dark cycle) by the Oxymax system (Columbus Instruments; Columbus OH). Initial 48 hours of acclimation time was not used for calculations.[109] Data was uploaded and analyzed in CalR, a web based analysis tool for indirect calorimetry data (www.CalRapp.org).[192]

**Moderate intensity treadmill:** Using an Exer 3/6 treadmill with electric stimulus (Columbus Instruments; Columbus OH) 3-4-month-old mice were trained for 3 rounds of ~12 minutes. Mice were then run starting at 4m/min. Speed was increased by 2m/min increments every 5 minutes until 16 m/min. Mice were additionally encouraged to run

by light brushing on the hind quarters with paper towels. Mice were run for 60 minutes or until exhaustion, defined as an unwillingness to mount a run despite encouragement.[109]

**High intensity treadmill:** 10–12-month-old mice were trained on an enclosed, metabolic treadmill with electric stimulus (Columbus Instruments; Columbus OH), which takes indirect calorimetry measurements via the Oxymax system. Mice were run starting at 5 m/min and speed increased by 2m/min every 3 minutes until 15 m/min or RER$\geq$1.0.

**Neurological testing:** For the behavioral studies, 10-month-old LCHADD (8 females and 6 males) and WT littermates (6 females and 4 males) were used. The mice were tested for performance in the wire hang test on 4/4/2021, for performance in the rotarod test on 4/6/21-4/8/21, and for activity in the open field and subsequently grip strength on 4/9/21, as described in detail below. All animal procedures were reviewed and approved by the OHSU IACUC and in accordance with AAALAC and ARRIVE guidelines. Researchers were blinded to the genotype throughout all experiments.

**Wire Hang:** Motor function was also assessed using the wire hang task, adopting the falls and reaches method described by van Putten 2016 [215] and summarized here. Mice were placed on a suspended metal wire so that they were hanging only by their front paws. In this method, mice start with a fall score of 10 and a reach score of 0. Over the duration of 180s, mice lost 1 point from the score every time they fell and gained 1 point

every time they reached one of the poles holding up the wire. The time of each fall or reach event was also recorded. Each time a mouse fell or reached, the timer was paused to replace the mouse in the center of the wire again. This test allows assessments of endurance and strength and exploring more complex motor coordination.

**Rotarod:** Sensorimotor function was assessed using the rotarod. Mice were placed on a rotating rod (diameter: 3 cm, elevated: 45 cm; Rotamex-5, Columbus Instruments, Columbus, OH, USA). Rotation speed started at 5.0 rpm and accelerated 1.0 rpm every 3 s. Latency to fall (s) was recorded using photo beams located below the rod. Mice received three trials each day for 3 subsequent days.

**Open Field:** General locomotion and anxiety-like behavior was measured in an open environment (40.6 cm in length) with transparent walls. Animals were placed into the maze for a single 10-min trial. Movement of the mice was recorded using video tracking with Ethovision XT 7 software (Noldus Information Technologies, Wageningen, The Netherlands). Dependent measures recorded were distance moved and time spent in the more anxiety-provoking center of the open field.

**Grip Strength:** We used a Harvard Apparatus grip test device for assessing grip strength in the mice. The grip strength meter allows the study of neuromuscular functions in rodents by determining the maximum force displayed by an animal. The grip strength meter was positioned horizontally, and the mice held by the tail and lowered towards

the apparatus. The mice were allowed to grasp the metal grid and pulled backwards in the horizontal plane. The force applied to the grid just before the mouse lost its grip was recorded as the peak tension. We performed 3 consecutive measurements at one-minute intervals.

**Retinal Evaluations:** *Optokinetic Tracking (OKT)* OKT thresholds were used to identify spatial frequencies of gratings (cycles/degree) which define visual performance for animals (OptoMotry; CerebralMechanics, Lethbridge, Alberta, Canada). Briefly, animals were placed on the pedestal in the OptoMotry system and given five minutes to acclimate to the new environment. A simple staircase method at 100% contrast in normal lighting conditions was used for testing. Right and left eyes were tested separately and averaged together to get one spatial frequency per animal.

**Electroretinography (ERG):** Mice were dark-adapted overnight. Under dim red light, mice were anesthetized with ketamine (100 mg/kg) and xylazine (10 mg/kg). Bilateral platinum electrodes were placed on the corneal surface to record the light-induced retinal potentials. The reference and ground electrodes placed subcutaneously in the forehead and tail, respectively. Scotopic a and b-wave ERG responses were recorded at increasing light intensities from −2.76 to 3.39 log cd · s/$m^2$. Scotopic c-wave flash responses were recorded with a separate flash at 1.51 log cd · s/$m^2$. Animals were then light adapted with bright white light for 10 minutes and photopic flashes were recorded at increasing light intensities from -0.23 to 1.02 log cd · s/$m^2$. Animals were recovered

from anesthesia with an i.p. injection of atipamezole 1mg/kg. Data presented in Figure 3-6 includes the scotopic c-wave flash at 1.51 log cd · s/$m^2$ and the maximum photopic flash at 1.02 log cd · s/$m^2$. Representative Scotopic a and b full waveforms are provided in supplementary Figure 3-5a.

**Fundus photography:** Live, *in-vivo* retinal imaging was performed with the Micron IV (Phoenix Research Laboratories, Pleasanton, CA). Mice were anesthetized with ketamine (100 mg/kg) and xylazine (10 mg/kg). Eyes were kept lubricated with 2.5% Hypromellose (Goniovisc). White light was used to acquire bright field images. Exposure settings were kept consistent between all animals. Images were scored yes/no for the presence of hypopigmented white spots by an independent reviewer.

**Histology:** Before enucleation, the superior edge of the eye was marked. Once enucleated, eyes were immediately placed in cold 4% paraformaldehyde and incubated for 2 hours at 4°C. Eyes were then placed in cassettes and stored in 70% ethanol at room temperature. Orientated eyes were processed and embedded in paraffin for sectioning (Tissue-Tek VIP 6, Tissue-Tek TEC 5; Sakura Finetek USA, Inc., Torrance, CA, USA). Sections were cut with a microtome to a thickness of 4 µm, stained with hematoxylin-eosin (H&E), and viewed on a Leica DMI3000 B microscope (Leica Microsystems GmbH, Wetzlar, Germany). All images were taken at a magnification of ×40. Presence of vacuoles in the RPE were scored by an independent reviewer. The percent of the RPE

visible on H&E with the presence of vacuoles was calculated for each eye. The patches of with vacuoles may not be contiguous but were averaged across the whole RPE.

**Spectral Domain Optical Coherence Tomography (SD-OCT):** Mice were sedated using 1.5% isoflurane delivered via a nose cone, corneas were anesthetized with 0.5% proparacaine, and pupils were dilated using a combination of 1% tropicamide and 2.5% phenylephrine. Artificial tears were used to maintain corneal clarity. Mice were seated in a Bioptigen AIM-RAS holder and SD-OCT images were obtained using an Envisu R2200-HR SD-OCT instrument (Bioptigen, Durham, NC).[216,217]Each eye was imaged using linear horizontal scans in the temporal and nasals quadrants and linear vertical scans in the superior and inferior quadrants. SD-OCT images were acquired when animals were 12 months old.

**Echocardiography:** High-frequency (40 MHz) two-dimensional and Doppler echocardiography was performed to assess the status of the aortic valve and LV (Vevo 2100, VisualSonics, Toronto, Canada). End-systolic and end-diastolic LV dimensions and wall thickness, and LV ejection fraction were measured from the parasternal long-axis view by the single plane modified Simpson's method. Stroke Volume was calculated as the product of the LV outflow tract cross-sectional area and time-velocity integral on pulsed-wave Doppler. Left ventricular mass was calculated by end-diastolic images in the mid-ventricular parasternal short-axis view by equation 1:

$$1.05\times(5/6A_1[l+t]-5/6A_2[l])$$

where $A_1$ and $A_2$ are the cross-sectional areas for the epicardium and endocardium, respectively; *l* is the distance from the apex to the mitral valve plane; and *t* is mean wall thickness.

**Statistics and Reproducibility:** Data were analyzed using SPSS (Chicago, IL), CalR (www.CalRapp.org) and Prism 9.0 software (GraphPad, San Diego, CA). Figures were generated using Prism software. Data were graphed as mean $\pm$ standard deviation of the mean with the individual data points. $p<0.05$ was considered statistically significant.

Western protein densitometry normalized to GAPDH and RT-qPCR, were compared by unpaired t-test between genotypes- LCHADD and WT by sex. Palmitate oxidation was completed as matched pairs (genotype and sex) and statistically compared by paired t-test between genotypes by sex. Indirect calorimetry results were analyzed in CalR software. CalR uses a general linear model (GLM) with ANOVA for differences independent of mass such as RER and an ANCOVA for variables impacted by mass such as $VO_2$, $VCO_2$, and energy expenditure.[192] Plasma acylcarnitines were compared by 2-way ANOVA (main effect: genotype and acylcarnitine species) by sex with post-hoc Sidak multiple comparison test. Fasting glucose and ketones and high intensity exercise RER and $VO_2$ studies were compared by a repeated measures ANOVA. Main effect p-values for group (G; LCHADD or WT), time (T) and their interaction are reported with a post-hoc Sidak multiple comparison test indicating specific timepoint differences. Differences between LCHADD and WT mice by sex (male and female) were compared by a 2-way Analysis of Variance (ANOVA) with a post-hoc Sidak multiple comparison test for

moderate intensity exercise, echocardiography outcomes, and tissue weights. Main effect p-values for group (G; LCHADD or WT), sex (S; male or female) and their interaction are reported. Neurological/behavior testing differences between LCHADD and WT mice by sex (male and female) were compared by a 2-way Analysis of Variance (ANOVA) with a post-hoc Least Squares Mean difference test. For behavior testing with changes over time such as rotarod testing, a 2-way repeated measures ANOVA compared group (G; LCHADD male, LCHADD female, WT male, WT female) over time (T) and their interaction with a post-hoc Least Squares Mean difference test was used. OKT, ERG, H&E disruption of RPE were compared by unpaired t-test between genotypes- LCHADD and WT. Presence or absence of hypopigmented areas were compared by Fishers exact test.

## Acknowledgements

This study was funded by generous support from the Scully-Peterson foundation and the National Eye Institute (R01EY032889). Eye tissue processing and sectioning was supported by the Casey Eye Institute, Leonard Christenson Eye Pathology Laboratory. This work was supported by the National Institutes of Health (Bethesda, MD) P30 EY010572 core grant, the Malcolm M. Marquis, MD Endowed Fund for Innovation, and an unrestricted grant from Research to Prevent Blindness (New York, NY) to Casey Eye Institute, Oregon Health & Science University.

# Chapter 4 : The LCHADD mouse model recapitulates early-stage chorioretinopathy in LCHADD patients

**The LCHADD mouse model recapitulates early-stage chorioretinopathy in LCHADD patients**

Shannon J. Babcock[1*], Allison G. Curtis[2], Garen Gaston[1], Gabriela Elizondo[1], Melanie B. Gillingham[1], Renee C. Ryals[1,2]

[1]Department of Molecular and Medical Genetics, Oregon Health & Science University, Portland, Oregon, USA, [2]Casey Eye Institute, Oregon Health & Science University, Portland, Oregon, USA

*Corresponding Author:

Renee C. Ryals, PhD

Email: ryals@ohsu.edu

Phone: 503-440-9247

Word Count: 4490

*Accepted to iVOS May 2024*

## Author Contributions

**SB was involved with conducting all visual assessments, TEM imaging, acylcarnitine profiling, and RNA-sequencing. SB was also responsible for all experiment design, data analysis, and writing.** AC was involved with visual assessments, conducted all retinal cross-section staining, participated in data analysis, and editing manuscript. GG was involved in mouse breeding, TEM imaging, and editing manuscript. GE was involved in mouse breeding and editing manuscript. MG was involved in experiment design, acquiring funding, and editing manuscript. RR was involved in experiment design, data analysis, acquiring funding, and editing manuscript.


## Abstract

Purpose: Recent studies have shown that the retinal pigment epithelium (RPE) relies on fatty acid oxidation (FAO) for energy, however its role in overall retinal health is unknown. The only FAO disorder that presents with chorioretinopathy is long-chain 3-hydroxyacyl-CoA dehydrogenase deficiency (LCHADD). Studying the molecular mechanisms can lead to new treatments for patients and elucidate the role of FAO in the RPE. This paper characterizes the chorioretinopathy progression in a recently reported LCHADD mouse model.

Methods: Visual assessments, such as optokinetic tracking and fundus imaging were performed in wildtype (WT) and LCHADD mice at 3, 6, 10, and 12-months of age. Retinal morphology was analyzed in 12-month retinal cross-sections using H&E, RPE65, CD68, and TUNEL staining, while RPE structure was assessed using transmission electron microscopy. Acylcarnitine profiles were measured in isolated RPE/sclera samples to

determine if FAO was blocked. Bulk RNA-sequencing of 12-month male WT and LCHADD RPE/sclera samples assessed gene expression changes.

Results: LCHADD RPE/sclera samples had a 5- to 7-fold increase in long-chain hydroxyacylcarnitines compared to WT, suggesting an impaired LCHAD step in long-chain FAO. LCHADD mice have progressively decreased visual performance and increased RPE degeneration starting at 6-months. LCHADD RPE have an altered structure and a 2-fold increase in macrophages in the subretinal space. Finally, LCHADD RPE/sclera have differentially expressed genes compared to WT, including downregulation of genes important for RPE function and angiogenesis.

Conclusions: Overall, this LCHADD mouse model recapitulates early-stage chorioretinopathy seen in LCHADD patients and is a useful model for studying LCHADD chorioretinopathy.

## Introduction

The retinal pigment epithelium (RPE) is the outermost retinal cell layer and is crucial for vision. Its ability to regulate the transport of nutrients and waste, to convert and store retinal pigments, and to phagocytose shed photoreceptor outer segments are all crucial in maintaining the function and health of the photoreceptors and choroid. Recent research has suggested that fatty acid β-oxidation (FAO) in the RPE is crucial in maintaining the metabolic homeostasis of the retina.[59] Specifically, the RPE uses FAO to degrade fatty acids from shed outer segments, create ATP, and suppress RPE glycolysis so that glucose can pass from the choroid to the glycolytic photoreceptors.[58, 57,64,68] FAO

also stimulates ketogenesis where the product, ketone bodies, can be passed to the photoreceptors as another source of energy.[60,61,57,69] Perturbations to this system, such as RPE cells becoming more glycolytic, may result in retinal degeneration.[70,72,218,219]

Though FAO has a role in retinal function, it is not clear if it is required for overall vision. Interestingly, in most genetic disorders where FAO is disrupted, patients do not present with vision loss suggesting that impaired FAO alone does not cause retinal degeneration. The only FAO disorder where patients present with chorioretinopathy is long-chain 3-hydroxyacyl-CoA dehydrogenase deficiency (LCHADD, OMIM# 609016). It is hypothesized that the chorioretinopathy is caused by an accumulation of hydroxyacylcarnitines and hydroxy-fatty acids, unique intermediates seen only in LCHADD, that are potentially toxic to the RPE. Therefore, studying vision in FAO disorders, particularly LCHADD, will help improve our understanding of the impact of FAO on retinal health as well as identify other pathogenic mechanisms involved in retinal degeneration.

The pathogenic variant, c.G1528C in *HADHA* which encodes the alpha subunit of the mitochondrial trifunctional protein (TFP), causes LCHADD in human patients. TFP is a heterotetramer made up of two alpha- and two beta-subunits and is responsible for the last three steps of long-chain FAO: enoyl-CoA hydratase, LCHAD, and thiolase (Figure 4-1:A-B). The G1528C pathogenic variant occurs in the LCHAD active site and hinders only the LCHAD activity while the stability and other enzymatic activities of TFP remain mostly intact.[25,26] This causes the unique accumulation of long-chain hydroxyacylcarnitines, which serves as a biomarker for LCHADD.

The progression of chorioretinopathy in LCHADD patients has been characterized. Young LCHADD patients first present with pigment clumping and hypopigmentation at the posterior pole on fundus images, indicating that the loss of the RPE initiates the chorioretinopathy. Patients then develop atrophy of the choroid at the posterior pole and report poor night vision. Finally, patients lose photoreceptors, RPE, and choroid in the central fundus which progresses to blindness.[53,55] The current treatment for LCHADD patients is dietary management consisting of fasting avoidance and a diet low in long-chain fats supplemented with medium-chain triglycerides or triheptanoin (odd-chain medium length fatty acids) that provide a fatty acid substrate that can be used for energy. While treatment can delay or slow progression, the diet does not prevent the chorioretinopathy, highlighting a need for a retina specific treatment for LCHADD chorioretinopathy.[43,45,46]

Unfortunately, research into LCHADD chorioretinopathy has been limited due to the lack of model organisms. To address this problem, we recently reported a novel LCHADD mouse model that is homozygous for the c.G1528C variant in *Hadha* and recapitulated many of the human phenotypes. The LCHADD mouse model has decreased FAO, an accumulation of circulating hydroxyacylcarnitines, cardiomyopathy, and a reduced ability to exercise. Additionally, it displays retinal degeneration at 1-year of age.[133] Here we aim to further characterize the progression of the chorioretinopathy in the LCHADD mouse model by taking visual assessments at 3, 6, 10, and 12 months of age and aim to investigate the molecular mechanisms involved.

## Results

To test if LCHADD RPE has reduced LCHAD activity and an impaired FAO, we measured acylcarnitine concentrations in RPE/sclera samples isolated from 15-month WT and LCHADD mice of mixed sex. LCHADD RPE/sclera show a statistically significant increase in long chain hydroxyacylcarnitines compared to WT RPE/sclera (Figure 4-1:C). Specifically, there was 7-fold and a 5-fold increase in C16-OH and C18-OH. Acetyl-CoA, the product of FAO and glycolysis that is important for the citric acid cycle and subsequently ATP production, is not different between LCHADD and WT RPE/sclera (Figure 4-1:D). While the high hydroxyacylcarnitines suggest LCHADD RPE/sclera have a block at the LCHAD step, the equivalent acetyl-CoA levels indicate there may not be an energy deficiency.

We have previously reported that LCHADD mice have a decrease in visual performance at 12-months of age.[133] To characterize the changes in visual performance over time, we measured the spatial frequency of WT and LCHADD mice at 3, 6, 10, and 12-months using optokinetic tracking (OKT) (Figure 4-2:A). The spatial frequency in LCHADD mice, while statistically significant, is only slightly decreased when compared to WT (0.33 vs 0.36 cycles/degree) at 3-months. This difference increased to 0.06 cycles/degree at 6-months (0.29 vs 0.35 cycles/degree), which is statistically significant and more biologically relevant than at 3-months. The difference between LCHADD and WT visual performance was the largest at 10-months (0.23 vs 0.32 cycles/degree) and remained the same at 12-months. This suggests that, by 6-months, LCHADD mice have decreased visual performance that progressively worsens compared to WT mice.

Next, fundus imaging was performed in WT (Figure 4-2:C) and LCHADD (Figure 4-2:D) mice at 3, 6, 10, and 12-months of age. RPE degeneration was evident and characterized by hypopigmented areas. Starting at 6-months of age, the percentage of LCHADD eyes with hypopigmentation was at least twice the number of WT eyes. In addition, the percentage of LCHADD eyes with hypopigmentation continued to increase from 11% at 3-months to 67% at 12-months, whereas the percentage of WT eyes with pigmentation remained between 10-17% until 10-months and only increased to 30% at 12-months (Figure 4-2:B). This suggests LCHADD mice have increased RPE degeneration compared to WT mice starting at 6-months that worsens over time. Optical coherence tomography (OCT) was used to look at overall retinal degeneration. Like previously reported findings, there was no difference in the thickness of the photoreceptor and RPE layers between WT and LCHADD mice (Figure 4-3), indicating photoreceptors have not degenerated by 12-months.[133] TUNEL staining on 12-month LCHADD central retinal cross-sections do indicate increased TUNEL-positive cells in the cross-sections compared to WT; however, this is not statistically significant ($p=0.06$) and the total number of TUNEL-positive cells is low (Supplemental Figure 4-1). This indicates that LCHADD mice may have minor degeneration in other layers of the retina compared to WT but not enough to alter the retinal structure. Overall, LCHADD mice have progressive vision loss and RPE degeneration compared to WT starting at 6-months of age, although not an overall change in retinal thickness.

To further analyze the RPE layer, hematoxylin and eosin (H&E) staining and RPE65 immunofluorescence showed that, at 12-months of age, LCHADD mice had increased

RPE disruptions and degenerations compared to WT. The RPE was characterized into four types: Type 1 indicates normal RPE where H&E and RPE65 staining show a consistent, continuous RPE layer (Figure 4-4:A); Type 2 indicates RPE that developed vacuoles seen in H&E staining (Figure 4-4:B); Type 3 indicates RPE with a loss of boundary rigidity and lack of uniform pigmentation in both stains (Figure 4-4:C); and Type 4 indicates RPE loss as seen from a loss of pigmentation on H&E or a severe thinning/complete absence of RPE65 fluorescence (Figure 4-4:D). When quantified, WT mice had minimal RPE disruption where 53% of the samples had normal RPE and 47% of the RPE had vacuoles (Type 1 and 2; Figure 4-4: E). In contrast, 88% of LCHADD samples had some degree of RPE disruption and 35% of samples had a loss of boundary rigidity and/or RPE loss (Type 3 and 4; Figure 4-4:F). Interestingly, we saw a large number of choroid vacuoles in the LCHADD samples compared to WT samples (44% vs 20%; Supplemental Figure 4-2). Further analysis is needed to determine the etiology and significance of these vacuoles.

Transmission electron microscopy (TEM) further suggests a change in RPE structure of 12-month LCHADD mice. WT RPE have a normal structure with some vacuoles present (Figure 4-5:A, Supplemental Figure 4-3:A-D). LCHADD RPE appear to have a loss of basal infoldings, loss of apical microvilli intertwining with photoreceptor outer segments, and photoreceptor outer segments that are abnormal and horizontal to the RPE (Figure 4-5:B-C, Supplemental Figure 4-3:E-H). TEM imaging also suggests mitochondria in LCHADD RPE trend larger than WT; however, this is not statistically significant ($p=0.11$; Supplemental Figure 4-4:A-C). There is no difference in the number of mitochondria between WT and LCHADD RPE/sclera (Supplemental Figure 4-4:D).

Future experiments, such as TEM imaging of RPE with higher magnification, are needed to further explore the mitochondrial morphology and function in LCHADD RPE. Overall, TEM indicates an altered RPE structure confirming H&E and RPE65 staining.

Increased macrophages in the RPE and subretinal space of a deceased 14-month LCHADD patient presenting with early-stage chorioretinopathy was previously reported.[220] An increase in CD68+ macrophages in the subretinal space have also been associated with ectopic RPE and RPE dystrophy in animal models of retinal degenerations, suggesting a role of CD68+ macrophages in the retinal inflammation commonly seen in retinopathies.[221] To determine if similar macrophage infiltration exists in the LCHADD mouse model, we stained retinal cross sections for CD68. The average number of macrophages present in the central retina of WT and LCHADD mice were 14 versus 27, suggesting increased macrophages in LCHADD mice (Figure 4-6).

Finally, RNA-sequencing on 12-month male WT and LCHADD RPE/sclera were used to investigate molecular mechanisms involved in LCHADD chorioretinopathy. LCHADD RPE/sclera have differentially expressed genes (DEGs) compared to WT mice (Figure 4-7:A). There were 16 statistically significant DEGS, all of which were downregulated in LCHADD RPE/sclera, and the most common gene ontology term taken from the DEGs was tissue development (Figure 4-7:B-C and Supplemental Table 4-1). Interestingly, many of the significant DEGs have been previously studied in the context of retinal degeneration, specifically playing a role in angiogenesis (Figure 4-7:C).[222-226] One gene of particular interest, *Mitf*, is expressed solely in the RPE and plays a crucial role in RPE function.[227-230] Loss of this gene has been connected to loss of RPE pigmentation

and loss of RPE phenotype, thus supporting the results seen from H&E staining and TEM.[231,232] Overall, this data supports that 12-month LCHADD male mice have an altered gene expression in the RPE/sclera, and in addition to RPE dysfunction, changes in the vasculature could be significantly contributing to the LCHADD chorioretinopathy.

Figures

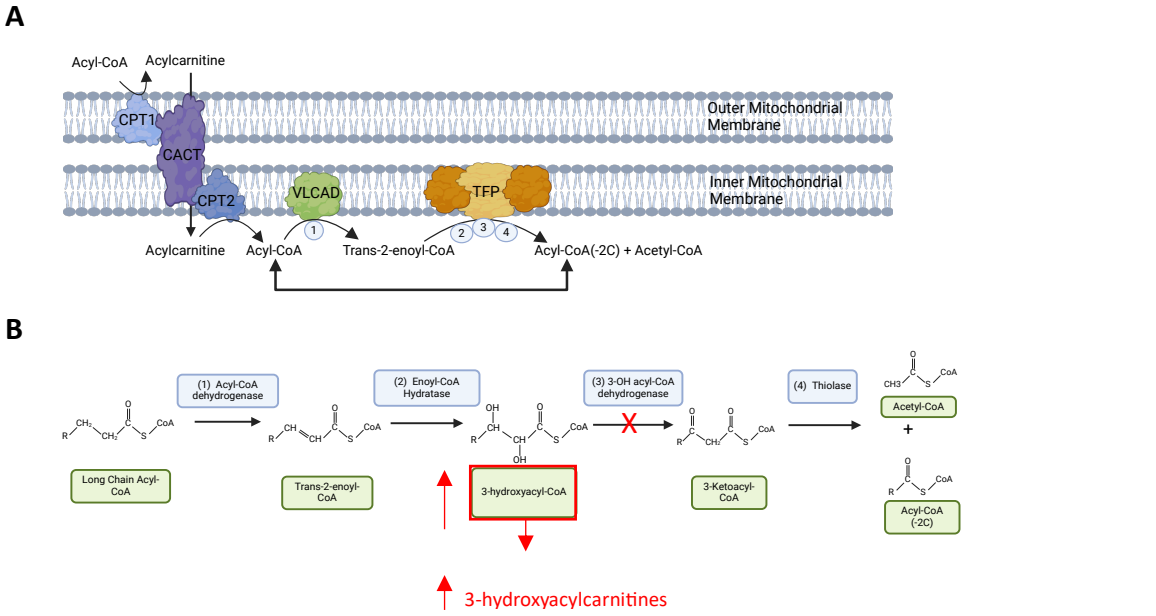


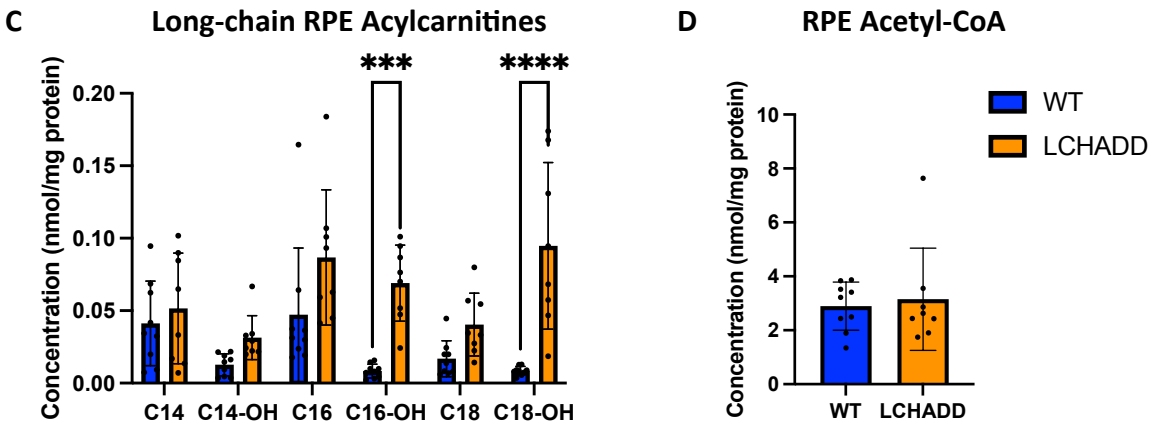


**Figure 4-1: LCHADD RPE displays an increase in hydroxyacylcarnitines but not a decrease in acetyl-CoA.** (A) Schematic of the proteins involved in long-chain fatty acid oxidation. (B) Enzymatic activity and intermediates involved in long-chain fatty acid oxidation. Red indicates the LCHADD G1528C pathogenic variant inhibits only the LCHAD activity and results in an accumulation of long-chain 3-hydroxyacylcarnitines, which serves as a biomarker for LCHADD. Figure was created using Biorender. (C-D) In isolated RPE/sclera samples, LCHADD (n=8) compared to WT (n=9) have (C) an increase in long-chain hydroxyacylcarnitines, suggesting a block in FAO at the LCHAD step. LCHADD samples have (D) equivalent acetyl-CoA which suggests that LCHADD RPE may not have an energy deficiency. Data presented as mean ± SD. A one-way ANOVA with Sidak's multiple comparison post-hoc test was used to calculate acylcarnitine statistics. An unpaired T-test was used to calculate acetyl-COA statistics. *p<0.05, ****p<0.0001, ns= not significant

A

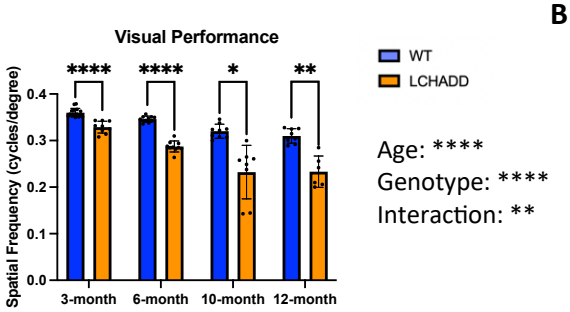


B

| Eyes with Hypopigmented Areas | | |
|---|---|---|
| | WT | LCHADD |
| 3-month | 4/30 (13%) | 2/18 (11%) |
| 6-month | 2/20 (10%) | 6/20 (30%) |
| 10-month | 3/18 (17%) | 8/15 (53%) |
| 12-month | 5/16 (31%) | 8/12 (67%) |

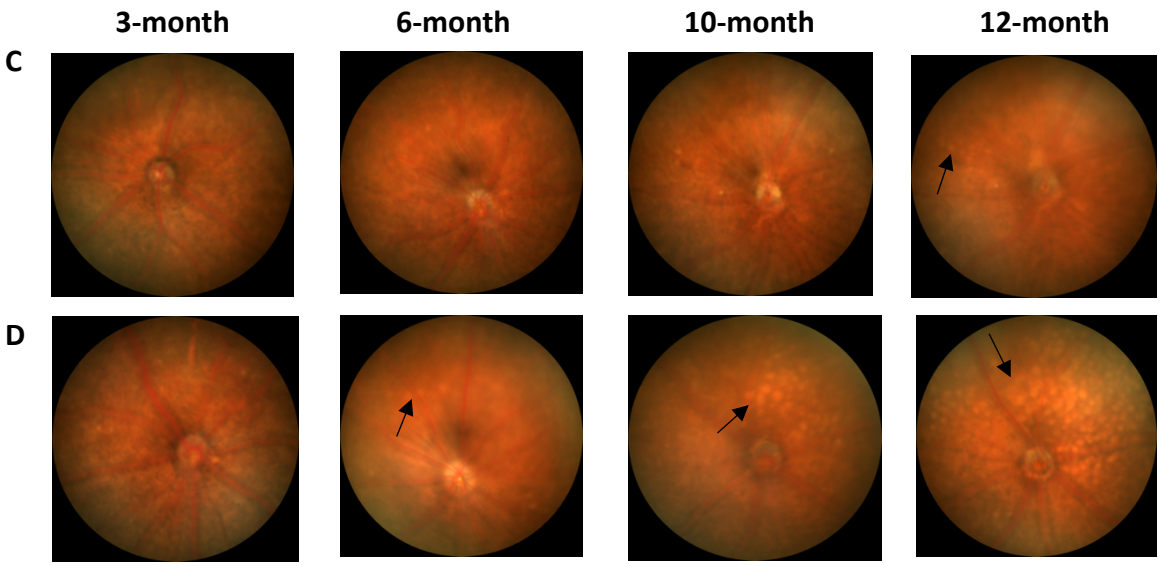


**Figure 4-2: LCHADD mice display a decreased visual performance due to increased RPE degeneration, starting at 6-months of age, that progressively worsens over time.** (A) OKT measurements in LCHADD mice (n=6-10 mice) show a significantly lower visual performance compared to WT mice (n=8-12 mice) that progressively decreases overtime. Data presented as mean ± SD. Stats were calculated by a mixed–effects model and Sidak's multiple comparisons post-hoc test. (B) Percentage of fundus images with white, hypopigmented spots in WT and LCHADD mice at 3-, 6-, 10-, and 12-months of age. C) Examples of WT eyes at 3, 6-, 10, and 12-months of age show white, hypopigmented spots are minimal in WT eyes even at 12-months of age. (D) Examples of LCHADD eyes at 3-, 6-, 10-, and 12-months of age that demonstrate white, hypopigmented spots that first appear at 6-months of age and increase over time, suggesting a progressive increase in RPE degeneration. Black arrows=hypopigmented spots. *p<0.05, **p<0.01, ****p<0.0001

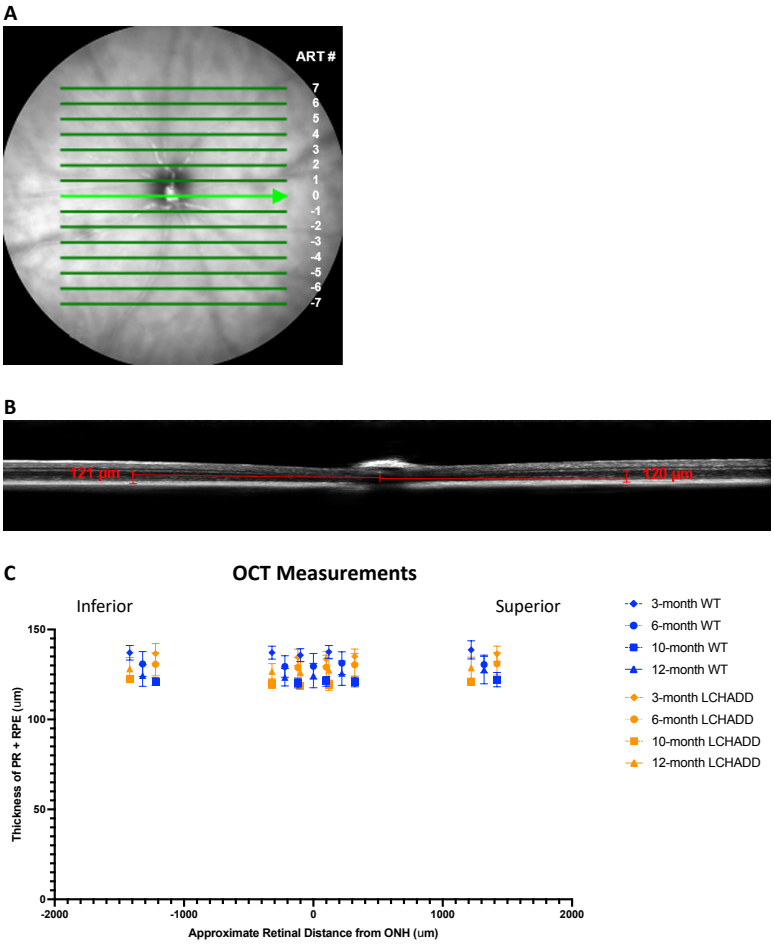


**Figure 4-3: No difference in retinal cell structure between WT and LCHADD mice at any age.** (A) A representative IR fundus image showing OCT image acquisition. The green lines demarcate the B-scans acquired and each are approximately 220 µm apart. The ART # is used as a label for each location. ART #0 scans through the center of the optic nerve head. (B) A representative 3-month LCHADD OCT image. The photoreceptor (PR) and RPE thickness was measured approximately 520 µm on the temporal and nasal side. The measurements were averaged together. (C) The thickness of the PR and RPE layers in WT (n=7-11 mice) and LCHADD mice (n=3-8 mice) at 3, 6, 10, and 12-months of age. The thickness of PR and RPE were measured at ART #s -6, -1, 0, 1, 6 (approximately -1320, -220, 0, 220, and 1320 µm from the center of the optic nerve head). Symbols were slightly displaced along the x-axis to allow for better visualization. There was no difference in PR and RPE thickness between WT and LCHADD mice at any age. Data presented as mean ± SD. A two-way ANOVA with a Sidak's multiple comparison analysis was used to calculate statistics for each age.

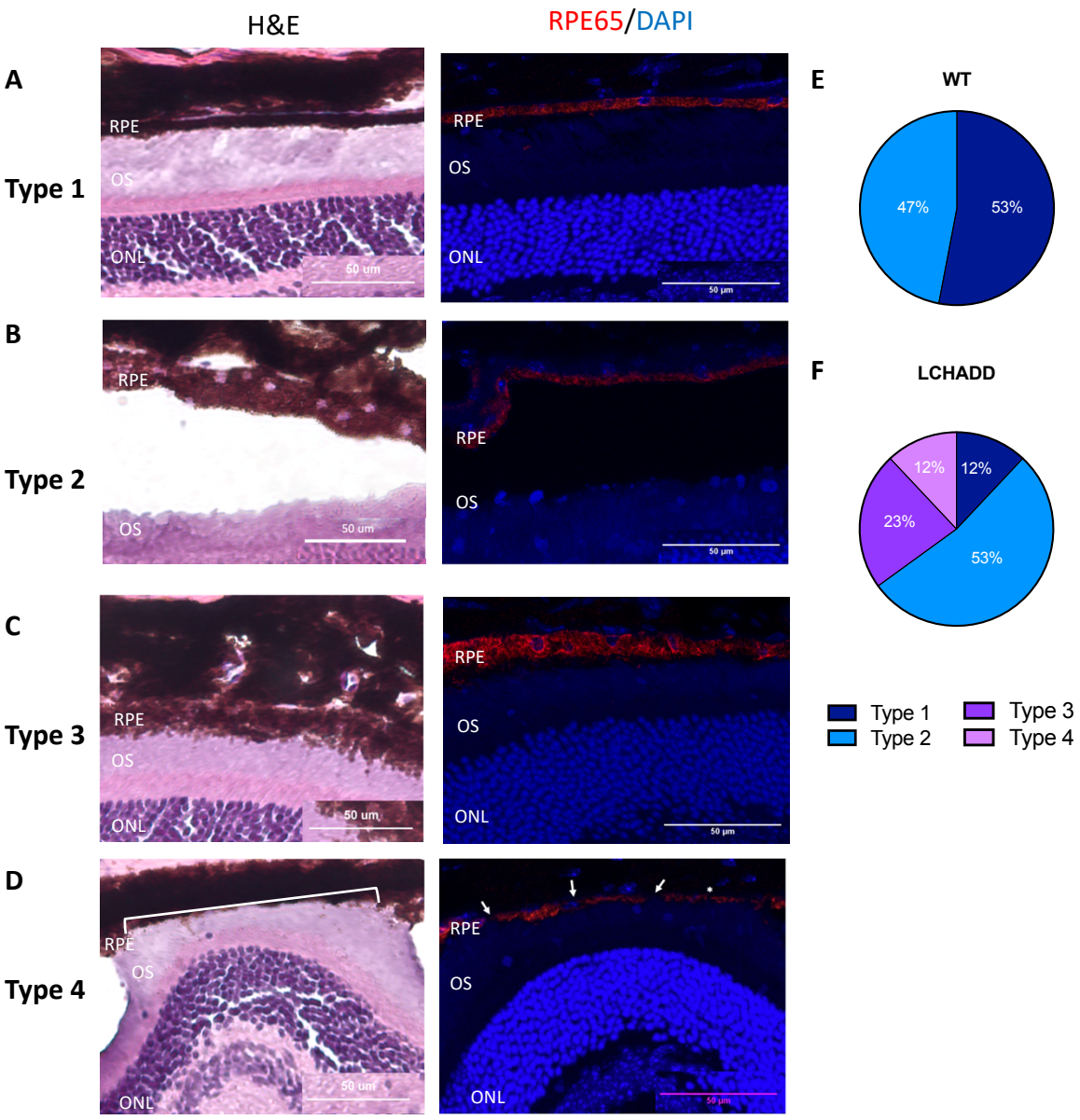


**Figure 4-4: 12-month LCHADD RPE show increased RPE disruptions ranging from RPE vacuoles to RPE loss in areas.** Four different types of RPE were seen from 12-month WT (n=15 central retina cross section from 5 eyes) and LCHADD (n=17 central retina cross section from 6 eyes) retinal cross sections stained with H&E or RPE65/DAPI (red/blue fluorescence). (A) Type 1 RPE were defined as normal, healthy RPE. (B) Type 2 RPE were defined as RPE with vacuoles in the RPE on H&E staining while RPE65 showed a normal RPE. (C) Type 3 RPE were defined as RPE that had a loss of rigidity and disintegration on both H&E and RPE65 staining. (D) Type 4 RPE were defined as areas where there was a loss of RPE on H&E staining (white bracket) and either significant thinning (white asterisk) or complete loss (white arrow) of RPE65 staining. (E-F) When the types of RPE were quantified, LCHADD samples had a higher percentage of RPE that were disrupted and had more severe disruptions (Type 3 and 4) when compared to WT mice.

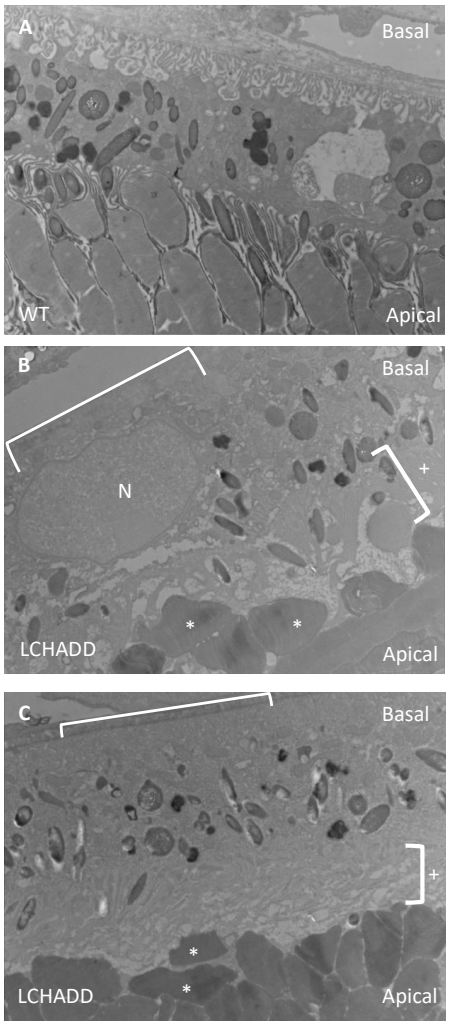


**Figure 4-5: TEM imaging shows 12-month LCHADD RPE display an altered RPE structure.** (A) RPE from 12-month WT mice have a relatively normal RPE structure with basal infoldings and apical microvilli. (B-C) Representative images of LCHADD RPE, on the other hand, display a loss of basal infoldings (bracket only), loss of apical microvilli (bracket with plus sign), and abnormal photoreceptor outer segments that are horizontal to the RPE (white asterisk). N=nucleus and V=vacuole.

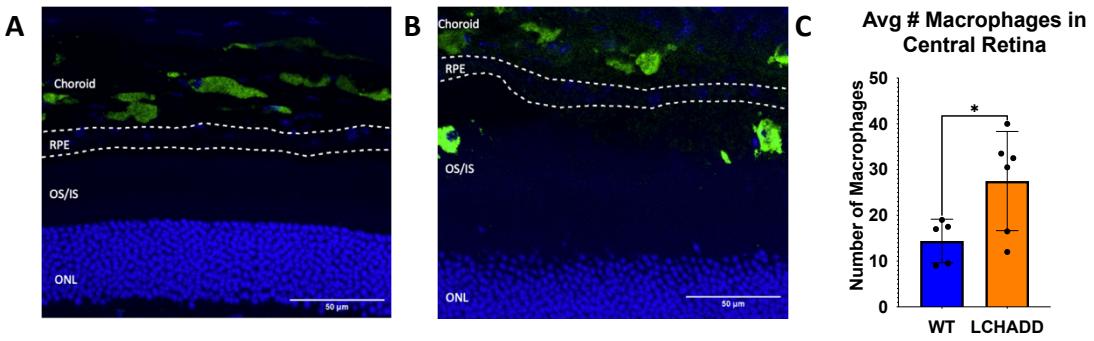


**Figure 4-6: 12-month LCHADD mice have increased infiltration of macrophages into the subretinal space when compared to WT mice suggesting increased inflammation.** (A-B) Representative images of (A) WT and (B) LCHADD retinal cross sections stained with CD68 (green) and DAPI (blue) suggest an increased number of macrophages that infiltrate the subretinal space of LCHADD mice. (C) Quantification of the average number of macrophages in the subretinal or neural retinal space in the central retina. This was calculated by averaging the number of macrophages in two central retinal cross sections taken from 12-month LCHADD (n=6) and WT (n=5) mice. Data presented as mean ± SD. Stats were measured using a two-tail T-test. *p<0.05

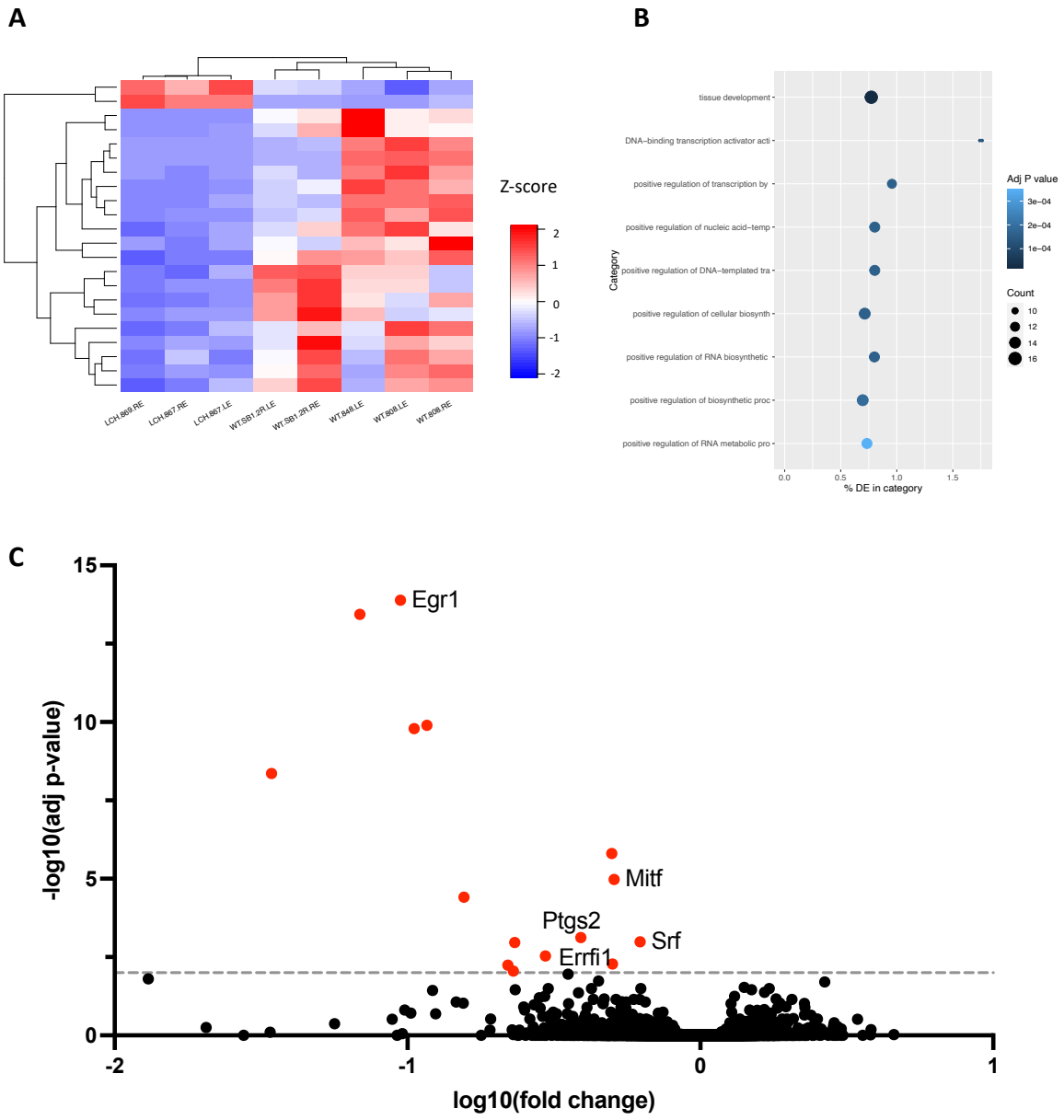


**Figure 4-7: RNA-sequencing of 12-month male WT (n=5) and LCHADD (n=3) RPE/sclera highlight genes that are differentially expressed in LCHADD RPE/sclera samples.** (A) Heatmap of Z-scores calculated from RNA-sequencing of 12-month male WT and LCHADD mice. (B) Top 10 gene ontology (GO) terms based on the DEG in LCHADD mice. The most over-represented category is tissue development. (C) Volcano plot of differentially expressed genes (DEGs) found in LCHADD mice compared to WT mice. Red highlighted points are significant DEGs with a -log10(adj p-value)>2. Points with labels indicate genes that have been previously studied in the retina. These genes have been shown to be involved vasculature and angiogenesis (*Egr1*, *Errfi1*, *Srf*, *Ptgs2*), and RPE function (*Mitf*).

Supplemental Figures

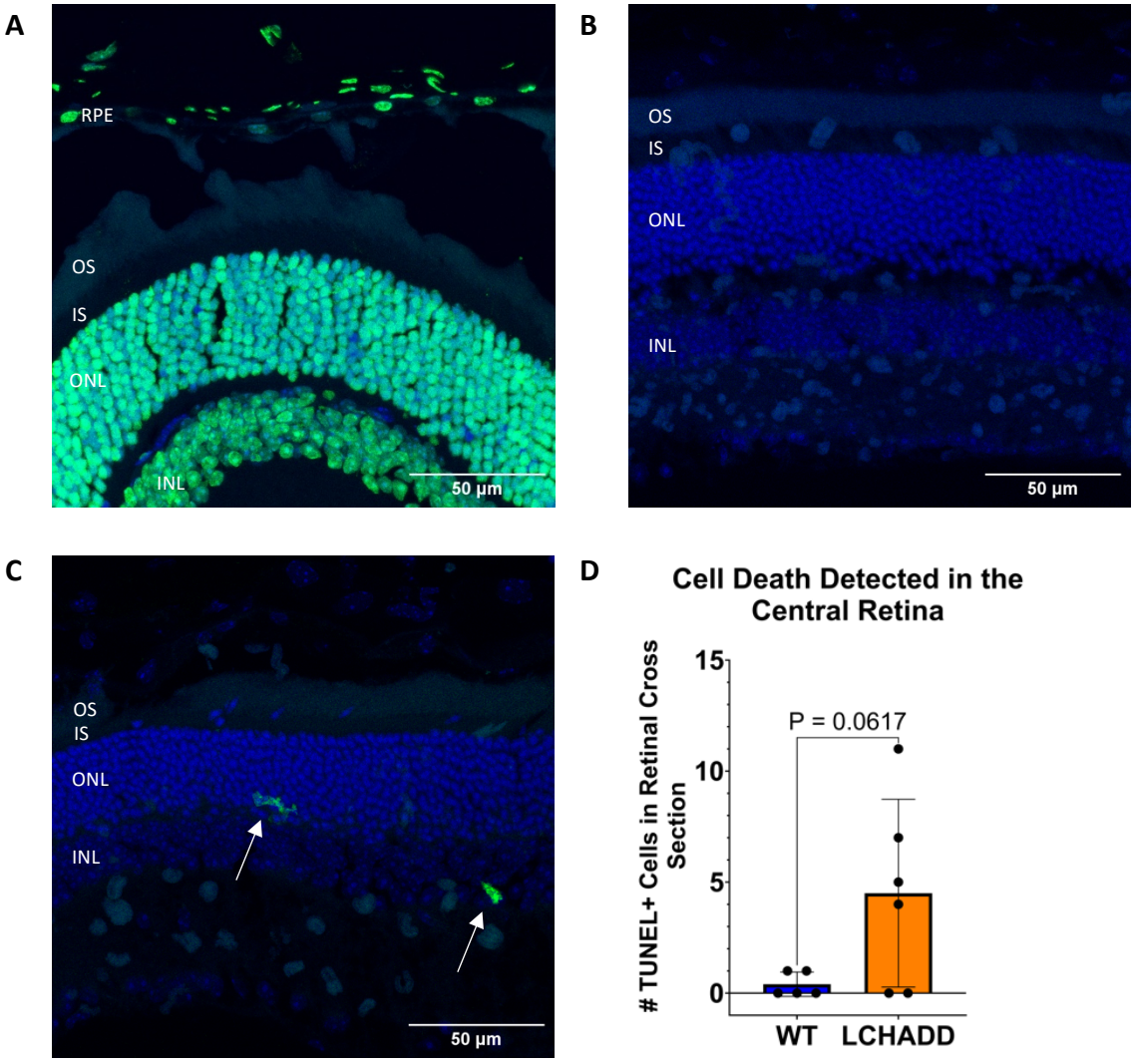


**Supplemental Figure 4-1: There is no statistically significant difference in apoptotic cells between the central retina cross-sections of 12-month WT and LCHADD mice, indicating no significant retinal degeneration.** (A-C) Representative images of (A) positive control, (B) 12-month WT, and (C) 12-month LCHADD retinal cross-sections stained with TUNEL staining (green) and DAPI (blue). Both WT and LCHADD retinal cross-sections have few apoptotic cells (white arrows), suggesting no retinal degeneration. (D) Quantification of the number of TUNEL-positive cells in the retinal cross-sections from 12-month WT and LCHADD central retina cross-sections. LCHADD mice have increased TUNEL-positive cells compared to WT cross-sections. Data presented as mean ± SD. Stats were measured using a two-tail T-test.

A

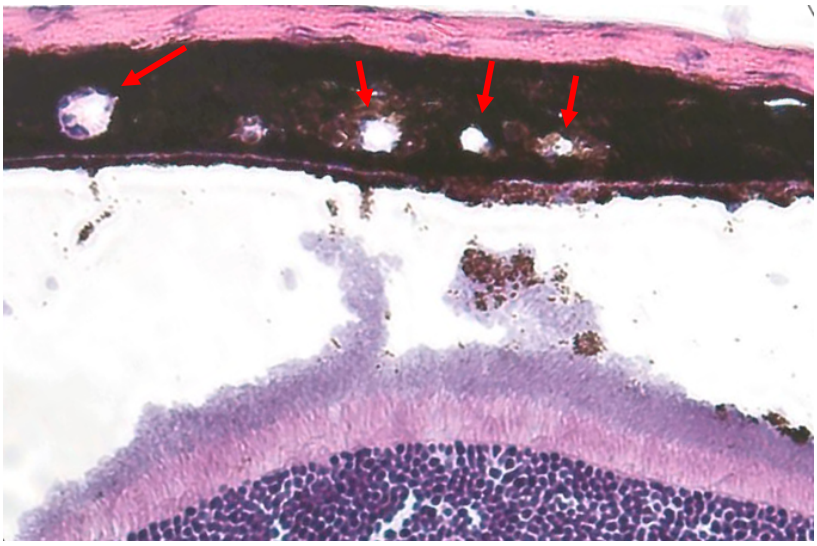

B WT C LCHADD

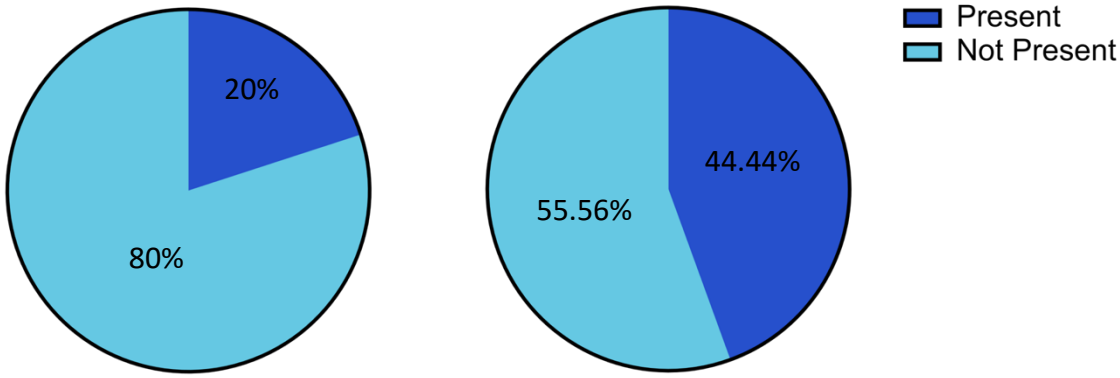


**Supplemental Figure 4-2: 12-month LCHADD mice have increased vacuoles in the choroid compared to WT mice.** (A) An example of vacuoles (red arrows) seen in choroid of 12-month LCHADD mice. (B-C) Percentage of H&E-stained retinal cross sections with vacuoles in choroid in 12-month (B) WT and (C) LCHADD mice.

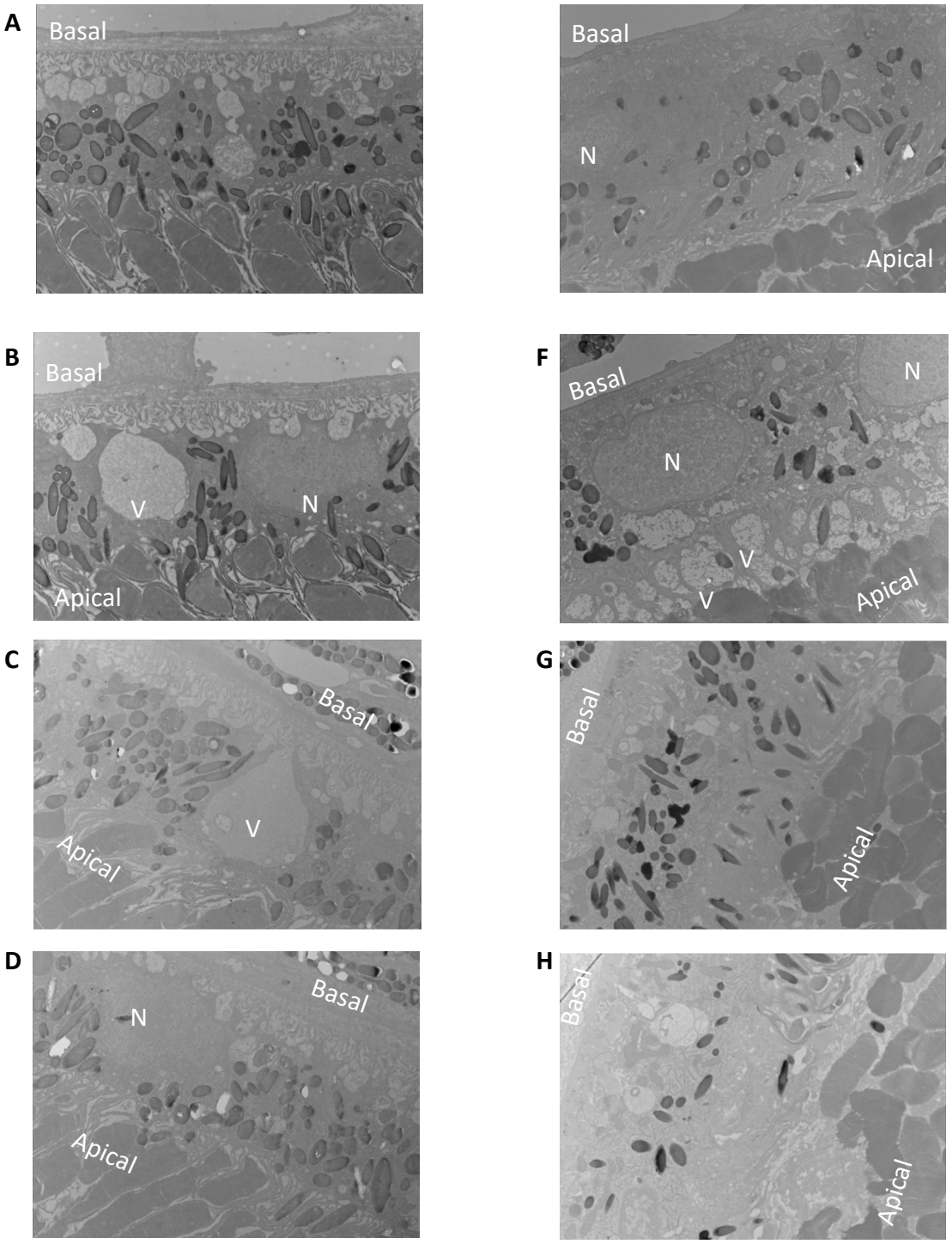


**Supplemental Figure 4-3: Additional TEM images of 12-month WT and LCHADD RPE.** (A-D) Additional WT RPE (n=2) that show a normal RPE that has basal infoldings and apical microvilli. (E-H) Additional LCHADD RPE (n=2) that have a loss of basal infoldings, loss of apical microvilli, and abnormal photoreceptor outer segment that are horizontal to RPE. N= nucleus and V= vacuoles.

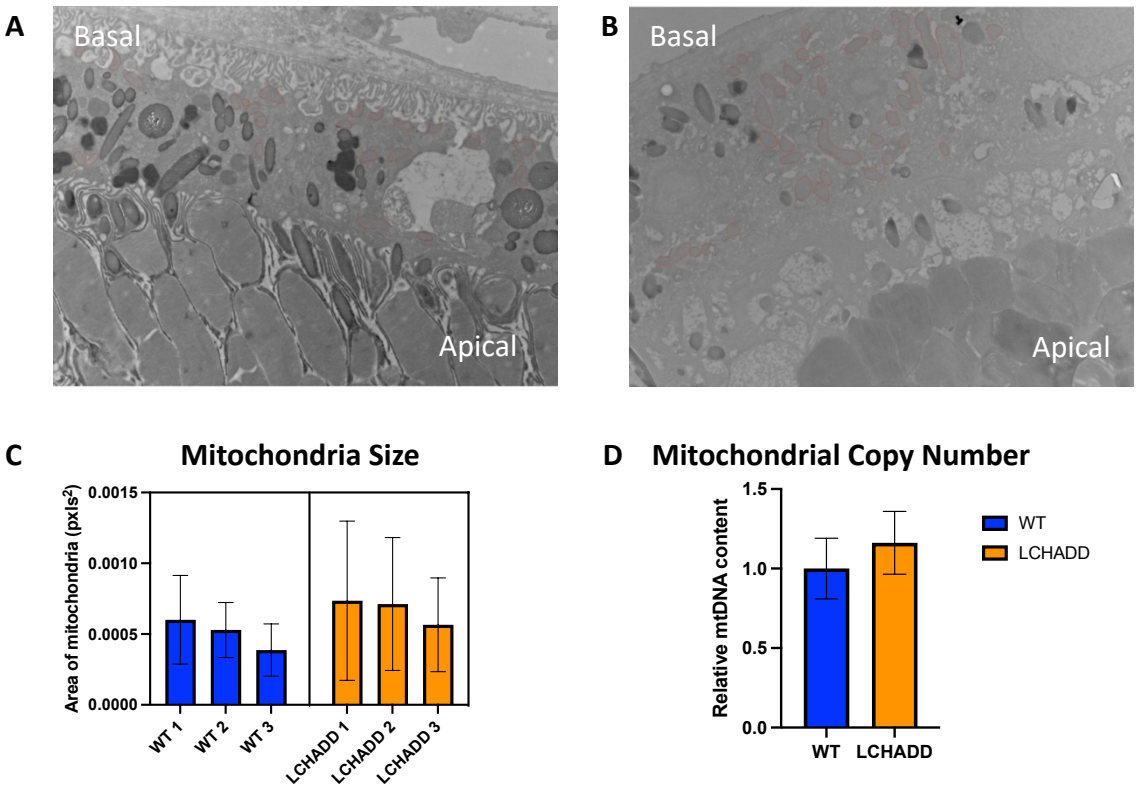


**Supplemental Figure 4-4: LCHADD RPE may have larger mitochondria than WT.** (A-B) Representative images of 12-month (A) WT and (B) LCHADD RPE showing that LCHADD RPE may have larger and more abnormally shaped mitochondria (outlined in red). (C) Quantification of the area of mitochondria in WT (n=3 eyes) and LCHADD (n=3 eyes) RPE. While not statistically significant (p=0.11), LCHADD mice trend toward larger mitochondria than WT. Statistics were calculated using a nested t-test. (D) There was no difference in the mitochondrial copy number of 12-month WT (n=4) and LCHADD (n=4) RPE/sclera. Statistics were calculated using a two-tailed T-test.

| DEG with -log10(adj p-value)>2 | | |
|---|---|---|
| **Gene** | **log10(Fold change)** | **-log10(adj p-value)** |
| Pde10a | 0.668510184 | 17.94811901 |
| Egr1 | -1.024054017 | 13.88853934 |
| Egr2 | -1.162715397 | 13.43977612 |
| Arc | -0.933497295 | 9.892134634 |
| Nr4a1 | -0.977054107 | 9.789660128 |
| Egr3 | -1.463945711 | 8.360534541 |
| Slc25a25 | -0.30267469 | 5.802827659 |
| Mitf | -0.29405198 | 4.97309374 |
| Myh2 | -0.80742496 | 4.411364701 |
| Errfi1 | -0.407837188 | 3.122906931 |
| Srf | -0.206117621 | 2.988229353 |
| Dusp1 | -0.633690292 | 2.967839128 |
| Ptgs2 | -0.529010862 | 2.534359789 |
| Dusp8 | -0.300325298 | 2.279426111 |
| Csrp3 | -0.657163733 | 2.242659713 |
| Lrrc30 | -0.638548796 | 2.051352381 |

**Supplemental Table 4-1: Significant differentially expressed genes (DEGs) in LCHADD mice.** Table of all significant DEGs in LCHADD mice. These genes have a -log10(adj p-value)>2 and are all the points highlighted in Figure 6C.

## Discussion

LCHADD is a rare, long-chain FAO disorder that was first reported in 1989 and affects between 1:250,000 to 1:750,000 people depending on location.[16,19,233] With more LCHADD patients living past infancy due to early detection and better treatments, patients must cope with chronic, later-onset symptoms such as chorioretinopathy which are not well researched nor preventable. Studying the molecular mechanisms involved in LCHADD chorioretinopathy will not only allow for the development of a better treatment, but it will elucidate the role of FAO in the RPE, a current area of research, and identify other pathogenic mechanisms that result in retinal degeneration. Results presented here show that the recently reported LCHADD mouse model recapitulates early-stage LCHADD chorioretinopathy in patients and provides a model to study the molecular mechanisms involved in LCHADD chorioretinopathy.

The causes of LCHADD chorioretinopathy are currently unknown; however, many believe that an accumulation of toxic intermediates and/or an energy deficiency contribute to RPE degeneration. Recent research suggested that fatty acids are a major energy source in RPE and the loss of FAO in RPE cells disrupts the energy production in RPE. This negatively impacts the metabolic homeostasis in the retina, eventually leading to retinal degeneration.[59-12] This hypothesis is challenged by the observation that LCHADD is the only FAO disorder that presents with chorioretinopathy. If an impaired FAO is sufficient in causing retinal degeneration, then one would expect other FAO disorders to also present with retinopathy. Since LCHADD is also the only FAO disorder that accumulates long-chain hydroxyacylcarnitines, it is hypothesized that hydroxyacylcarnitines are toxic to RPE cells. Previous reports have negatively correlated

the sum of hydroxyacylcarnitines in plasma of LCHADD patients with visual acuity.[43] In our results, we see no change in acetyl-CoA levels but a significant accumulation of hydroxyacylcarnitines in RPE/sclera from 15-month LCHADD mice. Acetyl-CoA is an important metabolic intermediate that regulates many cellular processes and signal transduction, so the levels of acetyl-CoA may reflect the metabolic state of the cells. As we do not see a decrease in acetyl-CoA levels, our data suggests that energy deficiency may not play a major role in LCHADD chorioretinopathy. In contrast, the higher level of hydroxyacylcarnitines is associated with vision loss indicating they are potentially toxic to the RPE. It is important to note that many different metabolic processes create and utilize acetyl-CoA and subcellular compartmentalization of acetyl-CoA can be a better gauge of cellular state[234]; therefore, more experiments need to be performed to confirm our findings including direct measurements of energy state, such as ATP, Krebs cycle intermediates, and lactate. In addition, while we expect hydroxyacylcarnitine accumulation in young mice because it can be detected in newborn LCHADD patients, acylcarnitine concentrations will need to be measured in RPE/sclera from 3 to 6-month-old mice to determine how they change overtime.

We show chorioretinopathy in the LCHADD mouse is initiated by RPE degeneration and there is increased macrophage presence in the subretinal space. Both findings are similar to what has been observed from patient studies[53,220]; however, this mouse model provides detailed information on the structural changes in LCHADD RPE. Our results suggest LCHADD RPE cells may be losing polarity and barrier function in LCHADD chorioretinopathy. RPE polarity is crucial in allowing the RPE to regulate

transport, whether that be through trafficking proteins to the apical or basal membrane, melanosome movement, or phagocytosing photoreceptor outer segments.[235] The apical microvilli and basal infoldings play a role in regulating transport with the choroid and photoreceptor outer segments and many important proteins are localized to the apical or basal membranes.[236] The loss of the basal infoldings and apical microvilli suggest that transport and integrity of the cell boundaries are compromised (Figure 4-5). This compromised transport and loss of barrier function can result in abnormal uptake, such as the increased presence of vacuoles seen in Type 2 RPE, and loss of boundaries and structure of RPE cells, as seen from the loss of rigidity in Type 3 RPE. The altered structure can result in RPE dysfunction and, eventually, degeneration. The downregulation of *Mitf* further supports RPE dysfunction and loss of boundary formation as this gene has been shown to be crucial in RPE development and differentiation and transepithelial transport.[229,230] Overall, the LCHADD mouse chorioretinopathy mirrors what has been observed in LCHADD patients and provides a useful model to study the molecular mechanisms involved with the chorioretinopathy.

Unexpectedly, we do see some retinal degeneration in the WT mice at 12-months of age. One possible explanation could be natural degeneration in C57BL/6J mice, which is the background of the LCHADD mice.[237] Another potential explanation could be a result of phototoxicity.[238] While the mice were housed in conditions where they were exposed to less than 6 lux of light, which is known to not cause phototoxicity, they could have been exposed to high light intensities during transportation or testing that caused damage. Finally, while none have been identified yet, this mouse line could be more

susceptible to retinal degeneration because of off-target mutations introduced by CRISPR/Cas9, which was used to create this LCHADD line[133]. This is an important factor to consider for future experiments on older mice.

This study has a few limitations. First, the progression of chorioretinopathy in the LCHADD mouse is slower and less severe when compared to patients. Patients with LCHADD present with chorioretinopathy usually in the first decade and quickly progress to the loss of the photoreceptors. This is evident as retinal thinning seen using OCT.[54] In this mouse model, we did not see a significant change in the photoreceptor layer nor any discernable changes in OCT, indicating that even at 12-months of age the LCHADD mice have early-stage chorioretinopathy (approximately stage 2A).[55] One potential explanation for this is that the mice are not stressed. During their 12-months, these mice had no metabolic crises initiated from exercising/fasting/illness, which are commonly seen in patients. Maintaining a low-fat diet (~10% of caloric intake) and avoiding metabolic crises have been shown to delay or slow the progression of the chorioretinopathy in patients, suggesting that these moments of stress accelerate the progression potentially by significantly increasing hydroxyacylcarnitine levels.[43,45,46] As these mice were never stressed (fasted/exercised/sick) and they normally eat a low-fat diet (~16% of calories provided by fat; Formulab Diet 5008, Irradiated), it is possible they are not being sufficiently challenged and we could potentially accelerate the progression by stressing the mice. Another limitation is that LCHADD patients can develop choroid neovascularization (CNV).[239,240] While we report here that LCHADD mice have increased vacuoles in the choroid and many DEGs in LCHADD mice have been reported to play a

role in angiogenesis and vasculature, the quality of the choroid was outside of the scope of this paper.[222-226,230] Therefore, it will be important to use appropriate techniques, such as OCT angiography, to assess the vasculature of this LCHADD mouse.

Because the current dietary treatment does not prevent LCHADD chorioretinopathy, this LCHADD mouse model will be crucial in the development of new retinal-specific treatments. Gene therapy has been investigated as a potential treatment for FAO disorders and is a promising treatment for LCHADD chorioretinopathy.[175-177,181] Because LCHAD is an autosomal recessive, monogenic disorder that is caused by a loss of LCHAD activity, adding a functional *HADHA* gene to the RPE may be sufficient in preventing the chorioretinopathy by restoring LCHAD activity and FAO in the retina and, ultimately, decreasing hydroxyacylcarnitines. This model will allow us to evaluate gene therapy as a potential treatment for LCHADD chorioretinopathy.

## Conclusion

Overall, we report that the new LCHADD mouse model develops early-stage chorioretinopathy and is a promising model when studying LCHADD chorioretinopathy. Similar to humans, chorioretinopathy in LCHADD mice is likely initiated by a loss of the RPE layer. This study provides evidence of the RPE losing barrier function and polarity, as seen on TEM and RNA-seq. While there is some optimization required with this model, such as increasing the rate of progression, this model will advance chorioretinopathy research and ultimately test the efficacy of therapies that can preserve visual function for patients living with LCHADD.

## Methods

### Animal Model

All animal procedures were reviewed and approved by the OHSU IACUC (eIACUC #B11243). Experiments were performed in accordance with AAALAC and ARRIVE guidelines. Experiments, except RNA-seq, was conducted using WT and LCHADD mice of mixed sex as no sex-specific differences were seen.

### Visual Acuity using Optokinetic Tracking (OKT)

OKT was performed as previously described with a camera calibrated to 22.08 pixels/cm.[133] Right and left eyes were tested and recorded separately.

### Fundus Photography

Mice were anesthetized with an intraperitoneal (IP) injection of ketamine (90 mg/kg) and xylazine (9 mg/kg) followed by an injection of 20% dextrose (10 μL/kg). Eyes were dilated prior to imaging with 1% atropine, 1% tropicamide, and 2.5% phenylephrine, then lubricated with 0.3% hypromellose eye gel. Fundus imaging performed same as previously described.[133] After imaging, mice were administered an IP injection of atipamezole (1 mg/kg) and 0.5% erythromycin ophthalmic ointment then placed on a heating pad.

### Spectral Domain Optical Coherence Tomography (SD-OCT)

Mice were anesthetized and the eyes dilated same as above. SD-OCT images were acquired with the SPECTRALIS HRA+OCT (Heidelberg Engineering; Heidelberg, Germany)

using a 55° lens. Fifteen linear horizontal B-scans generated from 1024 A-scans and averaging 50±2 frames were captured across the IR retinal image. B-scans at approximately -1320, -220, 0, 220, 1320 microns from the center of the optic nerve head were manually segmented to obtain the average thickness of the photoreceptors and RPE (Heidelberg Eye Explorer, v1.10.12). Thickness was compared between LCHADD and WT retinas. Post-testing animal care was the same as above.

**Tissue Sectioning and Staining**

Whole globes from 12-month mouse eyes were enucleated, fixed in 4% paraformaldehyde (PFA), dehydrated in 30% sucrose, embedded in optimal cutting temperature (O.C.T) compound, and snap-frozen. Embedded globes were sliced into 12 μm thick retinal cross sections (except for H&E) on a cryostat (Leica CM1860; Wetzlar, Germany) and stored at -20°C. All cryosections were thawed and rehydrated in 1X PBS prior to staining.

*Hematoxylin and Eosin (H&E) Staining*

Retinal cryosections were stained with H&E and viewed on a Leica DMI3000B microscope (Leica Microsystems GmbH, Wetzlar, Germany) using the 40X objective. Chorioretinal phenotypes observed across each eye were characterized and frequencies of each phenotype was compared between WT and LCHADD samples.

*Immunofluorescence (IF) on Retinal Cross Sections*

For RPE65 staining, cryosections were permeabilized in 0.1% Triton X-100, blocked with 1% bovine serum albumin (BSA), and incubated in a recombinant rabbit anti-RPE65 primary antibody (1:100 dilution; Abcam, ab231782). For CD68 staining, cryosections were permeabilized and blocked in 1% BSA/0.3% Triton X-100 and incubated in a rabbit anti-CD68 (1:100 in 1% BSA/0.3% Triton X-100; Invitrogen, PA5-78996) primary antibody. All sections were incubated with a donkey anti-rabbit Alexa Fluor 647 (1:500 dilution; Invitrogen, A-31573) secondary antibody followed by DAPI.

Cross-sections were mounted using Fluoromount-G and imaged with a Leica Microsystems TCS SP8 X confocal system. Z-stacks were taken at 1 μm intervals. Post-imaging processing was conducted using ImageJ.

*TUNEL Staining:*

Sections were stained with fluorescein-labeled dUTP according to manufacturer's protocol (Elabscience Bionovation; E-CK-A420). Slides were counter-stained with DAPI and mounted with Fluoromount-G. Imaging and post-imaging processing was conducted as described in IF section.

**Transmission Electron Microscopy**

12-month mice were anesthetized using isoflurane and perfused by flushing with PBS and administering fresh, EM-grade fixative (5% glutaraldehyde/2% paraformaldehyde in PBS; Electron Microscopy Sciences, cat #: 16220 and 15713). Mice were enucleated, the lens were removed, and samples were stored in fixative at 4°C.

Samples were processed in a Pelco Biowave Pro+ microwave with a SteadyTemp Pro chiller. The tissue was stained with an aqueous solution of 2% osmium tetroxide and 1.5% potassium ferricyanide, followed by staining with 1% uranyl acetate. The tissue was dehydrated in an increasing acetone series followed by infiltrated in EMbed812 resin. The tissue was flat embedded in coffin molds and polymerized in a 60°C oven. Once polymerized, the capsules were removed and sectioned. Sections were collected on slot grids and imaged on a Tecnai T12 transmission electron microscope equipped with an AMT Nanosprint12 camera, at 120kV.

**Acylcarnitine Detection**

15-month mouse eyes were enucleated and RPE/sclera was isolated.[241] The samples were flash frozen in liquid nitrogen and stored at -80°C. Samples were resuspended in sterile 1X PBS and homogenized using a pellet pestle motor and brief sonication. Acylcarnitines were analyzed by flow injection analysis tandem mass spectrometry (FIA-MS/MS) and quantified as previously published.[242,243]

**RNA-sequencing**

RPE/sclera of 12-month mice were isolated and stored like Acylcarnitine Detection samples. Samples were mechanically disrupted with the TissueLyser in QIAzol, run through a QIAshredder, and incubated in Proteinase K. RNA was isolated following RNeasy Micro (Qiagen, 74104) protocol with modifications added for fibrous tissue and

an on-column DNase treatment using a QIAcube isolation robot. RNA was eluted in nuclease-free water.

Bulk RNA-seq libraries were prepared using the TruSeq Stranded mRNA Library Prep Kit (Illumina). Briefly, RNA was profiled for integrity on a 2200 Bioanalyzer (Agilent). Poly(A)+ RNA was isolated using oligo-dT magnetic beads and then fragmented using divalent cations and heat. Fragmented RNA was converted to double stranded cDNA using random hexamer priming. The second strand was synthesized with dUTP in place of dTTP to prevent priming from this strand during amplification. The cDNA was ligated to adapters with dual unique indexes and amplified by limited rounds of polymerase chain reaction. The amplified material was cleaned using AMPure XP Beads (Beckman Coulter). The final library was profiled on a 4200 Tapestation (Illumina) and quantified using real time PCR with an NGS Library Quantification Kit (Roche/Kapa Biosystems) on a StepOnePlus Real Time PCR Workstation (Thermo/ABI).

Libraries were sequenced on a NovaSeq 6000 (Illumina) running RTA v3.4.4. BCL files were demultiplexed using bcl2fastq v2.20.0.422 (Illumina). Sequencing quality was checked with FastQC (Babraham Bioinformatics). Libraries were trimmed using Trimmomatic 0.36 (Bolger et al 2014, Bioinformatics 30, 2114-2120), then aligned using STAR 2.5.0a (Dobin et al. 2013, Bioinformatics 29, 15-21) and reference genome GRCm38. SAMtools 1.5 (Li et al. 2009, Bioinformatics 25, 2078-2079) was used to generate the bam formatted alignment.

RNA-seq was analyzed using the Galaxy Project.[244] "Reference-based RNA-Seq data analysis" and "Visualization of RNA-Seq results with Volcano Plot" tutorial was followed.[245-248]

## Mitochondrial Analysis

The size of the mitochondria was calculated by tracing mitochondria on TEM images (6800x magnification) and measuring the area using FIJI. 4 TEM images per eye were counted, the total number of mitochondria counted per animal ranged from 54-130, and the total number of mitochondria counted for WT and LCHADD animals were 276 and 266 mitochondria.

The mitochondria copy number was determined by isolating DNA from RPE/sclera using the DNeasy Blood and Tissue Kit (Qiagen, 69504). Quantitative PCR was performed using DNA, forward/reverse *Mt-Nd6* and *Polb* primers[249], and Power SYBR Green PCR Mastermix (ThermoFisher Scientific, 4368708) on a QuantStudio 5 Real-Time PCR System (Thermofisher). Amplification was performed at 95°C for 10 mins, followed by 40 cycles of 95°C for 15 s, 53°C for 15 s, 60°C for 45 s. The relative mitochondrial copy number was calculated as previously published.[250]

### Statistical Analysis

Statistical analysis was performed using GraphPad Prism 10.2 software. All data is presented as mean ± SD. Different statistical tests used include one-way ANOVA, unpaired two-tail T-test, a nested T-test, and a mixed-effects model. A Sidak's multiple

comparison post-hoc test was added when needed and figures indicate when each test was used. P-values of less than 0.05 were considered statistically significant.

**Acknowledgements**

H&E staining was supported by the Leonard Christensen Eye Pathology Laboratory at Casey Eye Institute at OHSU. TEM imaging was supported by the Multiscale Microscopy Core at OHSU. RNA isolation and RNA-sequencing was supported by the OHSU Gene Profiling Shared Resource and OHSU Massively Parallel Sequencing Shared Resource. Acylcarnitine detection was conducted by the Biochemical Genetics Laboratory at the Mayo Clinic.

## Funding

This study was funded by the generous support of the Scully-Peterson foundation; the National Eye Institute (RO1EY032889); an unrestricted grant from Research to Prevent Blindness New York, NY; NIH P30 EY010572 Core Grant; and the Malcolm M. Marquis, MD Endowed Fund for Innovation to Casey Eye Institute, Oregon Health & Science University.

**Disclosure Statement**

The authors have nothing to disclose.

# Chapter 5 : Gene Addition as a Potential Treatment for LCHADD Chorioretinopathy

**Gene Addition as a Potential Treatment for LCHADD Chorioretinopathy**

Shannon J. Babcock[1], Allison G. Curtis[2], Garen Gaston[1], Gabriela Elizondo[1], Renee C. Ryals[1,2], Melanie B. Gillingham[1]

[1]Department of Molecular and Medical Genetics, Oregon Health & Science University, Portland, Oregon, USA, [2]Casey Eye Institute, Oregon Health & Science University, Portland, Oregon, USA

*Unpublished data*

## Author Contributions

**SB was responsible for construction and validation of CAG-mHadha-3XFLAG plasmid, packaging and tittering of AAV5-CAG-mHadha-3XFLAG, dosage experiments, visual assessments (OKT, fundus imaging/OCT, ERG), acylcarnitine detection in RPE/sclera, RPE flatmount staining, and writing**. AC was involved in subretinal injections, visual assessments (fundus imaging/OCT), and H&E staining. GG and GE were involved with breeding, colony management, and revisions. MG was involved with experiment design, funding, and revisions. RR was involved with experiment design, subretinal injections, funding, and revisions.


## Abstract

Purpose: Gene therapy is a widely studied treatment for fatty acid oxidation disorders (FAODs) and retinal dystrophies, making it a potential treatment for long-chain 3-hydroxyacyl-CoA dehydrogenase deficiency (LCHADD) chorioretinopathy. We evaluate the efficacy of retinal pigment epithelium (RPE) gene addition in preventing LCHADD chorioretinopathy by comparing the visual performances of wildtype (WT) and LCHADD mice treated with a WT *Hadha* or phosphate buffered saline (PBS).

Methods: 2-month WT and LCHADD mice were subretinally injected with PBS or $1x10^{10}$ vg/mL of recombinant adeno-associated virus serotype 5 (rAAV5) that encodes a WT mouse *Hadha* (AAV5-CAG-*Hadha*-3XFLAG). Optimal dosing was determined by subretinally injecting AAV5-CAG-*Hadha*-3XFLAG in LCHADD heterozygous mice at different doses. After one-month, optimal dose was determined as the dose that transfected the majority of RPE without signs of toxicity. Visual assessments, such as

optokinetic tracking and fundus imaging, were performed at 12-months. Successful transfection of the RPE was assessed by measuring acylcarnitine concentrations in isolated RPE/sclera and using immunofluorescence on RPE flatmounts to detect the presence of the transgene.

Results: LCHADD mice treated with AAV5-CAG-*Hadha*-3XFLAG had preserved visual performance and less RPE degeneration compared to untreated mice. Transfected LCHADD RPE/sclera had decreased hydroxyacylcarnitine concentrations compared to untreated LCHADD RPE/sclera suggesting partial restoration of fatty acid oxidation (FAO).

Conclusions: Preliminary evidence suggests that adding a WT *Hadha* to LCHADD RPE slow LCHADD chorioretinopathy progression in LCHADD mice.

## Introduction

Gene therapy is a promising and widely studied strategy for treating monogenic disorders, including fatty acid oxidation disorders (FAODs). There have been many preclinical studies that have shown promising evidence of gene addition improving outcomes in FAOD mouse models, such as decreasing lipid accumulation and circulating acylcarnitine levels.[175-180] Episomal gene addition treatments for retinal dystrophies have been widely researched as a long-term treatment because the retina is made up of post-mitotic cells, and thus will maintain the transgene overtime. The retina is also an ideal target tissue because it can be treated directly with subretinal injections at a lower dosage, outcomes that assess efficacy of the treatment are easy to measure, and it is a sequestered tissue due to the blood-retinal barrier so less virus will be found in circulation. Gene addition has also been investigated in many clinical trials. Examples

that treat the retina, including the RPE, are Luxturna, which is the first FDA-approved gene addition treatment for patients with RPE65-mediated retinal dystrophy, and timrepigene emaparvovec, a treatment for choroideremia that reached a phase 3 clinical trial.[73,251] LCHADD chorioretinopathy would, therefore, be a perfect candidate for gene addition because it is a symptom of a monogenic disorder that can be treated by adding a functional *HADHA* gene directly to the retina.

There are many different delivery vehicles that can be used in gene therapy, but the most common delivery vehicle for gene addition is packaging the transgene into a recombinant adeno-associated virus (rAAV). The AAV2/5 serotype (AAV5) has been shown to successfully transduce human pluripotent stem cell-derived RPE, retinal pigment epithelium (RPE) and photoreceptor cells when subretinally injected in rodent models, and has been used in clinical trials.[252-254] Therefore, using AAV5 allows for these preclinical gene addition experiments to better translate into potential clinical trials.

In this chapter, we evaluate the effect of gene addition in preventing chorioretinopathy in the LCHADD mouse model. Specifically, we detail the successful construction and packaging of a mouse WT *Hadha* construct into AAV2/5, describe the dosage experiments used to identify the optimal dose for a subretinal injection, and provide evidence that suggests gene addition could be a potential treatment for LCHADD chorioretinopathy.

## Results

*Construction and packaging of AAV5-CAG-Hadha-3XFLAG*

A plasmid encoding the mouse *Hadha* gene was created where *Hadha* was constitutively expressed using a chicken beta-actin (CAG) promoter and three FLAG tags were attached on the C-terminus of the TFPα protein to allow for identification of the transgene product. AAV2 inverted terminal repeat sequences (ITRs) bookend this construct to allow for packaging into an AAV (Figure 5-1:A). Restriction digests were conducted to ensure the proper plasmid was created and Sanger sequencing ensured no mutations occurred in the *Hadha* gene (data not shown). To determine if a stable TFPα protein is made and could be detected, Hek293 cells were transfected with the construct. Immunofluorescence on transfected cells show that FLAG expression can be detected and that it co-localizes with TFPα (Figure 5-1:B; Supplemental Figure 5-1). Western blotting also shows that only cells transfected with the plasmid express FLAG and that the TFPα level is increased in those cells (Figure 5-1:C; Supplemental Figure 5-2). Overall, this confirms that the plasmid translates a stable TFPα protein that can be detected using FLAG antibodies. This vector was packaged into an AAV2/5 delivery system to allow for in vivo transfection of mouse RPE cells.

*Optimal Dose for Gene Addition is 1 μL of $1x10^{10}$ vg/mL of AAV5-CAG-Hadha-3XFLAG*

Dosage experiments were conducted to determine the dose of AAV5-CAG-*Hadha*-3XFLAG that allows for high transfection of the RPE but does not cause toxicity. LCHADD heterozygous mice were used because they do not present with any LCHADD phenotypes and can provide a healthy model that is of similar background as LCHADD

mice. LCHADD heterozygous male mice were subretinally injected with 1 μL of PBS, $1x10^{10}$, or $1x10^{11}$ vg/mL of AAV5-CAG-*Hadha*-3XFLAG at 2-months of age. One month after injection, eyes were analyzed for RPE toxicity, transfection efficiency, and localization of the transgene.

To look at RPE toxicity and transfection efficiency, RPE flatmounts were stained with an antibody against FLAG to detect presence of the transgene and phalloidin, which outlines the cell membrane of the RPE. As RPE cells are hexagonal, RPE toxicity is seen when RPE cells lose the hexagonal shape. Eyes injected with $1x10^{10}$ vg/mL retain the hexagonal shape whereas $1x10^{11}$ shows more abnormal RPE (Figure 5-2:A). This indicates that the $1x10^{10}$ vg/mL dose is not toxic to the RPE whereas the $1x10^{11}$ vg/mL dose shows some toxicity. Transfection efficiency was approximately the same between $1x10^{10}$ and $1x10^{11}$ vg/mL (23% vs 20%) suggesting $1x10^{10}$ vg/mL can transfect the same amount of RPE without causing the toxicity seen in $1x10^{11}$ vg/mL (Figure 5-2:B and Supplementary Method 5-1). Finally, transgene localization was determined by staining retinal cross sections with a FLAG antibody. Both $1x10^{10}$ and $1x10^{11}$ vg/mL resulted in transfection of predominantly the RPE layer (Figure 5-2:C). Overall, the optimal dose of AAV5-CAG-*Hadha*-3XFLAG was determined to be $1x10^{10}$ vg/mL because it was not toxic to the RPE, had good transfection, and transfected predominantly the RPE layer.

*Gene Addition as a Potential Treatment for LCHADD Chorioretinopathy*

In order to evaluate gene addition as a potential treatment for LCHADD chorioretinopathy, 2-month-old LCHADD and WT mice of mixed sex were administered a subretinal injection of 1 μL of $1x10^{10}$ vg/mL of AAV5-CAG-*Hadha*-3XFLAG or 5% sorbitol

in PBS. Optokinetic tracking (OKT) was conducted on mice at 6, 10, and 12-months of age to measure visual performance. Other visual assessments, such as fundal images, optical coherence tomography (OCT), and electroretinograms (ERG) were taken when untreated LCHADD mice had a significantly decreased visual performance, which happened to occur at 12-months of age (Figure 5-3:A).

Unexpectedly, when fundal images were taken at 12-months of age, there were many problems on the eyes that affect visual assessments, such as corneal abrasions, foggy vitreous/nicked lens, and extreme retinal degeneration (Supplemental Figure 5-3). Therefore, only visual assessments from eyes with normal fundal images and OCTs (n=3-6 eyes per group) were analyzed.

OKT results show that at 12-months of age, PBS-treated LCHADD mice have significantly lower visual performance when compared to WT mice. On the other hand, LCHADD mice treated with AAV5-CAG-*Hadha*-3XFLAG had preserved visual performance (Figure 5-3:B). The treatment with AAV5-CAG-*Hadha*-3XFLAG did not affect the WT mice suggesting the treatment did not affect the visual performance, and similar to what was expected, there was no difference between sex.

Treating LCHADD eyes with AAV5-CAG-*Hadha*-3XFLAG may also be protective against RPE degeneration in LCHADD mice as seen by a decreased percentage of virus treated LCHADD eyes that had white, hypopigmented areas on fundus images compared to PBS LCHADD eyes on fundus images (Figure 5-3:C). LCHADD eyes, both PBS and virus-treated, had a higher percentage of eyes with hypopigmentation compared to WT; however, 67% of virus-treated LCHADD eyes displayed areas of hypopigmentation

whereas 100% of the PBS LCHADD eyes had areas of hypopigmentation (Figure 5-3:D). 25% of PBS and virus-treated WT eyes presented with areas of hypopigmentation indicating the injection did not cause RPE degeneration. However, H&E staining on retinal cross sections did not support decreased RPE degeneration (Figure 5-4). Both LCHADD groups had more and worse RPE degeneration compared to WT, but there is no difference between LCHADD eyes treated with AAV5-CAG-*Hadha*-3XFLAG and PBS. One potential explanation for this discrepancy is that the cross-sections used in the H&E did not include the area of the eye that was injected. Overall, these results suggest that treating LCHADD mice with AAV5-CAG-*Hadha*-3XFLAG can slow the LCHADD chorioretinopathy as seen from a preserved visual performance and less RPE degeneration in LCHADD eyes treated with AAV5-CAG-*Hadha*-3XFLAG compared to PBS.

ERG amplitudes, a measurement of retinal cell function, were not different between any of the groups, indicating no photoreceptor degeneration (Supplemental Figure 5-4). OCT, which can be used to assess retinal structure, was also not different between any of the groups, supporting the ERG results (Supplemental Figure 5-5). This is similar to what has been previously reported (Chapter 3 and 4) and suggests that even at 12-months of age, the chorioretinopathy in LCHADD mice have not reached photoreceptor degeneration.

To determine if treating LCHADD eyes with a WT *Hadha* restored FAO, we measured long-chain acylcarnitines from plasma and isolated RPE/sclera of 12-month PBS and virus-treated WT and LCHADD mice (Figure 5-5). As expected in plasma, LCHADD mice had an accumulation of long-chain acylcarnitines, specifically

hydroxyacylcarnitines, and gene addition did not affect circulating acylcarnitine levels (Figure 5-5:A). PBS LCHADD RPE/sclera samples also had an increase in long-chain acylcarnitine concentrations and a 10- and 18-fold increase in C16-OH and C18-OH. LCHADD eyes treated with AAV5-CAG-*Hadha*-3XFLAG had decreased acylcarnitine levels compared to PBS LCHADD mice, although not to WT levels. Specifically, there was a statistically significantly decrease in C18-OH in treated eyes when compared to PBS LCHADD eyes (Figure 5-5:B). Similar to what has been previously reported in Chapter 4, there was no difference in RPE/sclera acetyl-CoA concentrations between any of the groups indicating that energy deficiency may not be involved in the chorioretinopathy (Chapter 4; Figure 5-5:C). Overall, this suggests that the addition of WT *Hadha* to the RPE partially restored FAO and resulted in decreased hydroxyacylcarnitine concentrations in LCHADD mice.

Figures

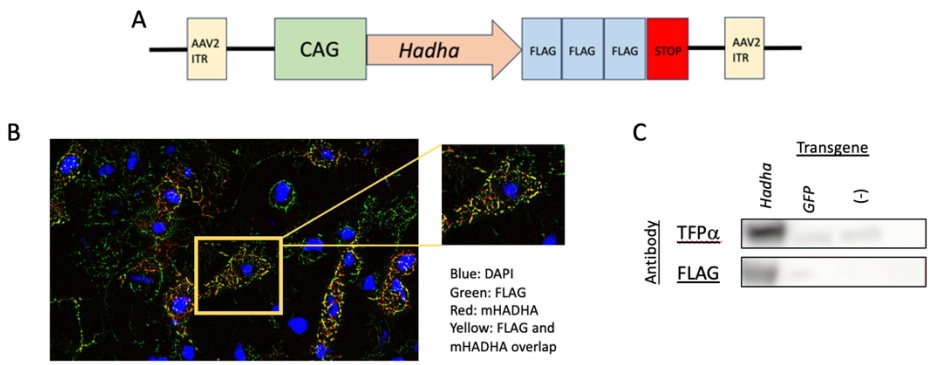


**Figure 5-1: Creation of a pAAV-CAG-*Hadha*-3XFLAG plasmid.** (A) Schematic of the pAAV-CAG-*Hadha*-3XFLAG construct. (B) Immunofluorescence of Hek293 cells transfected with the plasmid showing that FLAG (green) is expressed and co-localizes with TFPα (red). Yellow indicates the co-localization of FLAG and TFPα, and DAPI (blue) represent nuclei. (C) Western blot of Hek293 cells transfected with the pAAV-CAG-*Hadha*-3XFLAG, pAAV-CAG-GFP, or PBS. Results show that only cells transfected with the pAAV-CAG-*Hadha*-3XFLAG express FLAG and there is an increase in the TFPα concentration compared to the other conditions.

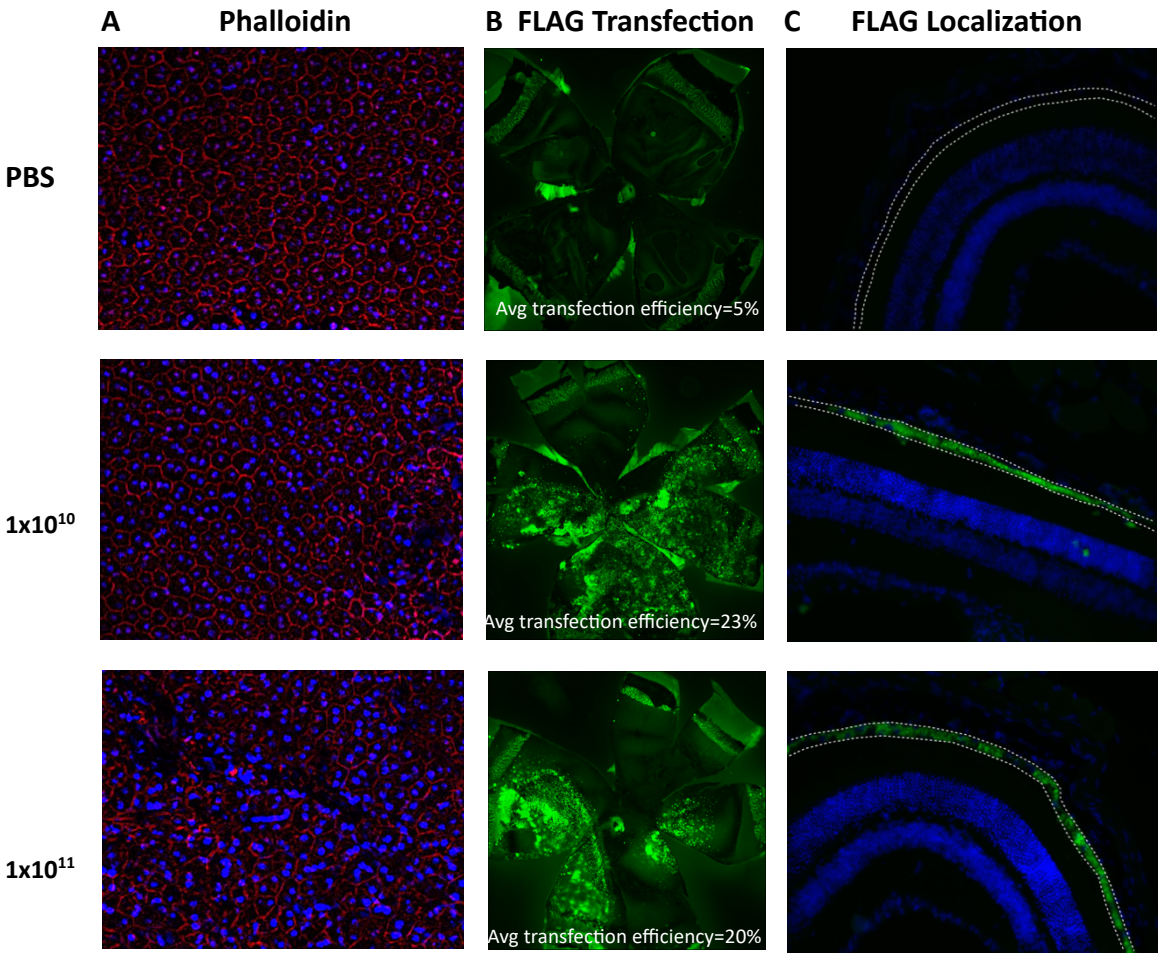


**Figure 5-2: 1x10$^{10}$ vg/mL is the optimal dose of AAV5-CAG-*Hadha*-3XFLAG for a subretinal injection.** LCHADD heterozygous mice were injected with PBS (n=4 eyes), 1x10$^{10}$ vg/mL of AAV5-CAG-*Hadha*-3XFLAG (n=6 eyes), 1x10$^{11}$ vg/mL of AAV5-CAG-*Hadha*-3XFLAG (n=8 eyes), or not injected (n=2 eyes). RPE flatmounts were stained with phalloidin (red) and antibody against FLAG (green) to assess (A) RPE toxicity and (B) transfection efficiency (n=3-4 per treatment). (A) Phalloidin (red) shows that 1x10$^{10}$ vg/mL is not toxic to the RPE whereas the 1x10$^{11}$ vg/mL can be moderately toxic. (B) Eyes treated with 1x10$^{10}$ vg/mL had an average transfection efficiency of around 23% whereas eyes transfected with 1x10$^{11}$ vg/mL was 20%. (C) Retinal cross sections stained against FLAG (green) (n=2-3 eyes per treatment) show that the RPE layer is the predominantly transfected layer at both 1x10$^{10}$ and 1x10$^{11}$ dose. DAPI (blue) indicated nuclei and RPE is indicated by dotted lines.

A

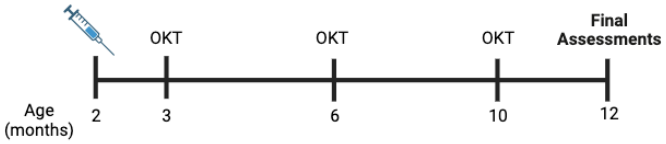


B. Visual Performance

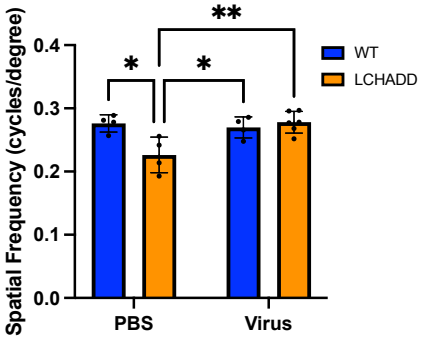


C

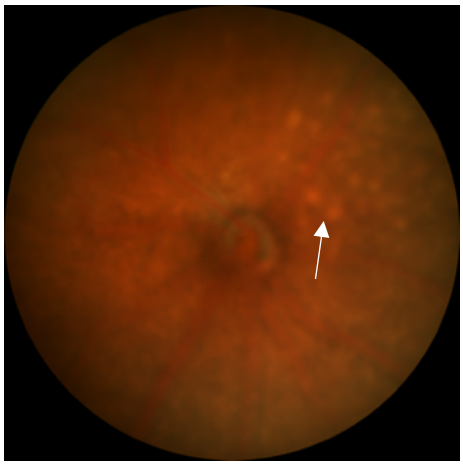

D

| Eyes with Hypopigmentation | |
|---|---|
| WT PBS | **1/4 (25%)** |
| WT Virus | **1/4 (25%)** |
| LCHADD PBS | **4/4 (100%)** |
| LCHADD Virus | **4/6 (67%)** |

**Figure 5-3: Gene addition can limit RPE degeneration and preserve visual performance in LCHADD mice.** (A) Schematic of the experiment. WT and LCHADD mice were subretinally injected with 1 µL $1x10^{10}$ vg/mL AAV5-CAG-*Hadha*-3XFLAG (WT: n=18; LCHADD: n=20) or 5% sorbitol in PBS (WT: n=16; LCHADD: n=14 eyes) at 2-months of age. Both eyes on the mouse were treated the same. Progression of chorioretinopathy was monitored using OKT at 3, 6, and 10-months of age, and the final assessments were collected at 12-months of age. There were problems on many of the eyes that could affect the visual performance, and thus only the eyes that had a clear fundal image were analyzed. (B) Visual performance of PBS treated LCHADD eyes were significantly lower compared to WT mice, and virus treated LCHADD eyes retained visual performance. Data presented as mean spatial frequency ± SD. Statistics calculated using a two-way ANOVA. (C) Fundal images were examined for hypopigmented areas, indicative of RPE degeneration. (D) Treating LCHADD eyes with AAV5-CAG-*Hadha*-3XFLAG did reduce the number of eyes with hypopigmentation compared to untreated LCHADD.

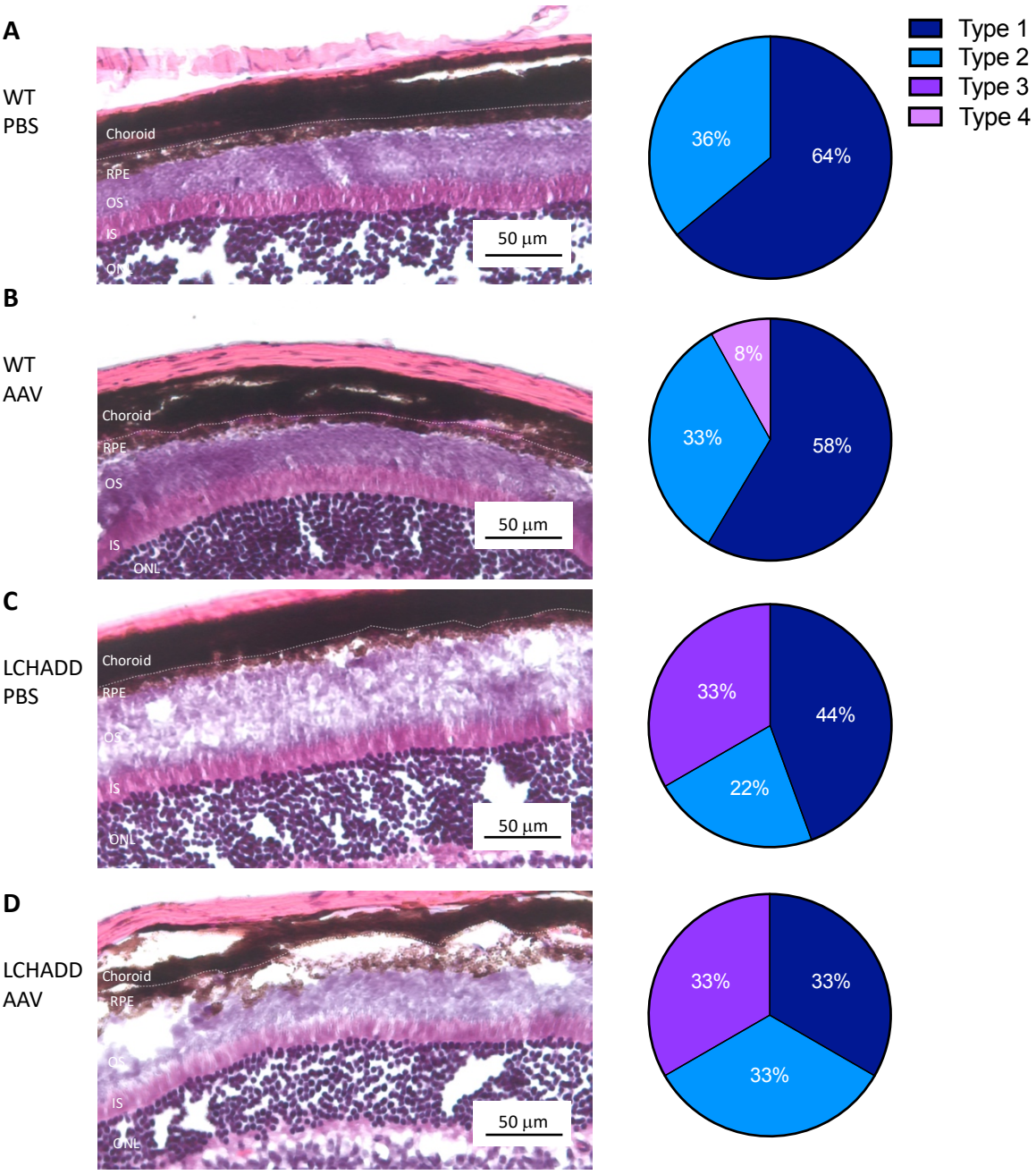


**Figure 5-4: Treated LCHADD eyes have a similar severity of RPE degeneration compared to untreated LCHADD eyes.** (A) Representative images (left) and percentage of each type of RPE (right) for (A) WT eyes treated with PBS, (B) WT eyes treated with AAV5-CAG-*Hadha*-3XFLAG, (C) LCHADD eyes treated with PBS, and (D) LCHADD eyes treated with AAV5-CAG-*Hadha*-3XFLAG suggest LCHADD eyes have increased RPE degeneration compared to WT, but there is no difference between LCHADD eyes treated with PBS and AAV5-CAG-*Hadha*-3XFLAG. The type of RPE is determined using the same criteria as Chapter 4: Type 1=normal; Type 2=Vacuoles in the RPE; Type 3=Loss of rigidity and disintegration of RPE; and Type 4=Loss of RPE layer. White dotted line on H&E staining separates the choroid and RPE layers.

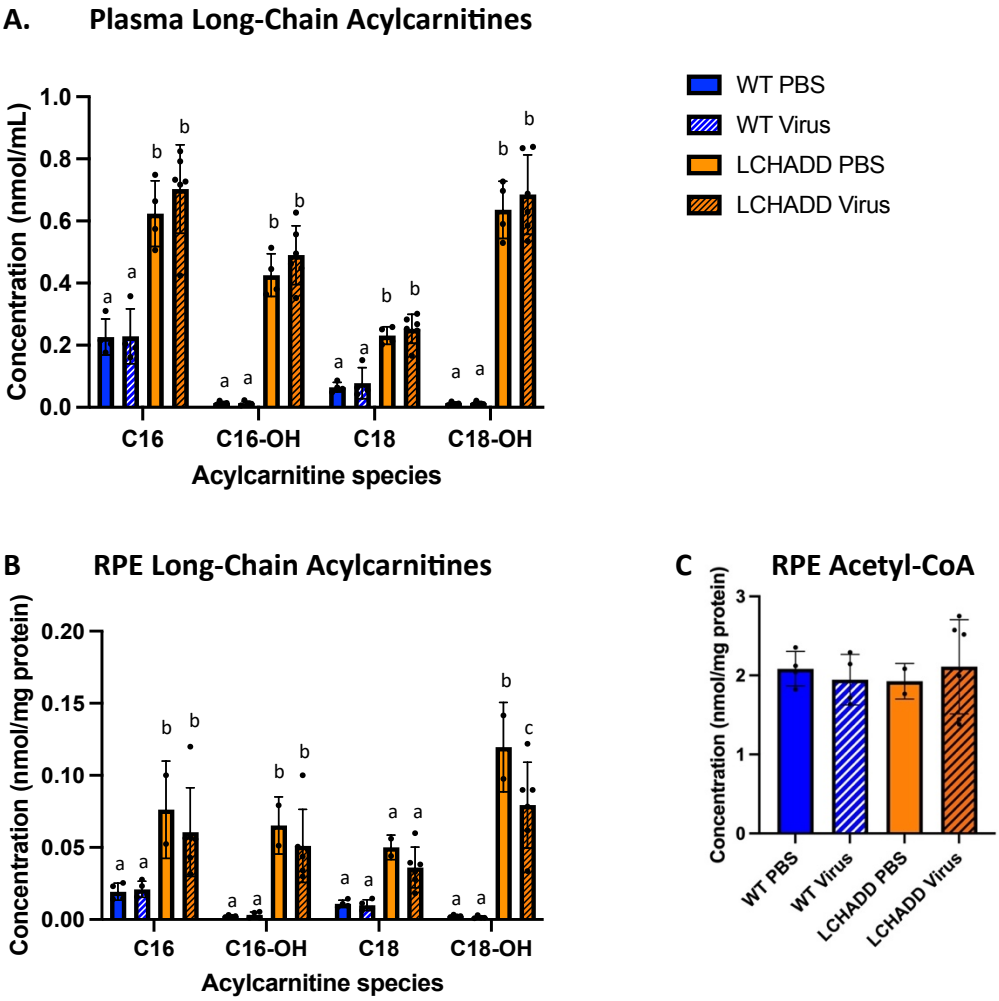


**Figure 5-5: Gene addition partially restored FAO to the RPE/sclera of 12-month LCHADD mice.** Acylcarnitines were measured from (A) plasma and (B) isolated RPE/sclera of 12-month WT and LCHADD mice. (A) As expected, untreated (n=4) and treated (n=6) LCHADD mice had an increase in plasma acylcarnitines compared to untreated (n=4) and treated (n=4) WT mice. (B) RPE/sclera samples from PBS treated LCHADD mice (n=2) had a statistically significant increase in acylcarnitine levels in all species except C18 compared to PBS (n=4) and virus treated (n=4) WT mice. Treated LCHADD RPE/sclera (n=6) had a decrease in acylcarnitines when compared to untreated LCHADD RPE/sclera, except the decrease was only statistically significant with C18-OH. Data is presented as mean concentration ± SD. Statistics were calculated using a two-way ANOVA with multiple comparisons. Bars with same letters indicate no statistically significant difference. For example, bars with "a" are not statistically significant whereas bars with "b" are statistically significant from "a", and "c" is statistically significant compared to "a" and "b".

Supplemental Figures

**A**

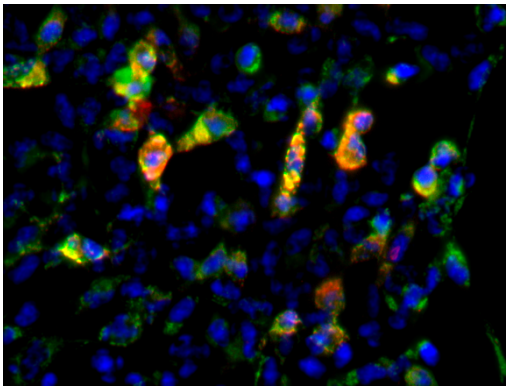

Blue: DAPI
Green: FLAG
Red: TFPα
Yellow/orange: FLAG and TFPα overlap

**B.** Data manipulation in ImageJ Protocol

1. Split channels
2. Blue channel
    - Subtract background: 50 pxls
    - Canvas size: Center 1920x1435
    - Brightness and Contrast Adjustment: 5306-7870
3. Green Channel:
    - Subtract background: 1 pxls
    - Canvas size: Top-center 1920x1435
    - Brightness and Contrast Adjustment: 50-750
4. Red Channel:
    - Subtract background: 1 pxls
    - Canvas size: Bottom-center 1920x1435
    - Brightness and contrast adjustment: 50-500.

**Supplemental Figure 5-1: Original images of Hek293 transfection and image manipulation.** (A) Original image of Figure 5-1: B representing immunofluorescence of Hek293 cells transfected with pAAV-CAG-*Hadha*-3XFLAG plasmid using FLAG and a *Hadha* antibody. The yellow/orange represent co-localization of FLAG and TFPα. (B) The data manipulation protocol using ImageJ for this image.

A


B

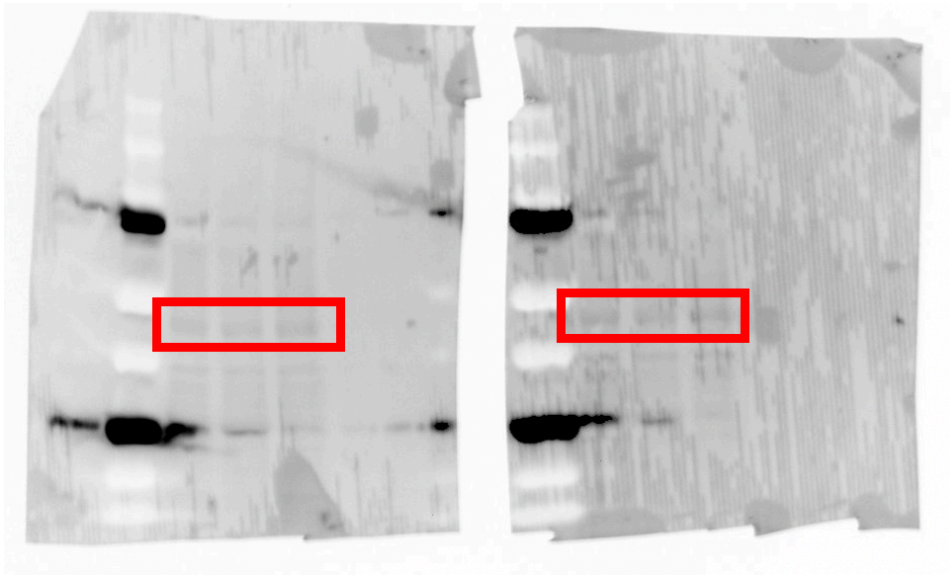

**Supplemental Figure 5-2: Western blot of Hek293 cells transfected with pAAV-CAG-*Hadha*-3XFLAG, GFP, or PBS.** (A) Original blot of membranes blotted with antibodies against FLAG (1:1000) or TFPα (1:1000). (B) The same blots as above imaged as total protein.

A

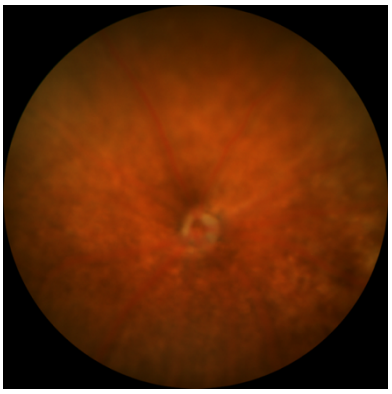

B

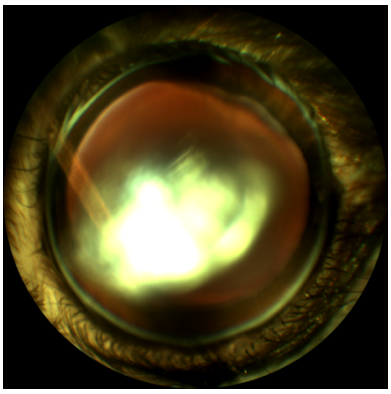

C

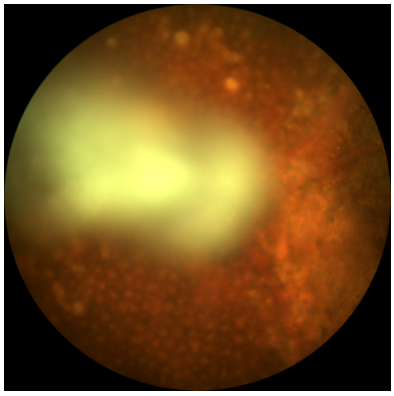

D

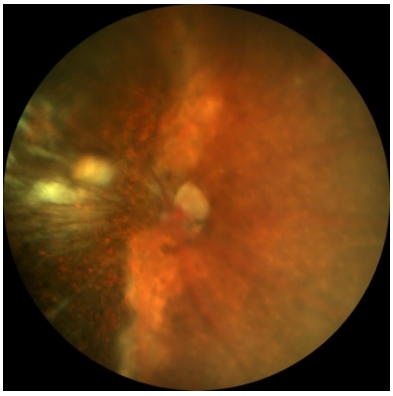

E

| Eye Problems | WT Ratio | LCHADD Ratio |
|---|---|---|
| Corneal Abrasions | 0/32 (PBS=0/14, Virus=0/18) | 6/36 (PBS=3/16, Virus=3/20) |
| Vitreous Problems (Bright spots masking fundus) | 9/32 (PBS=3/14); Virus=6/18) | 8/36 (PBS=5/16); Virus=3/20) |
| Retinal Detachment | 0/32 | 1/36 (Virus) |
| Retinal damage/degeneration | 7/32 (PBS=5/14; Virus=6/18) | 9/36 (PBS=3/16; Virus=6/20) |

**Supplemental Figure 5-3: Different types of fundal images seen in 12-month WT and LCHADD mice.** Fundal images of 12-month WT and LCHADD mice showed many of the eyes had some problems that could affect visual performance. These could be classified into four types: (A) Normal fundus, (B) eyes with corneal abrasions, (C) eyes with foggy vitreous/nicked lens, and (D) eyes with severe retinal degeneration. (E) Quantification of the number of eyes per treatment group show that most of these problems occur evenly between WT and LCHADD mice both treated with AAV5 and PBS, except corneal abrasions, which can be seen exclusively in LCHADD mice.

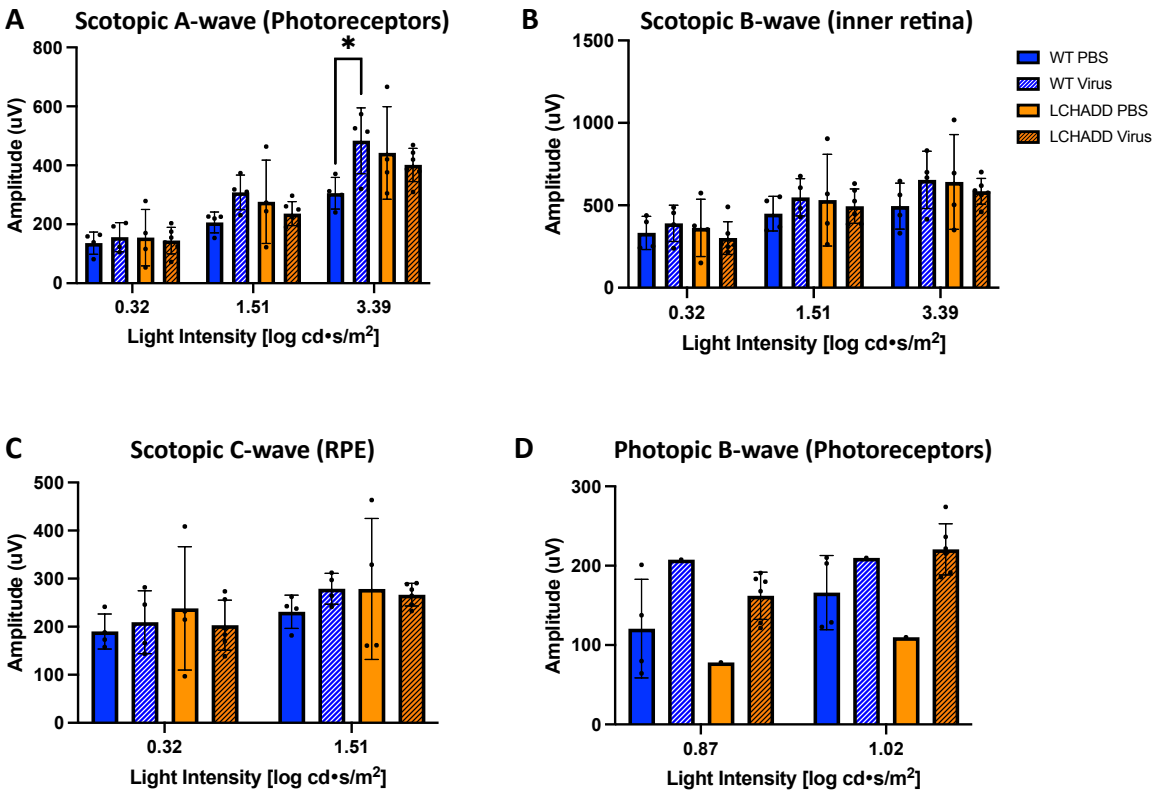


**Supplemental Figure 5-4: There is no difference in retinal cell function between any of the groups at 12-month of age.** ERGs were taken of 12-month untreated WT (n=4), treated WT (n=4), untreated LCHADD (n=4), and treated LCHADD (n=6) mice. (A) Scotopic a-wave, (B) scotopic b-wave, (C) scotopic C-wave, and (D) photopic b-wave amplitudes were not different between any of the groups. Data is presented as mean amplitude ± SD. Stats were measured using two-way ANOVA with multiple comparisons. *p<0.05.

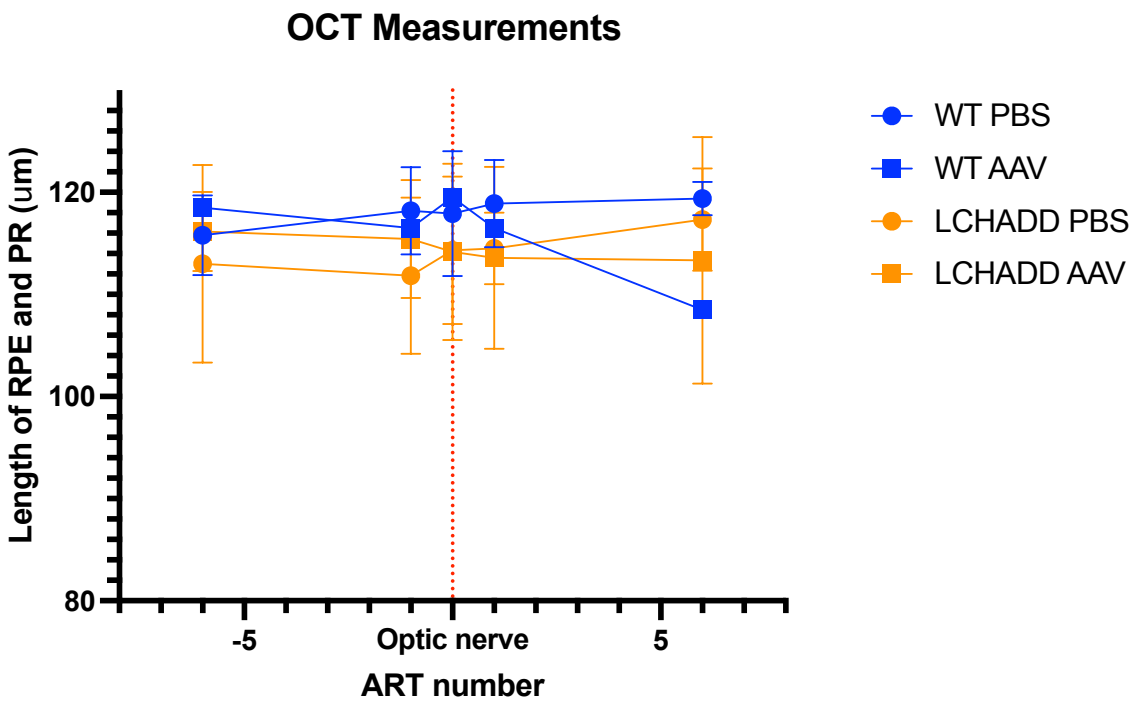


**Supplemental Figure 5-5: No difference in retinal cell structure between any of the groups at 12-month of age.** There was no difference in the length of the photoreceptor and RPE layer between WT PBS, WT virus-treated, LCHADD PBS, and LCHADD virus-treated anywhere in the eye. Measurements were collected same as in Chapter 4 (Figure 4-3:A-B). Data presented as mean ± SD. A two-way ANOVA with multiple comparisons was used to calculate statistics.

**Supplemental Table 5-1: Cloning fragment sequences**

| | |
|---|---|
| Fragment 1: pAAV-CAG-GFP-Backbone-Pst1-mHADHA | TTTTGGCAAAGAATTGGATCCTGCAGATGGTGGCGTCCCGGGCGATTGGCAGTCTCAGTCGCTTCT<br>CTGCCTTCAGGATCCTACGCTCCAGAGGCTGCATTTGCCGCAGCTTTACAACGTCTTCTGCTCTGC<br>TGACCAGAACCCATATTAATTATGGCGTCAAAGGGGATGTGGCAGTTATTCGGATTAACTCACCCA<br>ATTCAAAGGTAAATACATTGAATAAAGAAGTACAGTCAGAGTTCATAGAAGTCATGAACGAAATCT<br>GGGCCAACGACCAAATCAGGAGTGCTGTCCTTATCTCATCAAAGCCTGGCTGCTTTGTCGCAGGG<br>GCTGACATCAACATGCTATCCTCTTGTACAACCCCCCAAGAAGCAACACGAATATCACAGGAAGG<br>TCAGAGAATGTTTGAGAAACTTGAAAAGTCCCCAAAGCCCGTTGTGGCCGCCATCAGTGGATCCT<br>GCTTGGGAGGAGGACTTGAGCTTGCCATAGCATGCCAATACAGAATAGCAACAAAAGACAGAAA<br>AACAGTATTAGGTGTCCCTGAAGTGTTGCTGGGGATCTTACCAGGAGCCGGAGGTACCCAGAGAC<br>TGCCCAAAATGGTGGGTGTGCCTGCTGCATTTGACATGATGCTGACTGGCAGGAACATTCGTGCA<br>GACAGAGCAAAGAAAATGGGACTGGTTGACCAGTTGGTGGAACCGCTGGGACCAGGAATAAAAT<br>CACCAGAAGAAAGGACAATTGAATACCTAGAGGAAGTTGCAGTTAATTTTGCCAAAGGCCTGGCT<br>GATCGGAAAGTCTCTGCAAAGCAGAGCAAAGGCCTTGTGGAAAAGCTGACAACGTATGCCATGA<br>CTGTCCCATTTGTCAGACAACAGGTTTACAAAACAGTTGAAGAAAAAGTGAAGAAGCAGACTAA<br>AGGCCTTTATCCTGCCCCTTTGAAAATAATTGATGCTGTGAAGGCTGGACTTGAGCAAGGCAGTG<br>ACGCTGGTTATCTTGCTGAATCGCAGAAATTTGGAGAGCTTGCATTGACCAAAGAATCGAAGGCC<br>CTGATGGGGCTTTATAACGGCCAGGTCCTGTGCAAGAAAAATAAATTTGGAGCACCACAGAAGAA<br>CGTTCAGCAGCTAGCCATCCTTGGCGCAGGGCTGATGGGGGCTGGCATTGCCCAGGTCTCTGTGG<br>ATAAGGGACT |
| Fragment 2: mHADHA-Spe-3XFLAG-STOP-HindIII-pAAV-CAG-GFP Backbone | AGGTCTCTGTGGATAAGGGACTGAAAACTCTTCTTAAAGACACCACAGTGACGGGGCTGGGCCG<br>GGGACAGCAGCAAGTGTTCAAAGGGCTGAACGACAAAGTGAAGAAGAAAGCTCTCACATCATTT<br>GAAAGGGATTCCATCTTCAGCAACTTGATTGGGCAGCTGGATTACAAAGGCTTTGAGAAGGCCGA<br>CATGGTGATTGAGGCTGTGTTTGAGGACCTCGGTGTAAAGCACAAAGTGTTAAAGGAAGTGGAA<br>AGCGTGACTCCAGAACACTGTATCTTTGCCAGCAACACATCTGCTCTCCCAATCAATCAAATTGCT<br>GCTGTCAGCAAAAGGCCTGAGAAGGTGATCGGCATGCACTACTTCTCCCCCGTGGACAAGATGCA<br>GCTCCTAGAAATCATCACCACTGACAAAACCTCCAAGGACACAACGGCCTCTGCCGTGGCCGTGG<br>GGCTCAGGCAAGGGAAGGTCATCATTGTGGTCAAGGACGGACCCGGCTTCTACACCACCAGGTG<br>TCTTGCACCCATGATGTCTGAAGTCATGCGAATCCTCCAGGAAGGAGTTGACCCTAAGAAGCTGG<br>ACGCCTTGACCACAGGTTTCGGCTTCCCTGTGGGTGCTGCCACGCTGGCAGACGAAGTGGGTGTG<br>GATGTAGCACAGCACGTAGCAGAAGATCTAGGCAAAGCCTTTGGGGAGCGATTTGGAGGTGGCA<br>GCGTAGAACTGCTGAAACAGATGGTCTCCAAGGGCTTCTTAGGTCGCAAGTCTGGGAAGGGCTTT<br>TACATCTATCAGGAGGGCTCAAAGAATAAGAGTTTGAATTCTGAAATGGATAATATCTTGGCAAAT<br>CTGAGGCTGCCTGCCAAGCCCGAGGTCTCCTCTGATGAAGACGTCCAATACCGTGTGATAACAAG<br>GTTCGTGAACGAGGCAGTCCTGTGCCTACAGGAAGGGATCCTGGCCACACCGGCAGAGGGAGAC<br>ATCGGAGCTGTCTTTGGGCTTGGCTTTCCCCCTTGTCTCGGAGGGCCCTTCCGCTTTGTGGATCTG<br>TATGGTGCTCAGAAGGTAGTGGACCGGCTACGGAAGTACGAGTCTGCCTATGGAACACAGTTTAC<br>CCCATGCCAGCTGCTCCTCGACCACGCTAACAACTCTAGCAAGAAGTTCTACCAGttaActagttctgactac<br>aaagaccatgacggtgattataaagatcatgacatcgactacaaggatgacgatgacaagTAAAATTCGATATCAAGCTTATC |

**Supplemental Method 5-1: How to calculate transfection efficiency for dosage experiments**

To calculate the transfection efficiency, the RPE flatmounts were stained with a FLAG antibody (green) to detect the transgene and phalloidin to stain the RPE cell membranes. The percentage of RPE that was transfected was calculated by measuring the area that expressed FLAG by the total RPE flatmount area. In the transfected area, total cells were counted as determined by the phalloidin stain and the number of those cells that also expressed FLAG were counted. The fraction of transfected cells was multiplied by the transfected area divided by the total RPE area to get the transfection efficiency (See equation below).

Equation:

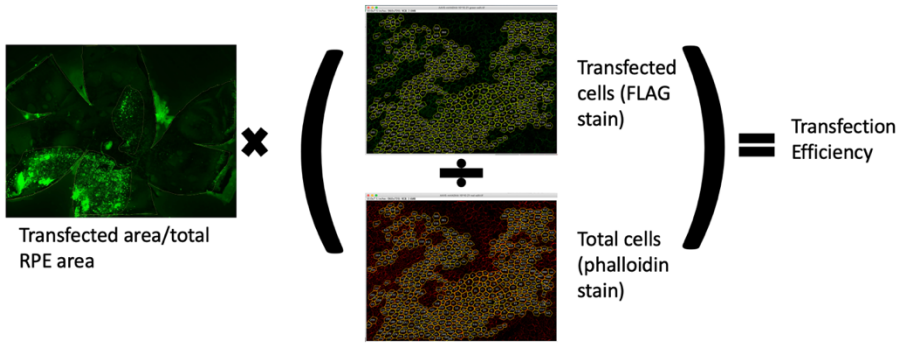


Results:

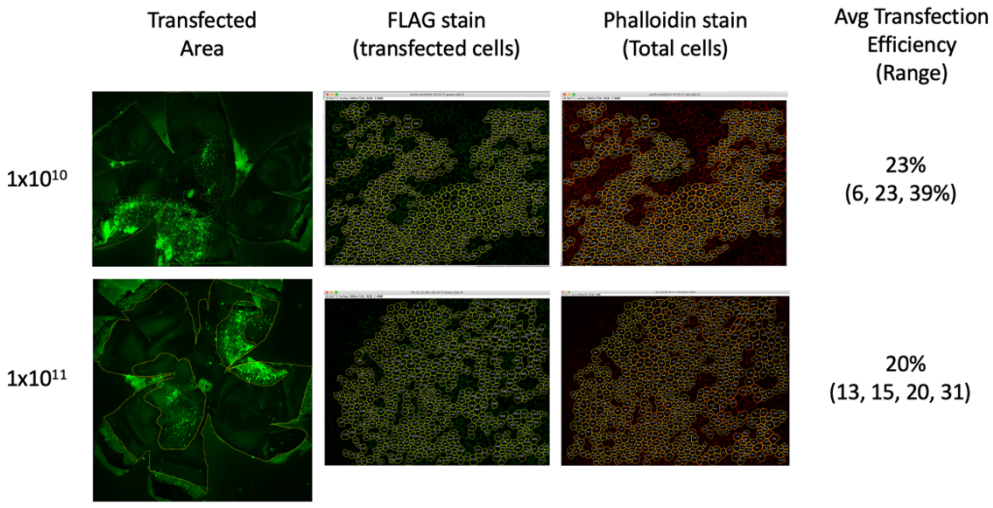

## Discussion

A new retinal-specific treatment for LCHADD chorioretinopathy is needed as patients, even with early intervention, eventually lose vision. LCHADD chorioretinopathy is a perfect candidate for gene addition as it is a monogenic disorder that affects the retina, which are post-mitotic cells that can be directly treated without loss of the transgene overtime. In this chapter, I show preliminary evidence that adding a WT *Hadha* to RPE cells may preserve visual performance and prevent RPE degeneration and that the LCHADD mouse model could be a preclinical trial model for LCHADD chorioretinopathy treatments.

LCHADD chorioretinopathy is believed to be caused by either an energy deficiency or an accumulation of toxic intermediates. This experiment does provide support for the hypothesis that the RPE degeneration is caused by an accumulation of toxic intermediates. For example, LCHADD treated eyes had a preserved visual performance and had decreased hydroxyacylcarnitines compared to untreated LCHADD eyes (Figure 5-5:B). In addition, there is no difference in acetyl-CoA concentrations between treated and untreated LCHADD eyes suggesting that the input into the Krebs cycle is not decreased and energy production may not be different (Figure 5-5:C). As acetyl-CoA is not a direct measurement for energy, as mentioned in Chapter 4, more direct measurements will need to be done in order to confirm energy availability in the retina.

One limitation in this study is the small sample size of healthy eyes per group due to the unexpected problems seen in the eyes (Supplemental Figure 5-3). As the problems can be seen across all the groups and there was no differences based on sex, it

is likely that the cause occurred during the injection process; therefore, future experiments will need to be done using an optimized injection protocol. The low sample size specifically prevented us from determining transfection efficiency in healthy eyes. The dosage experiments suggest a subretinal injection of 1 μL of $1x10^{10}$ vg/mL will result in ~20% transfection efficiency (Figure 5-2); however, it will be important to measure the transfection efficiency in future experiments. These studies will better correlate the transfection efficiency with RPE/sclera hydroxyacylcarnitine concentrations and visual outcomes, and it will provide insight into how much of the RPE needs to be treated in order to prevent the chorioretinopathy.

In conclusion, we show preliminary evidence that gene addition may be able to prevent LCHADD chorioretinopathy in the recently reported LCHADD mouse model. With some optimization this LCHADD mouse model could be an excellent preclinical model to evaluate potential treatments, such as gene addition, for LCHADD chorioretinopathy in patients.

## Methods

### Creation of pAAV-CAG-*Hadha*-3XFLAG

A pAAV-CAG-*Hadha*-3XFLAG plasmid was created using the NEBuilder HiFi DNA Assembly Kit (New England BioLabs, E5520S) with two fragments that encode the mouse *Hadha* gene and 3 FLAG tags (Supplementary Data) and pAAV-CAG-GFP (Gift from Edward Boyden (Addgene, Plasmid #37825)) that had GFP removed using EcoRI-HF and BamHI-HF restriction enzymes. Plasmid was chemically transformed into NEB Stable

Competent *E. coli* cells (New England BioLabs, C3040I). A midiprep was used to increase the amount of plasmid (Macherery-Nagel, 740420.10)

**Immunofluorescence on Hek293 cells**

Hek293 cells were transfected with pAAV-CAG-*Hadha*-3XFLAG using Lipofectamine 2000 (ThermoFisher Scientific, 11668019). Cells were fixed with 4% PFA. Cells were then permeabilized with 0.2% Triton-X and blocked with PBT buffer (5% Goat serum, 0.1% BSA, and 0.1% Triton-X). Cells were incubated with a mouse anti-FLAG (1:100, Millipore Sigma F1804) and rabbit anti-Hadha antibody (1:100, ThermoFisher Scientific PA5-27348) overnight at 4° C. Cells were then stained with Goat anti-mouse IgG-Alexa Fluor 488 (1:200, Invitrogen, A11029), goat anti-rabbit IgG-Alexa Fluor 555 (1:200, Invitrogen A21428), and DAPI (1:400) for one hour at room temperature. Cells were analyzed on a Nikon Eclipse Ts2 Inverted Microscope.

**Western Blots on Hek293 cells**

Hek293 cells were transfected with pAAV-CAG-*Hadha*-3XFLAG using Lipofectamine 2000 (ThermoFisher Scientific, 11668019). After 48 hours, cells were lysed in NP40 buffer and lysates were ran on a 10% TGX Stain-Free FastCast Acrylamide Gel (Bio-Rad, 1610182) in Tris/Glycine/SDS Buffer. Protein was transferred to a PVDF membrane using the Trans-Blot Turbo Transfer system (Bio-Rad). Membranes were blotted in 5% Milk in TBST (Tris-Buffered Saline and 0.1% Tween 20), then stained with a mouse anti-FLAG (1:1000, Millipore Sigma F1804) and rabbit anti-Hadha (1:1000, ThermoFisher Scientific PA5-

27348) antibody overnight at 4° C. Membranes were incubated in goat anti-mouse IgG-HRP (1:5000, Thermo Scientific 31432) and goat anti-rabbit IgG-HRP (1:5000, Thermo Scientific 31462), then activated with the SuperSignal West Pico PLUS chemiluminescent HRP substrate (Thermo Fisher Scientific, 34580). Membranes were imaged on an Azure Sapphire Biomolecular Imager and a stain-free total protein image was taken using the Bio-Rad Gel Doc EZ Imager.

**Packaging of pAAV-CAG-*Hadha*-3XFLAG into AAV2/5**

Confluent Hek293 cells on a 15 cm plate were transfected with pAAV2/5 (Gift from Melina Fan (Addgene plasmid #104964)), pAdDeltaF6 (Gift from James M. Wilson (Addgene plasmid #112867)), and pAAV-CAG-*Hadha*-3XFLAG at a ratio of 1:1:1 for 5 days. AAV5-CAG-*Hadha*-3XFLAG was then concentrated using an Amicon Ultra-15 Centrifugal Filter (Millipore Sigma, UFC9030) in 5% sorbitol/PBS and treated with benzoase endonuclease (Millipore Sigma, 101697) to clear any unpackaged plasmids. The concentration of the AAV5-CAG-*Hadha*-3XFLAG was measured using qPCR[255,256]. AAV5-CAG-*Hadha*-3XFLAG samples were treated with DNase 1 prior to qPCR. The standards used were free-ITR standards, created by cutting the AAV5-CAG-*Hadha*-3XFLAG with PvuII. Finally, samples and standards were run on qPCR with ITR FWD/RVS primers according to following protocol: 95°C for 10 mins; 40 cycles of 95°C for 15 sec, 53°C for 15 sec, and 60°C for 45 sec.

**Subretinal injection of AAV2/5-mHadha**

Mice were anesthetized through an intraperitoneal injection of ketamine (100 mg/kg) and xylazine (10 mg/kg) and eyes were dilated with atropine, phenylephrine, and tropicamide. 1 μL of AAV5-CAG-*Hadha*-3XFLAG or PBS was subretinally injected. After injection, mice were intraperitoneally injected with 1 mg/kg of atipamezole and erythromycin ointment added to the eye.

**RPE Flatmount Immunofluorescence**

Mice were euthanized via cervical dislocation. Eyes were removed, burn marked on the superior side of the cornea, and fixed in 4% PFA then 30% sucrose. Eyes were flash frozen in liquid nitrogen and stored at -80°C. At time of staining, fat and muscle were removed from the back of the eye and a RPE flatmount was created on a Superfrost Plus Microscope Slide (Fisherbrand). The RPE flatmount was blocked with blocking buffer (3% goat serum and 0.3% Triton-X in PBS). The flatmounts were then stained with primary rabbit anti-FLAG antibody (1:500 dilution, Novus NBP237833) overnight at 4°C in a humidified chamber. Flatmounts were stained with Alexa-488 conjugated to a goat anti-rabbit secondary antibody (1:200 dilution in PBS with 0.3% Triton-X, Invitrogen A11008), Alexa 647-Phalloidin (1:400 dilution in PBS, Invitrogen A22287), and DAPI (1:400 dilution in PBS). Flatmounts were mounted with Vectashield Antifade Mounting Medium with DAPI (Novus biologicals, H-1200-NB) and imaged on Keyence Fluorescence Cell Imager BZ-X800. Images were then analyzed using FIJI 2.

**Retinal Cross Section Immunofluorescence**

Eyes were burn marked on the superior side of the cornea, enucleated, and fixed in 4% PFA and 30% sucrose. Eyes were embedded into Tissue-Tek O.C.T Compound (Sakura, 4583) and 10 μm slices were made using a cryostat at -22°C along the dorsal-ventral axis onto a Superfrost Plus Microscope Slide (Fisherbrand). Slides were stored at -20°C.

Slices were rinsed in PBS and blocked in blocking buffer (3% goat serum and 0.3% Triton-X in PBS). Samples were stained with a rabbit anti-FLAG primary antibody (1:1000 dilution in blocking buffer, Novus NBP237833) overnight at 4°C in humidified chamber in the dark. The slides were stained with Alexa 488 conjugated goat anti-rabbit secondary antibody (1:200 dilution in PBS with 0.3% Triton-X, Invitrogen A11008) and DAPI (1:400 dilution in PBS) at room temperature in a humidified chamber in the dark. Finally, the slides were mounted with Vectashield Antifade Mounting Medium with DAPI (Novus biologicals, H-1200-NB). Cross sections were imaged on a Nikon Eclipse Ts2 Inverted Microscope and images were analyzed using FIJI 2.

**Optical Kinetic Tracking***:* Same as Chapter 4.

**Fundus Imaging and Optical Coherence Tomography:** Same as Chapter 4

**Electroretinogram:** Same as Chapter 4

**H&E Staining***:* Same as Chapter 4

**RPE/Sclera Acylcarnitine***:* Same as Chapter 4

## Acknowledgments

The pAAV-CAG-GFP plasmid was a gift from Edward Boyden (Addgene, Plasmid #37825), the pAAV2/5 plasmid was a gift from Melina Fan (Addgene plasmid #104964), and the pAdDeltaF6 plasmid was a gift from James M. Wilson (Addgene plasmid #112867). H&E staining was supported by the Leonard Christensen Eye Pathology Laboratory at Casey Eye Institute at OHSU. Acylcarnitine detection was conducted by the Biochemical Genetics Laboratory at the Mayo Clinic.

## Funding

This study was funded by the generous support of the Scully-Peterson foundation; the National Eye Institute (RO1EY03889); an unrestricted grant from Research to Prevent Blindness New York, NY; NIH P30 EY010572 Core Grant; and the Malcolm M. Marquis, MD Endowed Fund for Innovation to Casey Eye Institute, Oregon Health & Science University

## Disclosure Statement

The authors have nothing to disclose.

# Chapter 6 : Discussion and Future Directions

## Conclusion

As more LCHADD patients live past infancy due to improved detection by newborn screening and early treatment, patients must cope with later-onset, chronic symptoms, such as chorioretinopathy, that are less researched and unpreventable. Mouse models have been crucial to FAOD research, including being used to understand molecular mechanisms involved in phenotypes and to test potential treatments (Chapter 2). Unfortunately, research into LCHADD, especially into LCHADD-specific phenotypes, have been limited due to the lack of a LCHADD mouse model. In this dissertation, I report a new LCHADD mouse model that is homozygous for the LCHADD pathogenic variant, c.G1528C, and recapitulates many aspects of LCHADD, including chorioretinopathy (Chapter 3). The chorioretinopathy in this 12-month LCHADD mouse recapitulates early-stage chorioretinopathy in patients (Chapter 4) and will be crucial in understanding the pathomechanisms and investigating potential treatments, such as gene addition (Chapter 5).

## Accelerating chorioretinopathy progression in mice

As shown in Chapter 4, LCHADD mice have increased RPE degeneration and decreased visual performance, similar to LCHADD patients with early-stage chorioretinopathy. Patients will develop chorioretinopathy in the first decade of life that will progress to overall retinal degeneration, such as in the photoreceptor degeneration; however, LCHADD mice do not have photoreceptor degeneration even at 12-months of age, which is a later adult stage in the mouse.[54,55] One potential reason for the difference in severity between humans and mice is that these mice are not challenged to

utilize FAO. LCHADD patients are advised to avoid times where FAO is required, such as exercise, fasting, and illness, and to maintain a low long-chain FA intake (~10% of total energy); however, adherence is challenging.[257] Patients detected through NBS, which allows for earlier implementation of treatment and lowers metabolic crises events, generally have less severe chorioretinopathy compared to patients detected symptomatically, suggesting reliance on FAO is important for chorioretinopathy progression.[45] LCHADD mice always have consistent access to food that is low in fat (Formulab Diet, 5008C33; ~16% of calories from fat), are never forced to exercise, and are rarely sick. Therefore, LCHADD chorioretinopathy in mice may be less severe than patients because they are not challenged to rely on FAO.

Accelerating chorioretinopathy in mice will be important in studying the full progression of LCHADD chorioretinopathy, including photoreceptor degeneration. One potential way to speed up the progression is to encourage more FAO either through consistent fasting/exercise and/or increase fat intake. Preliminary evidence suggests that 12-month LCHADD mice fed a breeder diet (~30% calories from fat) for 3-months had decreased visual performance when compared to LCHADD mice kept on a normal diet (~16% calories from fat) indicating increased reliance on FAO can accelerate the chorioretinopathy (Appendix A1-2B). In addition, many LCHADD patients experience severe metabolic crises during infancy when the retina is still developing.[258] These events may be important for the progression by disrupting retinal development and making the retina more susceptible to degeneration. Therefore, challenging the mice

directly after weaning with a higher fat diet or regular fasting may also cause a more severe chorioretinopathy.

## Hydroxyacylcarnitines are potentially toxic to the RPE

The two leading hypotheses for the cause of LCHADD chorioretinopathy is energy deficiency and an accumulation of toxic intermediates, specifically hydroxyacylcarnitines. The results presented in this dissertation provide support that the hydroxyacylcarnitines cause the RPE degeneration seen in our model. First, isolated RPE/sclera in LCHADD mice have increased 3-hydroxyacylcarnitines compared to WT but do not have a decrease in acetyl-CoA, suggesting that while FAO is blocked, the Krebs cycle and energy production may not be impaired (Figure 4-1). We also show that feeding mice a diet that is higher in fat further decreases visual performance in LCHADD mice (Appendix 1) and gene addition to the RPE was shown to retain visual performance and decreases hydroxyacylcarnitine levels (Figure 5-3 and 5-5).

While these data provide support for hydroxyacylcarnitines causing LCHADD chorioretinopathy, more direct experiments will need to be conducted. First, many different metabolic processes create and utilize acetyl-CoA; therefore, experiments that more directly measure energy state, such as ATP and Krebs cycle intermediates will need to be performed to eliminate energy deficiency as a cause to the chorioretinopathy. In addition, experiments that better correlate hydroxyacylcarnitine concentrations in the RPE/sclera and visual performance will need to be performed. Studies that have correlated acylcarnitine levels and visual performance in patients have used plasma acylcarnitine levels. However, there is no evidence that suggests RPE/sclera acylcarnitine

concentrations are similar to plasma as the studies presented here are the first to directly measure acylcarnitine concentrations from RPE/sclera tissues.[43] Hydroxyacylcarnitine concentrations and visual performance cannot be conclusively correlated from our studies because RPE/sclera acylcarnitine concentrations were not collected in the high-fat diet experiment and the sample size was too small in the gene addition study. Therefore, more experiments will need to be done that correlate hydroxyacylcarnitine concentrations with visual performance in this LCHADD mouse model.

## Choroid and vasculature changes in LCHADD chorioretinopathy

Choroidal neovascularization (CNV) is an abnormal growth of vessels from the choroid into the retina that can contribute to vision loss and is seen in patients with retinal dystrophies such as age-related macular degeneration.[259,260] CNV was first reported in a 21-year-old LCHADD female patient by Sacconi et al. (2022). Since this finding, Wongchaisuwat et al. (2024) recently reported CNV in 21% of LCHADD patients, highlighting another complication of LCHADD chorioretinopathy.[239,240]

Results in this dissertation also suggest a change in the choroid and vasculature of LCHADD mice. Specifically, H&E staining of 12-month LCHADD retinal cross sections have increased vacuoles in the choroid when compared to WT cross sections (Supplemental Figure 4-2), and RNA-sequencing data from 12-month LCHADD RPE/sclera samples indicate altered expression of genes involved in angiogenesis and vasculature (Figure 4-7). Unfortunately, none of the experiments conducted directly assess the quality of the choroid or vasculature. Using modalities such as OCT angiography, a

noninvasive imaging modality that provides a three-dimensional visualization of the vasculature of the retina and choroid, will be crucial to investigate the possible changes in the choroid and other blood vessels in the LCHADD mice.[260,261]

## Improving gene addition experiment outcomes

Preliminary evidence in this dissertation suggests adding a WT *Hadha* gene to the RPE may preserve visual performance in LCHADD mice (Figure 5-3); however, the sample size was small due to unexpected complications post-injection that inhibited visual assessments (Supplemental Figure 5-3). First, many of the WT and LCHADD eyes, both untreated and treated, displayed severe retinal degeneration and/or cloudy vitreous suggesting a potential immune response to the injection. One potential reason for this could be an increased risk of infection from the injection. Other studies using subretinal injections have applied a topical antibiotic, erythromycin, post injection and allowed the animals to recover from the anesthesia without further manipulation. This allowed the antibiotic to stay on the eye for a prolonged period of time. However, LCHADD mice were more likely to die during anesthesia by ketamine/xylazine. To increase survivability, a reversal agent, atipamezole, was administered after testing in order to wake the mouse from sedation. Unfortunately, the administration of atipamezole reduces the amount of time the eyes are treated with erythromycin due to the mice waking from sedation faster and physically removing the antibiotic gel. It is possible that the reduced antibiotic treatment increases the rate of infection. To minimize this impact, the erythromycin treatment time could be extended by delaying the administration of the reversal agent.

Another unexpected problem we encountered was that only LCHADD eyes had corneal abrasions. As LCHADD mice have an impaired FAO, they are likely unable to maintain body temperature as well as WT. It is possible that during anesthesia, the body temperature of LCHADD mice dropped quicker than WT which could result in the corneal damage.[262] Therefore, ensuring the LCHADD mice are constantly on a heating source while under sedation could improve the number of LCHADD eyes without corneal abrasions.

Overall, altering the anesthesia protocol by adding an erythromycin treatment period and keeping LCHADD mice on a heating source at all times are two possible approaches that may increase the number of healthy eyes after injection and maintain an appropriate sample size for repeated gene addition experiments in the future.

## Base editing or Prime Editing as an alternative to gene addition

A more permanent alternative to gene addition would be gene editing using base editors or prime editing. LCHADD chorioretinopathy is a promising candidate for gene editing because LCHADD patients have the same c.G1528C pathogenic variant in *HADHA*; therefore, a one treatment could be used for all patients. The most common type of gene editing is CRISPR-Cas9 gene editing; however, because it relies on homology-directed repair, this type of editing would not work in post-mitotic cells, such as the RPE. Base editing and prime editing, on the other hand, can correct the G1528C mutation without introducing double-strand DNA breaks, thus making it a potential option for genetically editing the RPE.[263,264] While base editing and prime editing are not in any clinical trials currently, they have been shown to correct many inherited retinal

degenerations, such as Leber Congenital Amaurosis, in preclinical models.[263,265,266] Overall, base or prime editing could be a promising alternative to gene addition as a treatment for LCHADD chorioretinopathy.

## Final thoughts

My dissertation characterizes the chorioretinopathy seen in a novel LCHADD mouse model and uses this model to investigate molecular mechanisms and potential treatments for LCHADD chorioretinopathy. With optimization of this mouse model, such as increasing the rate and severity of retinal degeneration, this LCHADD mouse will provide an excellent model to study the pathomechanisms involved in LCHADD chorioretinopathy. This mouse could also serve as an excellent preclinical model where potential treatments for LCHADD chorioretinopathy, such as gene therapy, could be evaluated and optimized prior to clinical trials.

# Chapter 7 : References

1. Kowalski GM, Bruce CR. The regulation of glucose metabolism: implications and considerations for the assessment of glucose homeostasis in rodents. *Am J Physiol Endocrinol Metab*. Nov 15 2014;307(10):E859-71. doi:10.1152/ajpendo.00165.2014
2. DeBerardinis RJ, Chandel NS. Fundamentals of cancer metabolism. *Sci Adv*. 2016;
3. Liu G, Summer R. Cellular Metabolism in Lung Health and Disease. *Annu Rev Physiol*. Feb 10 2019;81:403-428. doi:10.1146/annurev-physiol-020518-114640
4. Camandola S, Mattson MP. Brain metabolism in health, aging, and neurodegeneration. *EMBO J*. Jun 1 2017;36(11):1474-1492. doi:10.15252/embj.201695810
5. Deprince A, Haas JT, Staels B. Dysregulated lipid metabolism links NAFLD to cardiovascular disease. *Mol Metab*. Dec 2020;42:101092. doi:10.1016/j.molmet.2020.101092
6. Palmer BF, Clegg DJ. Metabolic Flexibility and Its Impact on Health Outcomes. *Mayo Clin Proc*. Apr 2022;97(4):761-776. doi:10.1016/j.mayocp.2022.01.012
7. Goodpaster BH, Sparks LM. Metabolic Flexibility in Health and Disease. *Cell Metab*. May 2 2017;25(5):1027-1036. doi:10.1016/j.cmet.2017.04.015
8. Smith RL, Soeters MR, Wust RCI, Houtkooper RH. Metabolic Flexibility as an Adaptation to Energy Resources and Requirements in Health and Disease. *Endocr Rev*. Aug 1 2018;39(4):489-517. doi:10.1210/er.2017-00211
9. Vockley J. Long-Chain Fatty Acid Oxidation Disorders and Current Management Strategies. *The American Journal of Managed Care*. 2020;
10. Longo N, Frigeni M, Pasquali M. Carnitine transport and fatty acid oxidation. *Biochim Biophys Acta*. Oct 2016;1863(10):2422-35. doi:10.1016/j.bbamcr.2016.01.023
11. Houten SM, Wanders RJ. A general introduction to the biochemistry of mitochondrial fatty acid beta-oxidation. *J Inherit Metab Dis*. Oct 2010;33(5):469-77. doi:10.1007/s10545-010-9061-2
12. Rui L. Energy metabolism in the liver. *Compr Physiol*. Jan 2014;4(1):177-97. doi:10.1002/cphy.c130024
13. Puchalska P, Crawford PA. Multi-dimensional Roles of Ketone Bodies in Fuel Metabolism, Signaling, and Therapeutics. *Cell Metab*. Feb 7 2017;25(2):262-284. doi:10.1016/j.cmet.2016.12.022
14. Vishwanath VA. Fatty Acid Beta-Oxidation Disorders: A Brief Review. *Ann Neurosci*. Mar 2016;23(1):51-5. doi:10.1159/000443556
15. Spiekerkoetter U. Mitochondrial fatty acid oxidation disorders: clinical presentation of long-chain fatty acid oxidation defects before and after newborn screening. *J Inherit Metab Dis*. Oct 2010;33(5):527-32. doi:10.1007/s10545-010-9090-x
16. Merritt JL, 2nd, Norris M, Kanungo S. Fatty acid oxidation disorders. *Ann Transl Med*. Dec 2018;6(24):473. doi:10.21037/atm.2018.10.57
17. Yoo HW. Inborn Errors of Mitochondrial Fatty Acid Oxidation: Overview from a Clinical Perspective. *J Lipid Atheroscler*. Jan 2021;10(1):1-7. doi:10.12997/jla.2021.10.1.1
18. Ruiz-Sala P, Pena-Quintana L. Biochemical Markers for the Diagnosis of Mitochondrial Fatty Acid Oxidation Diseases. *J Clin Med*. Oct 22 2021;10(21)doi:10.3390/jcm10214855

19. Wanders RJAD, M.; Ijlst, L.; De Jager, J.P.; Van Gennip, A.H.; Jakobs, C.; Dorland, L.; Van Sprang, F.J. Sudden Infant Death and Long-Chain 3-Hydroxyacyl-CoA Dehydrogenase. *The Lancet*. 1989;
20. Wanders RJI, L; Van Gennip, A. H.; Jakobs, C.; De Jager, J. P.; Dorland, L.; Van Sprang, F. J.; Duran, M. Long-chain 3-Hydroxyacyl-CoA Dehydrogenase Deficiency: Identification of a new Inborn Error of Mitochondrial Fatty Acid B-Oxidation. *J Inher Metab Dis*. 1990;
21. Carpenter K, Pollitt RJ, Middleton B. Human liver long-chain 3-hydroxyacyl-coenzyme a dehydrogenase is a multifunctional membrane-bound beta-oxidation enzyme of mitochondria. *Biochemical and Biophysical Research Communications*. 1992;183(2):443-448. doi:10.1016/0006-291x(92)90501-b
22. Xia C, Fu Z, Battaile KP, Kim JP. Crystal structure of human mitochondrial trifunctional protein, a fatty acid beta-oxidation metabolon. *Proc Natl Acad Sci U S A*. Mar 26 2019;116(13):6069-6074. doi:10.1073/pnas.1816317116
23. Yang B-Z, Heng HHQ, Ding J-H, Roe CR. The Genes for the a and b Subunits of the Mitochondrial Trifunctional Protein are Both Located in the Same Region of the Human Chromosome 2p23. *Genomics*. 1996;37
24. Kamijo T, Aoyama T, Komiyama A, Hashimoto T. Structural analysis of cDNAs for subunits of human mitochondrial fatty acid beta-oxidation trifunctional protein. *Biochem Biophys Res Commun*. Mar 15 1994;199(2):818-25. doi:10.1006/bbrc.1994.1302
25. Ijlst L, Wanders RJ, Ushikubo S, Kamijo T, Hashimoto T. Molecular basis of long-chain 3-hydroxyacyl-CoA dehydrogenase deficiency: identification of the major disease-causing mutation in the alpha-subunit of the mitochondrial trifunctional protein. *Biochim Biophys Acta*. Dec 8 1994;1215(3):347-50. doi:10.1016/0005-2760(94)90064-7
26. Ijist L, Ruiter JP, Hoovers JM, Jakobs ME, Wanders RJ. Common missense mutation G1528C in long-chain 3-hydroxyacyl-CoA dehydrogenase deficiency. Characterization and expression of the mutant protein, mutation analysis on genomic DNA and chromosomal localization of the mitochondrial trifunctional protein alpha subunit gene. *J Clin Invest*. Aug 15 1996;98(4):1028-33. doi:10.1172/JCI118863
27. Orii KA, T.; Souri, M.; Jiang, L.; Orii, K.; Hayashi, S.; Yamaguch, S.; Kondo, N.; Orii, T.; Hashimoto, T. Formation of the Enzyme Complex in Mitochondria is Required for Function of Trifunctional B-Oxidation Protein. *Biochemical and Biophysical Research Communications*. 1996;
28. Ushikubo SA, T.; Kamijo, T.; Wanders, R.J.A; Rinaldo, P.; Vockley, J.; Hashimoto, T. Molecular Characterization of Mitochondrial Trifunctional Protein Deficiency: Formation of the Enzyme Complex is Important for Stabilization of Both a- and b-subunits. *Am J Hum Genet*. 1996;
29. Spiekerkoetter U, Khuchua Z, Yue Z, Bennett MJ, Strauss AW. General mitochondrial trifunctional protein (TFP) deficiency as a result of either alpha- or beta-subunit mutations exhibits similar phenotypes because mutations in either subunit alter TFP complex expression and subunit turnover. *Pediatr Res*. Feb 2004;55(2):190-6. doi:10.1203/01.PDR.0000103931.80055.06

30. Pons RR, M.; Riudor, E.; Ribes, A.; Briones, P.; Ortigosa, L.; Baldellou, A.; Gil-Gibernau, J.; Olesti, M.; Navarro, C.; Wanders, R.J.A. The Clinical Spectrum of Long-Chain 3-Hydroxyacyl-CoA Dehydrogenase Deficiency. *Pediatric Neurology*. 1996;
31. Tyni TaP, H. Long-chain 3-hydroxyacyl-CoA dehydrogenase deficiency. *Acta Paediatr*. 1999;
32. Elizondo G, Saini A, Gonzalez de Alba C, et al. Cardiac phenotype in adolescents and young adults with long-chain 3-hydroxyacyl CoA dehydrogenase (LCHAD) deficiency. *Genet Med*. Mar 16 2024:101123. doi:10.1016/j.gim.2024.101123
33. Lindner M, Hoffmann GF, Matern D. Newborn screening for disorders of fatty-acid oxidation: experience and recommendations from an expert meeting. *J Inherit Metab Dis*. Oct 2010;33(5):521-6. doi:10.1007/s10545-010-9076-8
34. Marsden D, Bedrosian CL, Vockley J. Impact of newborn screening on the reported incidence and clinical outcomes associated with medium- and long-chain fatty acid oxidation disorders. *Genet Med*. Jan 25 2021;doi:10.1038/s41436-020-01070-0
35. Gillingham MB, Connor WE, Matern D, et al. Optimal dietary therapy of long-chain 3-hydroxyacyl-CoA dehydrogenase deficiency. *Mol Genet Metab*. Jun 2003;79(2):114-23. doi:10.1016/s1096-7192(03)00073-8
36. Gillingham MB, Heitner SB, Martin J, et al. Triheptanoin versus trioctanoin for long-chain fatty acid oxidation disorders: a double blinded, randomized controlled trial. *J Inherit Metab Dis*. Nov 2017;40(6):831-843. doi:10.1007/s10545-017-0085-8
37. Maguolo A, Rodella G, Dianin A, et al. Diagnosis, genetic characterization and clinical follow up of mitochondrial fatty acid oxidation disorders in the new era of expanded newborn screening: A single centre experience. *Mol Genet Metab Rep*. Sep 2020;24:100632. doi:10.1016/j.ymgmr.2020.100632
38. Fraser H, Geppert J, Johnson R, et al. Evaluation of earlier versus later dietary management in long-chain 3-hydroxyacyl-CoA dehydrogenase or mitochondrial trifunctional protein deficiency: a systematic review. *Orphanet J Rare Dis*. Nov 15 2019;14(1):258. doi:10.1186/s13023-019-1226-y
39. Immonen T, Turanlahti M, Paganus A, Keskinen P, Tyni T, Lapatto R. Earlier diagnosis and strict diets improve the survival rate and clinical course of long-chain 3-hydroxyacyl-CoA dehydrogenase deficiency. *Acta Paediatr*. May 2016;105(5):549-54. doi:10.1111/apa.13313
40. Sykut-Cegielska J, Gradowska W, Piekutowska-Abramczuk D, et al. Urgent metabolic service improves survival in long-chain 3-hydroxyacyl-CoA dehydrogenase (LCHAD) deficiency detected by symptomatic identification and pilot newborn screening. *J Inherit Metab Dis*. Feb 2011;34(1):185-95. doi:10.1007/s10545-010-9244-x
41. Dulz S, Atiskova Y, Engel P, Wildner J, Tsiakas K, Santer R. Retained visual function in a subset of patients with long-chain 3-hydroxyacyl-CoA dehydrogenase deficiency (LCHADD). *Ophthalmic Genet*. Feb 2021;42(1):23-27. doi:10.1080/13816810.2020.1836658
42. Gillingham M, Van Calcar S, Ney D, Wolff J, Harding C. Dietary management of long-chain 3-hydroxyacyl-CoA dehydrogenase deficiency (LCHADD). A case report and survey. *J Inherit Metab Dis*. Apr 1999;22(2):123-31. doi:10.1023/a:1005437616934

43. Gillingham MB, Weleber RG, Neuringer M, et al. Effect of optimal dietary therapy upon visual function in children with long-chain 3-hydroxyacyl CoA dehydrogenase and trifunctional protein deficiency. *Mol Genet Metab*. Sep-Oct 2005;86(1-2):124-33. doi:10.1016/j.ymgme.2005.06.001
44. Immonen T, Ahola E, Toppila J, Lapatto R, Tyni T, Lauronen L. Peripheral neuropathy in patients with long-chain 3-hydroxyacyl-CoA dehydrogenase deficiency - A follow-up EMG study of 12 patients. *Eur J Paediatr Neurol*. Jan 2016;20(1):38-44. doi:10.1016/j.ejpn.2015.10.009
45. Fahnehjelm KT, Liu Y, Olsson D, et al. Most patients with long-chain 3-hydroxyacyl-CoA dehydrogenase deficiency develop pathological or subnormal retinal function. *Acta Paediatrica*. 2016;105(12):1451-1460. doi:10.1111/apa.13536
46. Fahnehjelm KT, Holmstrom G, Ying L, et al. Ocular characteristics in 10 children with long-chain 3-hydroxyacyl-CoA dehydrogenase deficiency: a cross-sectional study with long-term follow-up. *Acta Ophthalmol*. May 2008;86(3):329-37. doi:10.1111/j.1600-0420.2007.01121.x
47. Gillingham MB, Choi D, Gregor A, et al. Early diagnosis and treatment by newborn screening (NBS) or family history is associated with improved visual outcomes for long-chain 3-hydroxyacylCoA dehydrogenase deficiency (LCHADD) chorioretinopathy. *J Inherit Metab Dis*. Apr 16 2024;doi:10.1002/jimd.12738
48. Murillo-Cuesta S, Artuch R, Asensio F, et al. The Value of Mouse Models of Rare Diseases: A Spanish Experience. *Front Genet*. 2020;11:583932. doi:10.3389/fgene.2020.583932
49. Goetzman ES. Modeling disorders of fatty acid metabolism in the mouse. *Prog Mol Biol Transl Sci*. 2011;100:389-417. doi:10.1016/B978-0-12-384878-9.00010-8
50. Schuler AM, Wood PA. Mouse Models for Disorders of Mitochondrial Fatty Acid B-Oxidation. *ILAR Journal*. 2002;
51. Spiekerkoetter U, Wood PA. Mitochondrial fatty acid oxidation disorders: pathophysiological studies in mouse models. *J Inherit Metab Dis*. Oct 2010;33(5):539-46. doi:10.1007/s10545-010-9121-7
52. Houten SM, Violante S, Ventura FV, Wanders RJ. The Biochemistry and Physiology of Mitochondrial Fatty Acid beta-Oxidation and Its Genetic Disorders. *Annu Rev Physiol*. 2016;78:23-44. doi:10.1146/annurev-physiol-021115-105045
53. Tyni T, Kivelä T, Lappi M, Summanen P, Nikoskelainen E, Pihko H. Ophthalmologic findings in long-chain 3-hydroxyacyl-Coa dehydrogenase deficiency caused by the G1528C mutation. *Ophthalmology*. 1998;105(5):810-824. doi:10.1016/s0161-6420(98)95019-9
54. Boese EA, Jain N, Jia Y, et al. Characterization of Chorioretinopathy Associated with Mitochondrial Trifunctional Protein Disorders: Long-Term Follow-up of 21 Cases. *Ophthalmology*. Oct 2016;123(10):2183-95. doi:10.1016/j.ophtha.2016.06.048
55. Wongchaisuwat N, Gillingham MB, Yang P, et al. A proposal for an updated staging system for LCHADD retinopathy. *Ophthalmic Genet*. Jan 30 2024:1-7. doi:10.1080/13816810.2024.2303682
56. Boulton MD-B, P. The role of the retinal pigment epithelium: topographical variation and ageing changes. *Eye (Lond)*. 2001;

57. Kanow MA, Giarmarco MM, Jankowski CS, et al. Biochemical adaptations of the retina and retinal pigment epithelium support a metabolic ecosystem in the vertebrate eye. *Elife*. Sep 13 2017;6doi:10.7554/eLife.28899
58. Lakkaraju A, Umapathy A, Tan LX, et al. The cell biology of the retinal pigment epithelium. *Prog Retin Eye Res*. Feb 24 2020:100846. doi:10.1016/j.preteyeres.2020.100846
59. Sinha T, Naash MI, Al-Ubaidi MR. The Symbiotic Relationship between the Neural Retina and Retinal Pigment Epithelium Is Supported by Utilizing Differential Metabolic Pathways. *iScience*. Apr 24 2020;23(4):101004. doi:10.1016/j.isci.2020.101004
60. Adijanto J, Du J, Moffat C, Seifert EL, Hurle JB, Philp NJ. The retinal pigment epithelium utilizes fatty acids for ketogenesis. *J Biol Chem*. Jul 25 2014;289(30):20570-82. doi:10.1074/jbc.M114.565457
61. Reyes-Reveles J, Dhingra A, Alexander D, Bragin A, Philp NJ, Boesze-Battaglia K. Phagocytosis-dependent ketogenesis in retinal pigment epithelium. *J Biol Chem*. May 12 2017;292(19):8038-8047. doi:10.1074/jbc.M116.770784
62. Louer EMM, Yi G, Carmone C, et al. Genes Involved in Energy Metabolism Are Differentially Expressed During the Day-Night Cycle in Murine Retinal Pigment Epithelium. *Invest Ophthalmol Vis Sci*. May 11 2020;61(5):49. doi:10.1167/iovs.61.5.49
63. Tyni T. Mitochondrial Fatty Acid beta-Oxidation in the Retinal Pigment Epithelium. *Pediatric Research*. 2002;52(4):595-600. doi:10.1203/01.Pdr.0000030874.20888.2d
64. Yam M, Engel AL, Wang Y, et al. Proline mediates metabolic communication between retinal pigment epithelial cells and the retina. *J Biol Chem*. Jun 28 2019;294(26):10278-10289. doi:10.1074/jbc.RA119.007983
65. Du J, Yanagida A, Knight K, et al. Reductive carboxylation is a major metabolic pathway in the retinal pigment epithelium. *Proc Natl Acad Sci U S A*. Dec 20 2016;113(51):14710-14715. doi:10.1073/pnas.1604572113
66. Chao JR, Knight K, Engel AL, et al. Human retinal pigment epithelial cells prefer proline as a nutrient and transport metabolic intermediates to the retinal side. *J Biol Chem*. Aug 4 2017;292(31):12895-12905. doi:10.1074/jbc.M117.788422
67. Chinchore Y, Begaj T, Wu D, Drokhlyansky E, Cepko CL. Glycolytic reliance promotes anabolism in photoreceptors. *Elife*. Jun 9 2017;6doi:10.7554/eLife.25946
68. Petit L, Ma S, Cipi J, et al. Aerobic Glycolysis Is Essential for Normal Rod Function and Controls Secondary Cone Death in Retinitis Pigmentosa. *Cell Rep*. May 29 2018;23(9):2629-2642. doi:10.1016/j.celrep.2018.04.111
69. Klipfel L, Cordonnier M, Thiebault L, et al. A Splice Variant in SLC16A8 Gene Leads to Lactate Transport Deficit in Human iPS Cell-Derived Retinal Pigment Epithelial Cells. *Cells*. Jan 18 2021;10(1)doi:10.3390/cells10010179
70. Wang W, Kini A, Wang Y, et al. Metabolic Deregulation of the Blood-Outer Retinal Barrier in Retinitis Pigmentosa. *Cell Rep*. Jul 30 2019;28(5):1323-1334 e4. doi:10.1016/j.celrep.2019.06.093
71. Brown EE, DeWeerd AJ, Ildefonso CJ, Lewin AS, Ash JD. Mitochondrial oxidative stress in the retinal pigment epithelium (RPE) led to metabolic dysfunction in both the

RPE and retinal photoreceptors. *Redox Biol*. Jun 2019;24:101201. doi:10.1016/j.redox.2019.101201
72. Swarup A, Samuels IS, Bell BA, et al. Modulating GLUT1 expression in retinal pigment epithelium decreases glucose levels in the retina: impact on photoreceptors and Muller glial cells. *Am J Physiol Cell Physiol*. Jan 1 2019;316(1):C121-C133. doi:10.1152/ajpcell.00410.2018
73. Hu ML, Edwards TL, O'Hare F, et al. Gene therapy for inherited retinal diseases: progress and possibilities. *Clinical and Experimental Optometry*. 2021:1-11. doi:10.1080/08164622.2021.1880863
74. Pupo A, Fernandez A, Low SH, Francois A, Suarez-Amaran L, Samulski RJ. AAV vectors: The Rubik's cube of human gene therapy. *Mol Ther*. Dec 7 2022;30(12):3515-3541. doi:10.1016/j.ymthe.2022.09.015
75. N. Rudnick LK, J. Comander. Adeno-associated Viral Vectors in the Retina: Delivering Gene Therapy to the Right Destination. *International Ophthalmology Clinics*. 2022;
76. Russell S, Bennett J, Wellman JA, et al. Efficacy and safety of voretigene neparvovec (AAV2-hRPE65v2) in patients with RPE65-mediated inherited retinal dystrophy: a randomised, controlled, open-label, phase 3 trial. *Lancet*. Aug 26 2017;390(10097):849-860. doi:10.1016/S0140-6736(17)31868-8
77. Zhou R, Caspi RR. Ocular immune privilege. *F1000 Biol Rep*. Jan 18 2010;2doi:10.3410/B2-3
78. Babcock SJ, Houten SM, Gillingham MB. A review of fatty acid oxidation disorder mouse models. *Mol Genet Metab*. Feb 23 2024;142(1):108351. doi:10.1016/j.ymgme.2024.108351
79. Gillingham JVMBM. Mitochondrial Fatty Acid Oxidation Disorders. *The Online Metabolic and Molecular Bases of Inherited Disease*. 2019;doi:10.1036/ommbid.129
80. Hickman DL, Johnson J, Vemulapalli TH, Crisler JR, Shepherd R. Commonly Used Animal Models. *Principles of Animal Research*. 2017:117-175.
81. Nyman LR, Cox KB, Hoppel CL, et al. Homozygous carnitine palmitoyltransferase 1a (liver isoform) deficiency is lethal in the mouse. *Mol Genet Metab*. Sep-Oct 2005;86(1-2):179-87. doi:10.1016/j.ymgme.2005.07.021
82. Nyman LR, Tian L, Hamm DA, et al. Long term effects of high fat or high carbohydrate diets on glucose tolerance in mice with heterozygous carnitine palmitoyltransferase-1a (CPT-1a) deficiency: Diet influences on CPT1a deficient mice. *Nutr Diabetes*. Aug 22 2011;1:e14. doi:10.1038/nutd.2011.11
83. Ji S, You Y, Kerner J, et al. Homozygous carnitine palmitoyltransferase 1b (muscle isoform) deficiency is lethal in the mouse. *Mol Genet Metab*. 2008;93(3):314-322.
84. Wang M, Wang K, Liao X, et al. Carnitine Palmitoyltransferase System: A New Target for Anti-Inflammatory and Anticancer Therapy? *Front Pharmacol*. 2021;12:760581. doi:10.3389/fphar.2021.760581
85. Lee J, Ellis JM, Wolfgang MJ. Adipose fatty acid oxidation is required for thermogenesis and potentiates oxidative stress-induced inflammation. *Cell Rep*. Jan 13 2015;10(2):266-79. doi:10.1016/j.celrep.2014.12.023

86. Pereyra AS, Hasek LY, Harris KL, et al. Loss of cardiac carnitine palmitoyltransferase 2 results in rapamycin-resistant, acetylation-independent hypertrophy. *Journal of Biological Chemistry*. 2017;292(45):18443-18456. doi:10.1074/jbc.M117.800839
87. Pereyra AS, Harris KL, Soepriatna AH, et al. Octanoate is differentially metabolized in liver and muscle and fails to rescue cardiomyopathy in CPT2 deficiency. *J Lipid Res*. Mar 20 2021;62:100069. doi:10.1016/j.jlr.2021.100069
88. Pereyra AS, McLaughlin KL, Buddo KA, Ellis JM. Medium-chain fatty acid oxidation is independent of l-carnitine in liver and kidney but not in heart and skeletal muscle. *Am J Physiol Gastrointest Liver Physiol*. Oct 1 2023;325(4):G287-G294. doi:10.1152/ajpgi.00105.2023
89. Lee J, Choi J, Scafidi S, Wolfgang MJ. Hepatic Fatty Acid Oxidation Restrains Systemic Catabolism during Starvation. *Cell Rep*. Jun 28 2016;16(1):201-212. doi:10.1016/j.celrep.2016.05.062
90. Lee J, Choi J, Selen Alpergin ES, et al. Loss of Hepatic Mitochondrial Long-Chain Fatty Acid Oxidation Confers Resistance to Diet-Induced Obesity and Glucose Intolerance. *Cell Rep*. Jul 18 2017;20(3):655-667. doi:10.1016/j.celrep.2017.06.080
91. Wood PA, Amendt B, Rhead W, Millington DS, Inoue F, Armstrong D. Short-Chain Acyl-Coenzyme A Dehydrogenase Deficiency in Mice. *Pediatric Research*. 1989;25(1):38-43.
92. Armstrong D, Masiowski ML, Wood PA. Pathologic Characterization of Short-Chain Acyl-CoA Dehydrogenase Deficiency in BALB/cByJ Mice. *American Journal of Medical Genetics*. 1993;47(6):884-892.
93. Skilling H, Coen PM, Fairfull L, et al. Brown adipose tissue function in short-chain acyl-CoA dehydrogenase deficient mice. *Biochem Biophys Res Commun*. Sep 24 2010;400(3):318-22. doi:10.1016/j.bbrc.2010.08.053
94. Guerra C, Koza R, Walsh K, Kurtz D, Wood PA, Kozak L. Abnormal Nonshivering Thermogenesis in Mic with Inherited Defects of Fatty Acid Oxidation. *J Clin Invest*. 1998;102(9):1724-1731.
95. Tolwani RJ, Hamm DA, Tian L, et al. Medium-chain acyl-CoA dehydrogenase deficiency in gene-targeted mice. *PLoS Genet*. Aug 2005;1(2):e23. doi:10.1371/journal.pgen.0010023
96. Herrema H, Derks TG, van Dijk TH, et al. Disturbed hepatic carbohydrate management during high metabolic demand in medium-chain acyl-CoA dehydrogenase (MCAD)-deficient mice. *Hepatology*. Jun 2008;47(6):1894-904. doi:10.1002/hep.22284
97. Martines AMF, Gerding A, Stolle S, et al. Transcriptome analysis suggests a compensatory role of the cofactors coenzyme A and NAD(+) in medium-chain acyl-CoA dehydrogenase knockout mice. *Sci Rep*. Oct 10 2019;9(1):14539. doi:10.1038/s41598-019-50758-0
98. Cox KB, Hamm DA, Millington DS, et al. Gestational, pathologic and biochemical differences between very long-chain acyl-CoA dehydrogenase deficiency and long-chain acyl-CoA dehydrogenase deficiency in the mouse. *Human Molecular Genetics*. 2001;10(19):2069-2077.

99. Chegary M, Brinke H, Ruiter JP, et al. Mitochondrial long chain fatty acid beta-oxidation in man and mouse. *Biochim Biophys Acta*. Aug 2009;1791(8):806-15. doi:10.1016/j.bbalip.2009.05.006
100. Diekman EF, van Weeghel M, Wanders RJ, Visser G, Houten SM. Food withdrawal lowers energy expenditure and induces inactivity in long-chain fatty acid oxidation-deficient mouse models. *FASEB J*. Jul 2014;28(7):2891-900. doi:10.1096/fj.14-250241
101. Exil VJ, Roberts RL, Sims H, et al. Very-long-chain acyl-coenzyme a dehydrogenase deficiency in mice. *Circ Res*. Sep 5 2003;93(5):448-55. doi:10.1161/01.RES.0000088786.19197.E4
102. Spiekerkoetter U, Tokunaga C, Wendel U, et al. Changes in blood carnitine and acylcarnitine profiles of very long-chain acyl-CoA dehydrogenase-deficient mice subjected to stress. *European Journal of Clinical Investigation*. 2004;34(3):191-196.
103. Spiekerkoetter U, Tokunaga C, Wendel U, et al. Tissue carnitine homeostasis in very-long-chain acyl-CoA dehydrogenase-deficient mice. *Pediatr Res*. Jun 2005;57(6):760-4. doi:10.1203/01.PDR.0000157915.26049.47
104. Cox KB, Liu J, Tian L, Barnes S, Yang Q, Wood PA. Cardiac hypertrophy in mice with long-chain acyl-CoA dehydrogenase or very long-chain acyl-CoA dehydrogenase deficiency. *Lab Invest*. Dec 2009;89(12):1348-54. doi:10.1038/labinvest.2009.86
105. Gelinas R, Thompson-Legault J, Bouchard B, et al. Prolonged QT interval and lipid alterations beyond beta-oxidation in very long-chain acyl-CoA dehydrogenase null mouse hearts. *Am J Physiol Heart Circ Physiol*. Sep 2011;301(3):H813-23. doi:10.1152/ajpheart.01275.2010
106. Tucci S, Flogel U, Hermann S, Sturm M, Schafers M, Spiekerkoetter U. Development and pathomechanisms of cardiomyopathy in very long-chain acyl-CoA dehydrogenase deficient (VLCAD(-/-)) mice. *Biochim Biophys Acta*. May 2014;1842(5):677-85. doi:10.1016/j.bbadis.2014.02.001
107. ter Veld F, Primassin S, Hoffmann L, Mayatepek E, Spiekerkoetter U. Corresponding increase in long-chain acyl-CoA and acylcarnitine after exercise in muscle from VLCAD mice. *J Lipid Res*. Aug 2009;50(8):1556-62. doi:10.1194/jlr.M800221-JLR200
108. Riggs CE, Jr., Michaelides MA, Parpa KM, Smith-Blair NJ. The effects of aerobic interval training on the left ventricular morphology and function of VLCAD-deficient mice. *Eur J Appl Physiol*. Nov 2010;110(5):915-23. doi:10.1007/s00421-010-1578-4
109. Gaston G, Gangoiti JA, Winn S, et al. Cardiac tissue citric acid cycle intermediates in exercised very long-chain acyl-CoA dehydrogenase-deficient mice fed triheptanoin or medium-chain triglyceride. *J Inherit Metab Dis*. Nov 2020;43(6):1232-1242. doi:10.1002/jimd.12284
110. Goetzman ES, Tian L, Wood PA. Differential induction of genes in liver and brown adipose tissue regulated by peroxisome proliferator-activated receptor-alpha during fasting and cold exposure in acyl-CoA dehydrogenase-deficient mice. *Mol Genet Metab*. Jan 2005;84(1):39-47. doi:10.1016/j.ymgme.2004.09.010
111. Exil VJ, Gardner CD, Rottman JN, et al. Abnormal mitochondrial bioenergetics and heart rate dysfunction in mice lacking very-long-chain acyl-CoA dehydrogenase. *Am J Physiol Heart Circ Physiol*. Mar 2006;290(3):H1289-97. doi:10.1152/ajpheart.00811.2005

112. Spiekerkoetter U, Ruiter J, Tokunaga C, et al. Evidence for impaired gluconeogenesis in very long-chain acyl-CoA dehydrogenase-deficient mice. *Horm Metab Res*. Oct 2006;38(10):625-30. doi:10.1055/s-2006-954581
113. Tucci S, Primassin S, Spiekerkoetter U. Fasting-induced oxidative stress in very long chain acyl-CoA dehydrogenase-deficient mice. *FEBS J*. Nov 2010;277(22):4699-708. doi:10.1111/j.1742-4658.2010.07876.x
114. Zhang D, Christianson J, Liu Z-X, et al. Resistance to High-Fat Diet-Induced Obesity and Insulin Resistance in Mice with Very Long-Chain Acyl-CoA Dehydrogenase Deficiency. *Cell Metabolism*. 2010;11(5):402-411. doi:10.1016/j.cmet.2010.03.012
115. Tarasenko TN, Cusmano-Ozog K, McGuire PJ. Tissue acylcarnitine status in a mouse model of mitochondrial beta-oxidation deficiency during metabolic decompensation due to influenza virus infection. *Mol Genet Metab*. Sep 2018;125(1-2):144-152. doi:10.1016/j.ymgme.2018.06.012
116. Tucci S, Krogmann A, Herebian D, Spiekerkoetter U. Renal response to short- and long-term exercise in very-long-chain acyl-CoA dehydrogenase-deficient (VLCAD -/-) mice. *Molecular and Cellular Pediatrics*. 2014;1(1):5.
117. Zieger M, Keeler AM, Flotte TR, ElMallah MK. AAV9 gene replacement therapy for respiratory insufficiency in very-long chain acyl-CoA dehydrogenase deficiency. *J Inherit Metab Dis*. Sep 2019;42(5):870-877. doi:10.1002/jimd.12101
118. Kurtz D, Rinaldo P, Rhead W, et al. Targeted disruption of mouse long-chain acyl-CoA dehydrogenase gene reveals crucial roles for fatty acid oxidation. *Proc Natl Acad Sci U S A*. 1998;95(26):15592-15597.
119. Van Vlies N, Tian L, Overmars H, et al. Characterization of carnitine and fatty acid metabolism in the long-chain acyl-CoA dehydrogenase-deficient mouse. *Biochem J*. 2005;387:185-193.
120. Bakermans AJ, Dodd MS, Nicolay K, Prompers JJ, Tyler DJ, Houten SM. Myocardial energy shortage and unmet anaplerotic needs in the fasted long-chain acyl-CoA dehydrogenase knockout mouse. *Cardiovasc Res*. Dec 1 2013;100(3):441-9. doi:10.1093/cvr/cvt212
121. Bakermans AJ, van Weeghel M, Denis S, Nicolay K, Prompers JJ, Houten SM. Carnitine supplementation attenuates myocardial lipid accumulation in long-chain acyl-CoA dehydrogenase knockout mice. *J Inherit Metab Dis*. Nov 2013;36(6):973-81. doi:10.1007/s10545-013-9604-4
122. Houten SM, Herrema H, Te Brinke H, et al. Impaired amino acid metabolism contributes to fasting-induced hypoglycemia in fatty acid oxidation defects. *Hum Mol Genet*. Dec 20 2013;22(25):5249-61. doi:10.1093/hmg/ddt382
123. Zhang D, Liu ZX, Choi CS, et al. Mitochondrial dysfunction due to long-chain Acyl-CoA dehydrogenase deficiency causes hepatic steatosis and hepatic insulin resistance. *Proc Natl Acad Sci U S A*. Oct 23 2007;104(43):17075-80. doi:10.1073/pnas.0707060104
124. Shinde A, Luo J, Bharathi SS, et al. Increased mortality from influenza infection in long-chain acyl-CoA dehydrogenase knockout mice. *Biochem Biophys Res Commun*. Mar 4 2018;497(2):700-704. doi:10.1016/j.bbrc.2018.02.135

125. Goetzman ES, Alcorn JF, Bharathi SS, et al. Long-chain acyl-CoA dehydrogenase deficiency as a cause of pulmonary surfactant dysfunction. *J Biol Chem*. Apr 11 2014;289(15):10668-10679. doi:10.1074/jbc.M113.540260
126. Otsubo C, Bharathi S, Uppala R, et al. Long-chain Acylcarnitines Reduce Lung Function by Inhibiting Pulmonary Surfactant. *J Biol Chem*. Sep 25 2015;290(39):23897-904. doi:10.1074/jbc.M115.655837
127. Ibdah JAP, H.; Zhao, Y.; Binford, S.; Salleng, K.; Cline, M.; Matern, D.; Bennett, M.; Rinaldo, P.; Strauss, A. Lack of mitochondrial trifunctional protein in mice causes neonatal hypoglycemia and sudden death. *J Clin Invest*. 2001;107(11):1403-1409.
128. Fould B, Garlatti V, Neumann E, Fenel D, Gaboriaud C, Arlaud GJ. Structural and functional characterization of the recombinant human mitochondrial trifunctional protein. *Biochemistry*. Oct 5 2010;49(39):8608-17. doi:10.1021/bi100742w
129. Ibdah JA, Perlegas P, Zhao Y, et al. Mice heterozygous for a defect in mitochondrial trifunctional protein develop hepatic steatosis and insulin resistance. *Gastroenterology*. May 2005;128(5):1381-90. doi:10.1053/j.gastro.2005.02.001
130. Mejia EM, Ibdah JA, Sparagna GC, Hatch GM. Differential reduction in cardiac and liver monolysocardiolipin acyltransferase-1 and reduction in cardiac and liver tetralinoleoyl-cardiolipin in the alpha-subunit of trifunctional protein heterozygous knockout mice. *Biochem J*. Oct 1 2015;471(1):123-9. doi:10.1042/BJ20150648
131. Kao HJ, Cheng CF, Chen YH, et al. ENU mutagenesis identifies mice with cardiac fibrosis and hepatic steatosis caused by a mutation in the mitochondrial trifunctional protein beta-subunit. *Hum Mol Genet*. Dec 15 2006;15(24):3569-77. doi:10.1093/hmg/ddl433
132. Khare T, Khare S, Angdisen JJ, et al. Defects in long-chain 3-hydroxy acyl-CoA dehydrogenase lead to hepatocellular carcinoma: A novel etiology of hepatocellular carcinoma. *Int J Cancer*. Sep 1 2020;147(5):1461-1473. doi:10.1002/ijc.32943
133. Gaston G, Babcock S, Ryals R, et al. A G1528C Hadha knock-in mouse model recapitulates aspects of human clinical phenotypes for long-chain 3-hydroxyacyl-CoA dehydrogenase deficiency. *Commun Biol*. Aug 29 2023;6(1):890. doi:10.1038/s42003-023-05268-1
134. Koizumi T, Nikaido H, Hayakawa J, Nonomura A, Yoneda T. Infantile disease with microvesicular fatty infiltration of viscera spontaneously occuring in the C3H-H-2 strain of mouse with similarities to Reye's syndrome. *Laboratory Animals*. 1988;
135. Nezu J, Tama I, Oku A, et al. Primary systemic carnitine deficiency is caused by mutations in a gene encoding sodium ion-dependent carnitine transporter. *Nature Genetics*. 1999;21(1):91-94.
136. Horiuchi M, Kobayashi K, Yamaguchi S, et al. Primary defect of juvenile visceral steatosis (jvs) mouse with systemic carnitine deficiency is probably in renal carnitine transport system. *Biochimica et Biophysica Acta (BBA) - Molecular Basis of Disease*. 1994;1226(1):25-30.
137. Kuwajima M, Lu K, Sei M, et al. Characteristics of Cardiac Hypertrophy in the Juvenile Visceral Steatosis Mouse with Systemic Carnitine Deficiency. *Academic Press Limited*. 1997;

138. Yoshida G, Li MX, Horiuchi M, et al. Fasting-induced reduction in locomotor activity and reduced response of orexin neurons in carnitine-deficient mice. *Neurosci Res*. May 2006;55(1):78-86. doi:10.1016/j.neures.2006.02.003
139. Sakoguchi T, Horiuchi M, Asakawa A, et al. Failure of the feeding response to fasting in carnitine-deficient juvenile visceral steatosis (JVS) mice: involvement of defective acyl-ghrelin secretion and enhanced corticotropin-releasing factor signaling in the hypothalamus. *Biochim Biophys Acta*. Nov 2009;1792(11):1087-93. doi:10.1016/j.bbadis.2009.09.001
140. Li MX, Yoshida G, Horiuchi M, Kobayashi K, Saheki T. Prolonged effect of single carnitine administration on fasted carnitine-deficient JVS mice regarding their locomotor activity and energy expenditure. *Biochim Biophys Acta*. Oct 2006;1761(10):1191-9. doi:10.1016/j.bbalip.2006.08.013
141. Lahjouji K, Elimrani I, Wu J, Mitchell G, Qureshi I. A heterozygote phenotype is present in the jvs+/- mutant mouse livers. *Mol Genet Metab*. 2002;76(1):76-80.
142. Hashimoto N, Suzuki F, Tamai I, et al. Gene-Dose Effect on Carnitine Transport Activity in Embryonic Fibroblasts of JVS Mice as a Model of Human Carnitine Transporter Deficiency. *Biochemical Pharmacology*. 1998;55(10):1729-1732.
143. Takahashi R, Asai T, Murakami H, et al. Pressure overload-induced cardiomyopathy in heterozygous carrier mice of carnitine transporter gene mutation. *Hypertension*. Sep 2007;50(3):497-502. doi:10.1161/HYPERTENSIONAHA.107.088609
144. Sinsheimer A, Mohsen AW, Bloom K, et al. Development and characterization of a mouse model for Acad9 deficiency. *Mol Genet Metab*. Sep-Oct 2021;134(1-2):156-163. doi:10.1016/j.ymgme.2021.09.002
145. Liang K. Mitochondrial CPT1A: Insights into structure, function, and basis for drug development. *Front Pharmacol*. 2023;14:1160440. doi:10.3389/fphar.2023.1160440
146. Violante S, Achetib N, van Roermund CWT, et al. Peroxisomes can oxidize medium- and long-chain fatty acids through a pathway involving ABCD3 and HSD17B4. *FASEB J*. Mar 2019;33(3):4355-4364. doi:10.1096/fj.201801498R
147. Mozolewska P, Duzowska K, Pakiet A, Mika A, SledziNski T. Inhibitors of Fatty Acid Synthesis and Oxidation as Potential Anticancer Agents in Colorectal Cancer Treatment. *Anticancer Res*. Sep 2020;40(9):4843-4856. doi:10.21873/anticanres.14487
148. Tserng KY, Jin SJ, Hoppel CL. Spiropentaneacetic acid as a specific inhibitor of medium-chain acyl-CoA dehydrogenase. *Biochemistry*. 1991;30(44):10755-10760.
149. Wang W, Palmfeldt J, Mohsen AW, Gregersen N, Vockley J. Fasting induces prominent proteomic changes in liver in very long chain Acyl-CoA dehydrogenase deficient mice. *Biochem Biophys Rep*. Dec 2016;8:333-339. doi:10.1016/j.bbrep.2016.08.014
150. Bakermans AJ, Geraedts TR, van Weeghel M, et al. Fasting-induced myocardial lipid accumulation in long-chain acyl-CoA dehydrogenase knockout mice is accompanied by impaired left ventricular function. *Circ Cardiovasc Imaging*. Sep 2011;4(5):558-65. doi:10.1161/CIRCIMAGING.111.963751
151. Xiong D, He H, James J, et al. Cardiac-specific VLCAD deficiency induces dilated cardiomyopathy and cold intolerance. *Am J Physiol Heart Circ Physiol*. Feb 2014;306(3):H326-38. doi:10.1152/ajpheart.00931.2012

152. Ranea-Robles P, Pavlova NN, Bender A, et al. A mitochondrial long-chain fatty acid oxidation defect leads to tRNA uncharging and activation of the integrated stress response in the mouse heart. *Cardiovasc Res*. Apr 7 2022;doi:10.1093/cvr/cvac050
153. Tucci S, Mingirulli N, Wehbe Z, Dumit VI, Kirschner J, Spiekerkoetter U. Mitochondrial fatty acid biosynthesis and muscle fiber plasticity in very long-chain acyl-CoA dehydrogenase-deficient mice. *FEBS Lett*. Jan 2018;592(2):219-232. doi:10.1002/1873-3468.12940
154. Tucci S, Herebian D, Sturm M, Seibt A, Spiekerkoetter U. Tissue-specific strategies of the very-long chain acyl-CoA dehydrogenase-deficient (VLCAD-/-) mouse to compensate a defective fatty acid beta-oxidation. *PLoS One*. 2012;7(9):e45429. doi:10.1371/journal.pone.0045429
155. Miniou P, Tiziano D, Frugier T, Roblot N, Le Meur M, Melki J. Gene targeting restricted to mouse striated muscle lineage. *Oxford University Press*. 1999;
156. McCarthy JJ, Srikuea R, Kirby TJ, Peterson CA, Esser KA. Inducible Cre transgenic mouse strain for skeletal muscle-specific gene targeting. *Skelet Muscle*. May 7 2012;2(1):8. doi:10.1186/2044-5040-2-8
157. Mitchell GA, Gauthier N, Lesimple A, Wang SP, Mamer O, Qureshi I. Hereditary and acquired diseases of acyl-coenzyme A metabolism. *Mol Genet Metab*. May 2008;94(1):4-15. doi:10.1016/j.ymgme.2007.12.005
158. Yang H, Zhao C, Wang Y, Wang SP, Mitchell GA. Hereditary diseases of coenzyme A thioester metabolism. *Biochem Soc Trans*. Feb 28 2019;47(1):149-155. doi:10.1042/BST20180423
159. Zhang YM, Chohnan S, Virga KG, et al. Chemical knockout of pantothenate kinase reveals the metabolic and genetic program responsible for hepatic coenzyme A homeostasis. *Chem Biol*. Mar 2007;14(3):291-302. doi:10.1016/j.chembiol.2007.01.013
160. van Eunen K, Volker-Touw CM, Gerding A, et al. Living on the edge: substrate competition explains loss of robustness in mitochondrial fatty-acid oxidation disorders. *BMC Biol*. Dec 7 2016;14(1):107. doi:10.1186/s12915-016-0327-5
161. Odendaal C, Jager EA, Martines AMF, et al. Personalised modelling of clinical heterogeneity between medium-chain acyl-CoA dehydrogenase patients. *BMC Biol*. Sep 4 2023;21(1):184. doi:10.1186/s12915-023-01652-9
162. Kuwajima M, Horiuchi M, Harashima H, et al. Cardiomegaly in the juvenile visceral steatosis (JVS) mouse is reduced with acute elevation of heart short-chain acyl-carnitine level after L-carnitine injection. *FEBS Lett*. Jan 29 1999;443(3):261-6. doi:10.1016/s0014-5793(98)01732-3
163. Ozaki K, Sano T, Tsuji N, Matsuura T, Narama I. Carnitine is necessary to maintain the phenotype and function of brown adipose tissue. *Lab Invest*. May 2011;91(5):704-10. doi:10.1038/labinvest.2011.6
164. Ranea-Robles P, Yu C, van Vlies N, Vaz FM, Houten SM. Slc22a5 haploinsufficiency does not aggravate the phenotype of the long-chain acyl-CoA dehydrogenase KO mouse. *J Inherit Metab Dis*. May 2020;43(3):486-495. doi:10.1002/jimd.12204
165. Primassin S, ter Veld F, Mayatepek E, Spiekerkoetter U. Carnitine Supplementation Induces Acylcarnitine Production in Tissues of Very Long-Chain Acyl-

CoA Dehydrogenase Deficient Mice, Without Replenishing Low Free Carnitine. *Pediatric Research*. 2008;63(6):632-637.
166. Schuler AM, Gower BA, Matern D, Rinaldo P, Wood PA. Influence of dietary fatty acid chain-length on metabolic tolerance in mouse models of inherited defects in mitochondrial fatty acid beta-oxidation. *Mol Genet Metab*. Dec 2004;83(4):322-9. doi:10.1016/j.ymgme.2004.08.010
167. Tucci S, Pearson S, Herebian D, Spiekerkoetter U. Long-term dietary effects on substrate selection and muscle fiber type in very-long-chain acyl-CoA dehydrogenase deficient (VLCAD(-/-)) mice. *Biochim Biophys Acta*. Apr 2013;1832(4):509-16. doi:10.1016/j.bbadis.2013.01.006
168. Primassin S, Tucci S, Spiekerkoetter U. Hepatic and muscular effects of different dietary fat content in VLCAD deficient mice. *Mol Genet Metab*. Dec 2011;104(4):546-51. doi:10.1016/j.ymgme.2011.09.011
169. Primassin S, Tucci S, Herebian D, et al. Pre-exercise medium-chain triglyceride application prevents acylcarnitine accumulation in skeletal muscle from very-long-chain acyl-CoA-dehydrogenase-deficient mice. *J Inherit Metab Dis*. Jun 2010;33(3):237-46. doi:10.1007/s10545-010-9105-7
170. Tucci S, Behringer S, Spiekerkoetter U. De novo fatty acid biosynthesis and elongation in very long-chain acyl-CoA dehydrogenase-deficient mice supplemented with odd or even medium-chain fatty acids. *FEBS J*. Nov 2015;282(21):4242-53. doi:10.1111/febs.13418
171. Tucci S, Primassin S, Ter Veld F, Spiekerkoetter U. Medium-chain triglycerides impair lipid metabolism and induce hepatic steatosis in very long-chain acyl-CoA dehydrogenase (VLCAD)-deficient mice. *Mol Genet Metab*. Sep 2010;101(1):40-7. doi:10.1016/j.ymgme.2010.05.005
172. Tucci S, Flogel U, Spiekerkoetter U. Sexual dimorphism of lipid metabolism in very long-chain acyl-CoA dehydrogenase deficient (VLCAD-/-) mice in response to medium-chain triglycerides (MCT). *Biochim Biophys Acta*. Jul 2015;1852(7):1442-50. doi:10.1016/j.bbadis.2015.04.009
173. Wehbe Z, Alatibi K, Jellusova J, Spiekerkoetter U, Tucci S. The fate of medium-chain fatty acids in very long-chain acylCoA dehydrogenase deficiency (VLCADD): A matter of sex? *Biochim Biophys Acta Mol Cell Biol Lipids*. Nov 2019;1864(11):1591-1605. doi:10.1016/j.bbalip.2019.08.001
174. Alatibi KI, Wehbe Z, Spiekerkoetter U, Tucci S. Sex-specific perturbation of complex lipids in response to medium-chain fatty acids in very long-chain acyl-CoA dehydrogenase deficiency. *FEBS J*. Aug 2020;287(16):3511-3525. doi:10.1111/febs.15221
175. Keeler AM, Conlon T, Walter G, et al. Long-term correction of very long-chain acyl-coA dehydrogenase deficiency in mice using AAV9 gene therapy. *Mol Ther*. Jun 2012;20(6):1131-8. doi:10.1038/mt.2012.39
176. Merritt JL, 2nd, Nguyen T, Daniels J, Matern D, Schowalter DB. Biochemical correction of very long-chain acyl-CoA dehydrogenase deficiency following adeno-associated virus gene therapy. *Mol Ther*. Mar 2009;17(3):425-9. doi:10.1038/mt.2008.295

177. Zhao XJ, Mohsen AW, Mihalik S, et al. Synthetic mRNA rescues very long-chain acyl-CoA dehydrogenase deficiency in patient fibroblasts and a murine model. *Mol Genet Metab*. Dec 23 2022;138(1):106982. doi:10.1016/j.ymgme.2022.106982
178. Kelly CL, Rhead W, Kutschke W, et al. Functional correction of short-chain acyl-CoA dehydrogenase deficiency in transgenic mice: implications for gene therapy of human mitochondrial enzyme deficiencies. *Human Molecular Genetics*. 1997;6(9):1451-1455.
179. Beattie SG, Goetzman E, Conlon T, et al. Biochemical correction of short-chain acyl-coenzyme A dehydrogenase deficiency after portal vein injection of rAAV8-SCAD. *Hum Gene Ther*. Jun 2008;19(6):579-88. doi:10.1089/hum.2007.168
180. Beattie SG, Goetzman E, Tang Q, et al. Recombinant adeno-associated virus-mediated gene delivery of long chain acyl coenzyme A dehydrogenase (LCAD) into LCAD-deficient mice. *J Gene Med*. Oct 2008;10(10):1113-23. doi:10.1002/jgm.1242
181. Zhao XJ, Mohsen AW, Mihalik S, et al. Messenger RNA rescues medium-chain acyl-CoA dehydrogenase deficiency in fibroblasts from patients and a murine model. *Hum Mol Genet*. Jul 4 2023;32(14):2347-2356. doi:10.1093/hmg/ddad076
182. Lefevre CR, Labarthe F, Dufour D, et al. Newborn Screening of Primary Carnitine Deficiency: An Overview of Worldwide Practices and Pitfalls to Define an Algorithm before Expansion of Newborn Screening in France. *Int J Neonatal Screen*. Feb 1 2023;9(1)doi:10.3390/ijns9010006
183. Ijlst L, Ruiter JP, Hoovers JM, Jakobs ME, Wanders RJ. Common missense mutation G1528C in long-chain 3-hydroxyacyl-CoA dehydrogenase deficiency. Characterization and expression of the mutant protein, mutation analysis on genomic DNA and chromosomal localization of the mitochondrial trifunctional protein alpha subunit gene. *J Clin Invest*. 1996;98(4):1028-33.
184. Tyni T, Rapola J, Paetau A, Palotie A, Pihko H. Pathology of long-chain 3-hydroxyacyl-CoA dehydrogenase deficiency caused by the G1528C mutation. *Pediatric pathology & laboratory medicine : journal of the Society for Pediatric Pathology, affiliated with the International Paediatric Pathology Association*. May-Jun 1997;17(3):427-47.
185. Liang K, Li N, Wang X, et al. Cryo-EM structure of human mitochondrial trifunctional protein. *Proc Natl Acad Sci U S A*. Jul 3 2018;115(27):7039-7044. doi:10.1073/pnas.1801252115
186. Spiekerkoetter U, Lindner M, Santer R, et al. Management and outcome in 75 individuals with long-chain fatty acid oxidation defects: results from a workshop. *J Inherit Metab Dis*. Aug 2009;32(4):488-97. doi:10.1007/s10545-009-1125-9
187. Grunert SC, Eckenweiler M, Haas D, et al. The spectrum of peripheral neuropathy in disorders of the mitochondrial trifunctional protein. *J Inherit Metab Dis*. Jul 2021;44(4):893-902. doi:10.1002/jimd.12372
188. Grunert SC, Eckenweiler M, Spiekerkoetter U. Reversible sensory neuropathy in mitochondrial trifunctional protein deficiency. *JIMD reports*. May 2022;63(3):207-210. doi:10.1002/jmd2.12279
189. Ibdah JA, Paul H, Zhao Y, et al. Lack of mitochondrial trifunctional protein in mice causes neonatal hypoglycemia and sudden death. *J Clin Invest*. 2001;107(11):1403-9.

190. Kurtz DM, Rinaldo P, Rhead WJ, et al. Targeted disruption of mouse long-chain acyl-CoA dehydrogenase gene reveals crucial roles for fatty acid oxidation. *Proc Natl Acad Sci U S A*. Dec 22 1998;95(26):15592-7.
191. Cox KB, Hamm DA, Millington DS, et al. Gestational, pathologic and biochemical differences between very long-chain acyl-CoA dehydrogenase deficiency and long-chain acyl-CoA dehydrogenase deficiency in the mouse. *Human Molecular Genetics*. 2001;10(19):2069-77.
192. Mina AI, LeClair RA, LeClair KB, Cohen DE, Lantier L, Banks AS. CalR: A Web-Based Analysis Tool for Indirect Calorimetry Experiments. *Cell Metab*. Oct 2 2018;28(4):656-666 e1. doi:10.1016/j.cmet.2018.06.019
193. Elizondo G, Matern D, Vockley J, Harding CO, Gillingham MB. Effects of fasting, feeding and exercise on plasma acylcarnitines among subjects with CPT2D, VLCADD and LCHADD/TFPD. *Mol Genet Metab*. Sep - Oct 2020;131(1-2):90-97. doi:10.1016/j.ymgme.2020.09.001
194. Cox KB, Liu J, Tian L, Barnes S, Yang Q, Wood PA. Cardiac hypertrophy in mice with long-chain acyl-CoA dehydrogenase or very long-chain acyl-CoA dehydrogenase deficiency. Research Support, N.I.H., Extramural. *Laboratory investigation; a journal of technical methods and pathology*. Dec 2009;89(12):1348-54. doi:10.1038/labinvest.2009.86
195. Bakermans AJ, Geraedts TR, van Weeghel M, et al. Fasting-induced myocardial lipid accumulation in long-chain acyl-CoA dehydrogenase knockout mice is accompanied by impaired left ventricular function. Comparative Study
Research Support, Non-U.S. Gov't. *Circ Cardiovasc Imaging*. Sep 2011;4(5):558-65. doi:10.1161/CIRCIMAGING.111.963751
196. Tyni T, Pihko H, Kivela T. Ophthalmic pathology in long-chain 3-hydroxyacyl-CoA dehydrogenase deficiency caused by the G1528C mutation. *Curr Eye Res*. 1998;17(6):551-9.
197. Saudubray JM, Martin D, de Lonlay P, et al. Recognition and management of fatty acid oxidation defects: a series of 107 patients. *J Inherit Metab Dis*. Jun 1999;22(4):488-502. doi:10.1023/a:1005556207210
198. Tyni T, Immonen T, Lindahl P, Majander A, Kivela T. Refined staging for chorioretinopathy in long-chain 3-hydroxyacyl coenzyme A dehydrogenase deficiency. *Ophthalmic Res*. 2012;48(2):75-81. doi:10.1159/000334874
199. Ji S, You Y, Kerner J, et al. Homozygous carnitine palmitoyltransferase 1b (muscle isoform) deficiency is lethal in the mouse. *Mol Genet Metab*. Mar 2008;93(3):314-22. doi:S1096-7192(07)00445-3 [pii]
10.1016/j.ymgme.2007.10.006
200. Chegary M, Brinke H, Ruiter JP, et al. Mitochondrial long chain fatty acid beta-oxidation in man and mouse. Research Support, N.I.H., Extramural
Research Support, Non-U.S. Gov't. *Biochimica et Biophysica Acta*. Aug 2009;1791(8):806-15. doi:10.1016/j.bbalip.2009.05.006
201. Diekman EF, van Weeghel M, Wanders RJ, Visser G, Houten SM. Food withdrawal lowers energy expenditure and induces inactivity in long-chain fatty acid oxidation-deficient mouse models. *FASEB J*. Mar 19 2014;doi:10.1096/fj.14-250241

202. Gaston G, Gangoiti JA, Winn SR, et al. Cardiac tissue citric acid cycle intermediates in exercised very long-chain acyl-CoA dehydrogenase-deficient mice fed triheptanoin or medium-chain trilgyceride. *Journal of Inherited Metabolic Disease*. 2020;doi:10.1002/jimd.12284
203. Spiekerkoetter U, Tokunaga C, Wendel U, et al. Changes in blood carnitine and acylcarnitine profiles of very long-chain acyl-CoA dehydrogenase-deficient mice subjected to stress. *Eur J Clin Invest*. Mar 2004;34(3):191-6. doi:10.1111/j.1365-2362.2004.01308.x
ECI1308 [pii]
204. Raimo S, Zura-Miller G, Fezelinia H, et al. Mitochondrial morphology, bioenergetics and proteomic responses in fatty acid oxidation disorders. *Redox Biol*. May 2021;41:101923. doi:10.1016/j.redox.2021.101923
205. Kamijo T, Wanders RJ, Saudubray JM, Aoyama T, Komiyama A, Hashimoto T. Mitochondrial trifunctional protein deficiency. Catalytic heterogeneity of the mutant enzyme in two patients. Research Support, Non-U.S. Gov't. *J Clin Invest*. Apr 1994;93(4):1740-7. doi:10.1172/JCI117158
206. Ushikubo S, Aoyama T, Kamijo T, et al. Molecular characterization of mitochondrial trifunctional protein deficiency: formation of the enzyme complex is important for stabilization of both alpha- and beta-subunits. *Am J Hum Genet*. 1996;58(5):979-88.
207. Fletcher AL, Pennesi ME, Harding CO, Weleber RG, Gillingham MB. Observations regarding retinopathy in mitochondrial trifunctional protein deficiencies. *Mol Genet Metab*. May 2012;106(1):18-24. doi:10.1016/j.ymgme.2012.02.015
208. Wang ZV, Li DL, Hill JA. Heart failure and loss of metabolic control. *J Cardiovasc Pharmacol*. Apr 2014;63(4):302-13. doi:10.1097/FJC.0000000000000054
209. Dyke PC, 2nd, Konczal L, Bartholomew D, McBride KL, Hoffman TM. Acute dilated cardiomyopathy in a patient with deficiency of long-chain 3-hydroxyacyl-CoA dehydrogenase. Case Reports. *Pediatr Cardiol*. May 2009;30(4):523-6. doi:10.1007/s00246-008-9351-8
210. Bonnet D, Martin D, Pascale De L, et al. Arrhythmias and conduction defects as presenting symptoms of fatty acid oxidation disorders in children. *Circulation*. Nov 30 1999;100(22):2248-53.
211. Mathur A, Sims HF, Gopalakrishnan D, et al. Molecular heterogeneity in very-long-chain acyl-CoA dehydrogenase deficiency causing pediatric cardiomyopathy and sudden death. Research Support, U.S. Gov't, P.H.S. *Circulation*. Mar 16 1999;99(10):1337-43.
212. Saudubray JM, Martin D, de Lonlay P, et al. Recognition and management of fatty acid oxidation defects: a series of 107 patients. *J Inherit Metab Dis*. 1999;22(4):488-502.
213. Knottnerus SJG, Bleeker JC, Ferdinandusse S, et al. Subclinical effects of long-chain fatty acid beta-oxidation deficiency on the adult heart: A case-control magnetic resonance study. *J Inherit Metab Dis*. Sep 2020;43(5):969-980. doi:10.1002/jimd.12266
214. Huynh FK, Green MF, Koves TR, Hirschey MD. Measurement of fatty acid oxidation rates in animal tissues and cell lines. *Methods Enzymol*. 2014;542:391-405. doi:10.1016/B978-0-12-416618-9.00020-0

215. van Putten M. The use of hanging wire tests to monitor muscle strength and condition over time. Standard Operating Procedure. 2016;DMD_M.2.1.004.
216. Pennesi ME, Michaels KV, Magee SS, et al. Long-term characterization of retinal degeneration in rd1 and rd10 mice using spectral domain optical coherence tomography. *Invest Ophthalmol Vis Sci*. Jul 10 2012;53(8):4644-56. doi:10.1167/iovs.12-9611
217. Ryals RC, Andrews MD, Datta S, et al. Long-term Characterization of Retinal Degeneration in Royal College of Surgeons Rats Using Spectral-Domain Optical Coherence Tomography. *Invest Ophthalmol Vis Sci*. Mar 1 2017;58(3):1378-1386. doi:10.1167/iovs.16-20363
218. Nolan ND, Caruso SM, Cui X, Tsang SH. Renormalization of metabolic coupling treats age-related degenerative disorders: an oxidative RPE niche fuels the more glycolytic photoreceptors. *Eye (Lond)*. Feb 2022;36(2):278-283. doi:10.1038/s41433-021-01726-4
219. Zhang M, Jiang N, Chu Y, et al. Dysregulated metabolic pathways in age-related macular degeneration. *Sci Rep*. Feb 12 2020;10(1):2464. doi:10.1038/s41598-020-59244-4
220. Tyni T, Pihko H, Kivelä T. Ophthalmic pathology in long-chain 3-hydroxyacyl-CoA dehydrogenase deficiency caused by the G1528C mutation. *Curr Eye Res*. 1998;17(6):551-559. doi:10.1080/02713689808951227
221. Choudhary M, Malek G. CD68: Potential Contributor to Inflammation and RPE Cell Dystrophy. *Adv Exp Med Biol*. 2023;1415:207-213. doi:10.1007/978-3-031-27681-1_30
222. Karthikkeyan G, Nareshkumar RN, Aberami S, Sulochana KN, Vedantham S, Coral K. Hyperglycemia induced early growth response-1 regulates vascular dysfunction in human retinal endothelial cells. *Microvasc Res*. May 2018;117:37-43. doi:10.1016/j.mvr.2018.01.002
223. Sharma YV, Cojocaru RI, Ritter LM, et al. Protective gene expression changes elicited by an inherited defect in photoreceptor structure. *PLoS One*. 2012;7(2):e31371. doi:10.1371/journal.pone.0031371
224. Liu L, Xing L, Chen R, et al. Mitogen-Inducible Gene 6 Inhibits Angiogenesis by Binding to SHC1 and Suppressing Its Phosphorylation. *Front Cell Dev Biol*. 2021;9:634242. doi:10.3389/fcell.2021.634242
225. Gunter A, Sothilingam V, Orlich MM, Nordheim A, Seeliger MW, Muhlfriedel R. Mural Serum Response Factor (SRF) Deficiency Provides Insights into Retinal Vascular Functionality and Development. *Int J Mol Sci*. Aug 9 2023;24(16)doi:10.3390/ijms241612597
226. Chin MS, Chandrasekharam NN, Hooper LC, Detrick B, Hooks JJ. Cyclooxygenase-2 gene expression and regulation in human retinal pigment epithelial cells. *Invest Ophthalmol Vis Sci*. 2001;42(10):2338-2346.
227. Han S, Chen J, Hua J, et al. MITF protects against oxidative damage-induced retinal degeneration by regulating the NRF2 pathway in the retinal pigment epithelium. *Redox Biol*. Jul 2020;34:101537. doi:10.1016/j.redox.2020.101537

228. Garcia-Llorca A, Aspelund SG, Ogmundsdottir MH, Steingrimsson E, Eysteinsson T. The microphthalmia-associated transcription factor (Mitf) gene and its role in regulating eye function. *Sci Rep*. Oct 28 2019;9(1):15386. doi:10.1038/s41598-019-51819-0
229. Ma X, Li H, Chen Y, et al. The transcription factor MITF in RPE function and dysfunction. *Prog Retin Eye Res*. Nov 2019;73:100766. doi:10.1016/j.preteyeres.2019.06.002
230. Danielsson SB, Garcia-Llorca A, Reynisson H, Eysteinsson T. Mouse microphthalmia-associated transcription factor (Mitf) mutations affect the structure of the retinal vasculature. *Acta Ophthalmol*. Dec 2022;100(8):911-918. doi:10.1111/aos.15140
231. Garcia-Llorca A, Olafsson KH, Sigurdsson AT, Eysteinsson T. Progressive Cone-Rod Dystrophy and RPE Dysfunction in Mitf(mi/+) Mice. *Genes (Basel)*. Jul 17 2023;14(7)doi:10.3390/genes14071458
232. Adijanto J, Castorino JJ, Wang ZX, Maminishkis A, Grunwald GB, Philp NJ. Microphthalmia-associated transcription factor (MITF) promotes differentiation of human retinal pigment epithelium (RPE) by regulating microRNAs-204/211 expression. *J Biol Chem*. Jun 8 2012;287(24):20491-503. doi:10.1074/jbc.M112.354761
233. Prasun P, LoPiccolo M, Ginevic R. Long-Chain Hydroxyacyl-CoA Dehydrogenase Deficiency/Trifunctional Protein Deficiency. *GeneReviews*. 2022;
234. Pietrocola F, Galluzzi L, Bravo-San Pedro JM, Madeo F, Kroemer G. Acetyl coenzyme A: a central metabolite and second messenger. *Cell Metab*. Jun 2 2015;21(6):805-21. doi:10.1016/j.cmet.2015.05.014
235. Storm T, Burgoyne T, Futter CE. Membrane trafficking in the retinal pigment epithelium at a glance. *J Cell Sci*. Aug 27 2020;133(16)doi:10.1242/jcs.238279
236. Bonilha VL, Rayborn ME, Bhattacharya SK, et al. The retinal pigment epithelium apical microvilli and retinal function. *Adv Exp Med Biol*. 2006;572:519-24. doi:10.1007/0-387-32442-9_72
237. Ferdous S, Liao KL, Gefke ID, et al. Age-Related Retinal Changes in Wild-Type C57BL/6J Mice Between 2 and 32 Months. *Invest Ophthalmol Vis Sci*. Jun 1 2021;62(7):9. doi:10.1167/iovs.62.7.9
238. De Vera Mudry MC, Kronenberg S, Komatsu S, Aguirre GD. Blinded by the light: retinal phototoxicity in the context of safety studies. *Toxicol Pathol*. Aug 2013;41(6):813-25. doi:10.1177/0192623312469308
239. Wongchaisuwat N, Wang J, Yang P, et al. Optical coherence tomography angiography of choroidal neovascularization in long-chain 3-hydroxyacyl-CoA dehydrogenase deficiency (LCHADD). *Am J Ophthalmol Case Rep*. Dec 2023;32:101958. doi:10.1016/j.ajoc.2023.101958
240. R. Sacconi FB, G. Querques. Choroidal Neovascularization Associated with Long-Chain 3-Hydroxyacyl-CoA Dehydrogenase Deficiency. *Retinal Cases and Brief Reports*. 2022;
241. Fernandez-Godino R, Garland DL, Pierce EA. Isolation, culture and characterization of primary mouse RPE cells. *Nat Protoc*. Jul 2016;11(7):1206-18. doi:10.1038/nprot.2016.065

242. Rinaldo P, Cowan TM, Matern D. Acylcarnitine profile analysis. *Genet Med*. Feb 2008;10(2):151-6. doi:10.1097/GIM.0b013e3181614289
243. Smith EH, Matern D. Acylcarnitine analysis by tandem mass spectrometry. *Curr Protoc Hum Genet*. Jan 2010;Chapter 17:Unit 17 8 1-20. doi:10.1002/0471142905.hg1708s64
244. Galaxy C. The Galaxy platform for accessible, reproducible and collaborative biomedical analyses: 2022 update. *Nucleic Acids Res*. Jul 5 2022;50(W1):W345-W351. doi:10.1093/nar/gkac247
245. Batut B, Freeber M, Heydarian M, et al. Reference-based RNA-Seq data analysis (Galaxy Traning Materials). Online. doi:https://training.galaxyproject.org/training-material/topics/transcriptomics/tutorials/ref-based/tutorial.html
246. Hiltemann S, Rasche H, Gladman S, et al. Galaxy Training: A powerful framework for teaching! *PLoS Comput Biol*. Jan 2023;19(1):e1010752. doi:10.1371/journal.pcbi.1010752
247. Batut B, Hiltemann S, Bagnacani A, et al. Community-Driven Data Analysis Training for Biology. *Cell Syst*. Jun 27 2018;6(6):752-758 e1. doi:10.1016/j.cels.2018.05.012
248. Doyle M. Visualization of RNA-Seq results with Volcano Plot (Galaxy Training Materials). doi:https://training.galaxyproject.org/training-material/topics/transcriptomics/tutorials/rna-seq-viz-with-volcanoplot/tutorial.html
249. Zhang H, Shen Y, Kim IM, Weintraub NL, Tang Y. The Impaired Bioenergetics of Diabetic Cardiac Microvascular Endothelial Cells. *Front Endocrinol (Lausanne)*. 2021;12:642857. doi:10.3389/fendo.2021.642857
250. Quiros PM, Goyal A, Jha P, Auwerx J. Analysis of mtDNA/nDNA Ratio in Mice. *Curr Protoc Mouse Biol*. Mar 2 2017;7(1):47-54. doi:10.1002/cpmo.21
251. MacLaren RE, Fischer MD, Gow JA, et al. Subretinal timrepigene emparvovec in adult men with choroideremia: a randomized phase 3 trial. *Nat Med*. Oct 2023;29(10):2464-2472. doi:10.1038/s41591-023-02520-3
252. Xia X, Guo X. Adeno-associated virus vectors for retinal gene therapy in basic research and clinical studies. *Front Med (Lausanne)*. 2023;10:1310050. doi:10.3389/fmed.2023.1310050
253. Gonzalez-Cordero A, Goh D, Kruczek K, et al. Assessment of AAV Vector Tropisms for Mouse and Human Pluripotent Stem Cell-Derived RPE and Photoreceptor Cells. *Hum Gene Ther*. Oct 2018;29(10):1124-1139. doi:10.1089/hum.2018.027
254. Jacobson SG, Cideciyan AV, Ho AC, et al. Safety and improved efficacy signals following gene therapy in childhood blindness caused by GUCY2D mutations. *iScience*. May 21 2021;24(5):102409. doi:10.1016/j.isci.2021.102409
255. Suoranta T, Laham-Karam N, Yla-Herttuala S. Optimized Protocol for Accurate Titration of Adeno-Associated Virus Vectors. *Hum Gene Ther*. Oct 2021;32(19-20):1270-1279. doi:10.1089/hum.2020.318
256. AddGene. AAV Titration by qPCR Using SYBR Green Technology. Website. 2019;
257. Mutze U, Ottenberger A, Gleich F, et al. Neurological outcome in long-chain hydroxy fatty acid oxidation disorders. *Ann Clin Transl Neurol*. Jan 23 2024;doi:10.1002/acn3.52002

258. Graven SN, Browne JV. Visual Development in the Human Fetus, Infant, and Young Child. *Newborn and Infant Nursing Reviews*. 2008;8(4):194-201. doi:10.1053/j.nainr.2008.10.011
259. Yeo NJY, Chan EJJ, Cheung C. Choroidal Neovascularization: Mechanisms of Endothelial Dysfunction. *Front Pharmacol*. 2019;10:1363. doi:10.3389/fphar.2019.01363
260. Patel RC, Gao SS, Zhang M, et al. Optical Coherence Tomography Angiography of Choroidal Neovascularization in Four Inherited Retinal Dystrophies. *Retina*. Dec 2016;36(12):2339-2347. doi:10.1097/IAE.0000000000001159
261. Rocholz R, Corvi F, Weichsel J, Schmidt S, Staurenghi G. OCT Angiography (OCTA) in Retinal Diagnostics. In: Bille JF, ed. *High Resolution Imaging in Microscopy and Ophthalmology: New Frontiers in Biomedical Optics*. 2019:135-60.
262. Koehn D, Meyer KJ, Syed NA, Anderson MG. Ketamine/Xylazine-Induced Corneal Damage in Mice. *PLoS One*. 2015;10(7):e0132804. doi:10.1371/journal.pone.0132804
263. Yee T, Wert KJ. Base and Prime Editing in the Retina-From Preclinical Research toward Human Clinical Trials. *Int J Mol Sci*. Oct 16 2022;23(20)doi:10.3390/ijms232012375
264. Porto EM, Komor AC, Slaymaker IM, Yeo GW. Base editing: advances and therapeutic opportunities. *Nat Rev Drug Discov*. Dec 2020;19(12):839-859. doi:10.1038/s41573-020-0084-6
265. Choi EH, Suh S, Foik AT, et al. In vivo base editing rescues cone photoreceptors in a mouse model of early-onset inherited retinal degeneration. *Nat Commun*. Apr 5 2022;13(1):1830. doi:10.1038/s41467-022-29490-3
266. Jo DH, Jang HK, Cho CS, et al. Visual function restoration in a mouse model of Leber congenital amaurosis via therapeutic base editing. *Mol Ther Nucleic Acids*. Mar 14 2023;31:16-27. doi:10.1016/j.omtn.2022.11.021

# Appendix 1: High Fat Diet Accelerates LCHADD Chorioretinopathy

Introduction: One limitation of the LCHADD mouse model is that it is that the chorioretinopathy is not as severe as patients. Specifically, 12-month mice display RPE degeneration but no degeneration in the photoreceptors. One possible explanation for this is that mice eat a diet lower in fat than humans, which can result in lower levels of the potentially toxic hydroxyacylcarnitines. The purpose of these experiments was to determine if raising the acylcarnitine levels by feeding mice a higher-fat diet would accelerate retinal degeneration and vision loss.

Results: 3-month WT and LCHADD mice were first placed on a high-fat diet (HFD; ~45% of calories from fat) for 3-months. After the 3-months of HFD, the LCHADD male mice did not gain the same amount of weight as WT mice suggesting they were not eating the food (Figure A1: A-C). In addition, 62% of LCHADD eyes had a problem, such as corneal abrasions and foggy vitreous, while only 5% of WT eyes had a problem (Figure A1: D-E). These problems hindered visual assessments. Overall, these results suggested that these mice were unhealthy and 3-months on a 45% fat diet was too high in fat for the LCHADD mice.

Next, 10-month WT and LCHADD mice were placed on either a normal diet (~16% calories from fat) or a breeder chow (~30% calories from fat) for 2-months. After 2-months, visual performance and retinal health was assessed using optokinetic tracking (OKT) and fundus imaging. LCHADD mice had the same body weight as WT mice on the

breeder chow, suggesting LCHADD mice were able to tolerate the breeder chow (Figure A2: A). Visual performance in LCHADD mice were statistically worse compared to WT, but the LCHADD mice on breeder chow was significantly worse than LCHADD mice on a normal diet suggesting a higher-fat diet increases vision loss (Figure A2: B). RPE degeneration was evaluated by counting the number of eyes with hypopigmented areas on fundus images. The number of LCHADD eyes with hypopigmentation was significantly higher than the number of WT eyes, but the number of eyes of LCHADD mice on breeder chow was not different than the number of LCHADD mice on a normal diet (Figure A2:C), indicating similar RPE degeneration between LCHADD mice on breeder and normal diet. Overall, breeder chow did accelerate vision loss in LCHADD mice without visibly impacting the overall health.

Conclusion: Overall, this data suggests that increasing the fat intake of LCHADD mice accelerates the vision loss. While LCHADD mice do not tolerate a diet with 45% calories from fat, as evidenced by decrease in body weight, LCHADD mice do tolerate the breeder diet (~30% calories from fat). While LCHADD mice on the breeder diet for 2-months has a significantly lower visual performance compared to LCHADD mice on a normal diet, there was no evidence of increased RPE degeneration on the fundal images. One reason for this could be that fundus imaging is not sensitive enough to detect the differences. Therefore, evaluating the visual performance and RPE degeneration in 6-month LCHADD mice that were on a breeder diet for 3-months will be important in

determining if a higher fat diet speeds up the initial presentation of the chorioretinopathy.

Figures

A

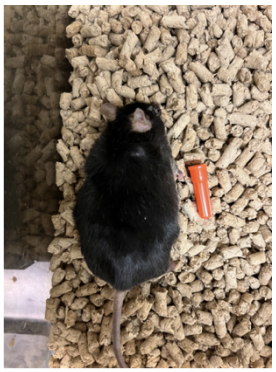

B

C.

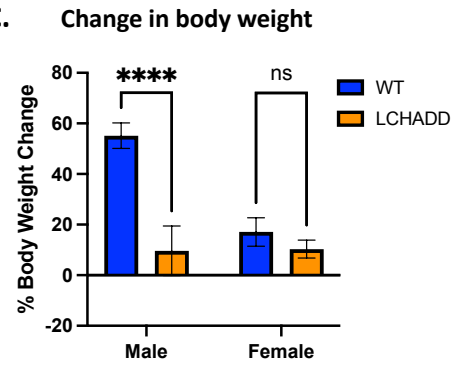


D

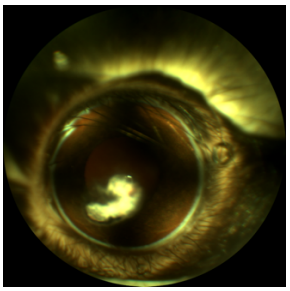

E

| | WT | LCHADD |
|---|---|---|
| Healthy Eyes | **19/20** | **5/13** |
| Corneal Abrasion | **0/20** | **5/13** |
| Cloudy Vitreous | **1/20** | **3/13** |

**Figure A1: LCHADD mice do not tolerate 3-months on a high-fat diet (45% calories from fat).** (A-B) Representative images of 6-month (A) WT and (B) LCHADD mice after 3-months on a high-fat diet. (C) LCHADD male mice, after 3-months on a high-fat diet, did not have the same increase in body weight as WT male mice, indicating mice were not eating the food. Female LCHADD mice did not increase in body weight as much as WT female mice, although this is not statistically significant. Data presented as mean ± SD. Statistics calculated by a two-way ANOVA. ****$p<0.0001$ (D) Representative image of a corneal abrasion seen on many LCHADD eyes after 3-months on a high-fat diet. (E) Quantification of the type of eyes in WT and LCHADD mice after 3-months on a high-fat diet show that LCHADD mice have more eye problems that would affect visual assessment when compared to WT.

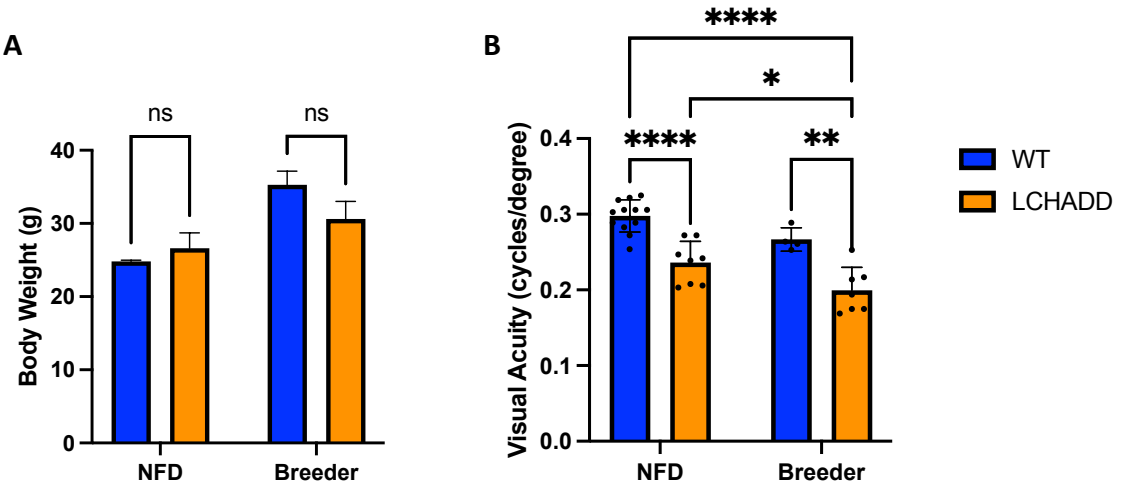


C

| Eyes with Hypopigmentation | | |
|---|---|---|
| | WT | LCHADD |
| NFD | **2/12 (17%)** | **5/8 (63%)** |
| Breeder | **1/4 (25%)** | **5/8 (63%)** |

**Figure A2: LCHADD mice can tolerate 2-months on a breeder chow (30% calories from fat) and accelerates vision loss in LCHADD mice.** (A) Female 12-month LCHADD mice, both on a normal diet and a breeder diet, had similar weights when compared to WT mice fed the same diet, indicating LCHADD mice are eating and can tolerate a breeder chow for 2-month. Data presented as mean ± SD and statistics calculated using a two-way ANOVA. (B) Visual performance of 12-month LCHADD mice were significantly lower that WT mice and LCHADD mice fed a breeder diet for 2-months has a significantly lower visual performance compared to LCHADD mice fed a normal diet. This suggests a higher-fat diet does accelerate the retinopathy in LCHADD mice. Data presented as mean ± SD and statistics calculated using a two-way ANOVA. (C) Quantification of the number of eyes with hypopigmentation suggests LCHADD eyes have increased hypopigmentation compared to WT, but LCHADD mice on a breeder chow do not have increased hypopigmentation compared to LCHADD mice on a normal diet. *p<0.05, **p<0.01, ***p<0.001, ****p<0.0001.